Institute of Space and Aeronautical Science, University of Tokyo
Report No. 453, August 1970

Detailed Measurements in the Transition Region of a Two-Dimensional Wake

By

Hiroshi SATO and Yoshio ONDA

Summary: Detailed measurements were made on the laminar-turbulent transition of a two-dimensional wake with three kinds of imposed disturbances, the natural disturbance in a wind tunnel, a sound of single frequency, and a sound of two frequencies from outside. In all cases the transition to turbulence is gradual. The production of the fluctuation energy from the mean motion can be negative in a certain stage of the transition. When a sound of single frequency is introduced into the wake, the induced velocity fluctuation is regular and periodic and it persists, resulting in a transition delay.

When a sound of two frequencies (f_1 and f_2) is introduced, two velocity fluctuations are induced. They grow independently while amplitudes are small. When amplitudes exceed certain values, two fluctuatoins interact and both amplitudes are reduced. Another result is the generation of velocity fluctuations of frequencies of f_1-f_2, $2(f_1-f_2)$, ..., and f_1+f_2, $2(f_1+f_2)$, ... The behavior of a slow, irregular fluctuation found in the natural transition resembles that of f_1-f_2 component in many respects. Both fluctuations must be generated by the same process. The amplification of randomness in the transition process may be accomplished by the mutual suppression of amplitudes and by the generation of low-frequency components from high-frequency components.

CONTENTS

1. INTRODUCTION

A small-amplitude disturbance imposed on a laminar shear flow grows or decays according to its frequency or wave length. The predition of the linear stability theory on the growth agrees very well with experimental results in various flows including the boundary layer along a flat plate, jets and wakes. If the wave

This document is provided by JAXA.

length of a disturbance lies in the unstable zone of the stability theory, the disturbance grows exponentially in the flow direction. As a result of the selective amplification an almost sinusoidal velocity fluctuation is produced in the "natural" transition. When the amplitude of the sinusoidal fluctuation reaches a certain threshold value, the growth rate becomes less. At the same time, the wave-form of the fluctuation changes. The linear theory is not valid for such a large-amplitude fluctuation. Second-order terms which are neglected in the linear theory become significant. The basic flow is distorted due to the interaction with the large-amplitude fluctuation and this distortion, in turn, modifies the growth of the fluctuation. Interaractions also take place among velocity fluctuations. The equation of motion is highly nonlinear. Existing nonlinear theories deal with simplified cases. [*1*][*2*][*3*]

Experimental investigations on the transition process have been made in various flows, and results indicate that the process is very much different for different flows. For instance, in the boundary layer along a plate a spanwise variation of the amplitude of the periodic fluctuation leads to abrupt breakdowns. [*4*] On the contrary, in free layers such as jets and wakes, the periodic fluctuation gradually changes into random turbulence. [*5*][*6*][*7*][*8*][*9*]

Among free layers the tr,ansition process of a wake is different from that of a separated layer. For example, the nonlinear interaction in the separated layer results in the production of subharmonics—the fluctuation with the frequency half of the fundamental component. [*7*][*10*] On the other hand, no such subharmonics have been found in the wake yet. [*5*] The reason for this difference is not known.

The structure of a fully-developed turbulence should not depend on the nature of the disturbance which initiated the transition. But the transition process is closely related to the initial disturbance. On example is the "turbulent spot" created in a boundary layer by a finite-amplitude disturbance. The development of the spot is entirely different from that of a two-dimensional fluctuation initiated by a vibrating ribbon. These facts suggest that more extensive and more ditailed experimental investigations are still wanted for a full understanding of the transition process.

The transition region connects two distinct states. One is the laminar flow which is deterministic in nature. If initial and boundary conditions are specified, the laminar flow must be uniquely determined. The other state is the random and turbulent motions which are not deterministic. Therefore, in the transition the "randomization process" is included. The abrupt breakdown is one example of randomization and the gradual change of the wave-form is another. Existing nonlinear theories are diterministic in nature. Even if complicated nonlinear equations are used for thories, the ramdomization process is not properly taken into account. In experimental works the randomization process has not been clarified.

The purpose of the present experimental investigation is to make a detailed experiment on the nonlinear inte action of velocity fluctuations as well as to obtain

This document is provided by JAXA.

informations on the randomization. We have already published several papers on the transition of free layers, including jet, wake and separated layer. They are concerned partly with the linear growth of fluctuations and partly with the non-linear development. In the present work we have made detailed measurements on the nonlinear interaction in the two-dimensional wake of a flat plate placed parallel to the uniform flow. Three types of initial disturbance were employed. One is the "natural" disturbance in the wind-tunnel. The natural transition is initiated by the natural disturbance. The second experiment is the transition with sound from a loudspeaker. The sound is a sinusoidal wave with one frecuency. The effect of the sound on the transition process was investigated. The last case is with a sound composed of two sinusoidal waves of different frequencies. The interaction of two discrete velocity fluctuations induced in the wake was investigated.

2. Experimental Arrangement

The whole experiment was conducted in the No. 2 Low-Turbulence Wind-Tunnel at the Institute of Space and Aeronautical Science. The wind-tunnel is of straight, blow-out type and has a test-section of 60 cm×60 cm cross-section and 3 m length (Fig. 2-1). The air-intake was specially designed for minimizing the non-uniformity of the approaching flow to the fan. The cross section of the settling chamber is 2.4 m×2.4 m and the contraction ratio is 16. Eleven fine-mesh screens were installed in the settlting chamber for reducing velocity fluctuations. The residual longitudinal fluctuation level in the test-section, $\sqrt{\overline{u^2}}$ is about 0.04 percent of the free-stream velocity at 10 m/sec. The streamwise distribution of the static pressure was made uniform within 1 percent of the dynamic pressure by adjusting two flexible side walls. One of side walls has slits in lateral and longitudinal directions. A static-pressure probe and a hot-wire anemometer are mounted on a three-dimensional traversing mechanism and inserted into the test-section through those slits. Portions of slits not in use are covered.

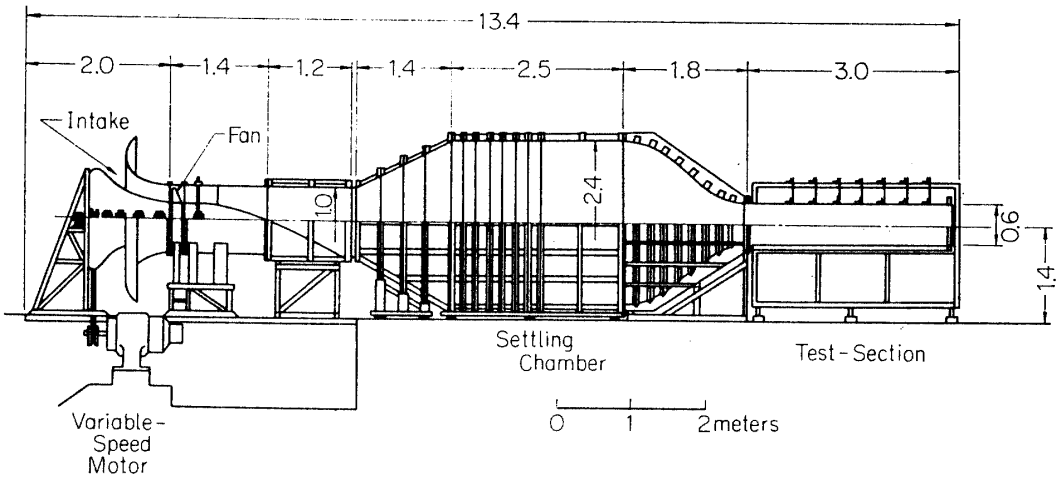

FIG. 2-1. No. 2 Low-Turbulence Wind-Tunnel. Flow, from left to right. All dimensions in meters.

This document is provided by JAXA.

A thin bakelite plate was spanned vertically in the center of the test-section for producing a two-dimensional wake. The bakelite was found to be better than metals because it exhibits less elongation and warping due to machining. The length of the plate is 30 cm and the span is equal to the height of the test section (60 cm). The maximum thickness of the plate is 3 mm. The leading edge was machined to form a half of a 10:1 ellipse and the trailing edge was filed to form a sharp and thin edge (Fig. 2-2). A compromise was necessary between the thinness and the straightness of the trailing edge. If the plate is field too thin, the trailing edge can not be kept straight and the two-dimentionality of the wake is destroyed. If the trailing dege is too thick, a dead-water region is formed behind the plate. In our previous work [5], the trailing dege was made as thin as possible and as a result it was slightly wavy. In the present experiment, we made the trailing edge as straight as possible with the expense of the thinness. The thickness was about 0.2 mm in contrast to 0.1 mm of our previous work. This difference seems to result in a small difference in the streamwise development of the laminar portion of the wake. The plate was aligned to the free stream so that the velocity distribution at the trailing edge becomes symmetrical with respect to the center-line. The arrangement of the test-section is shown in Fig. 2-3.

A loudspeaker was placed at the end of the wind-tunnel for introducing a sound into the wake. A sinusoidal output from an audiofrequency oscillator was fed to the loudspeaker. Two oscillators were used for producing sound with two frequencies.

The coordinate system has an origin at the center of the trailing edge. The X-axis is in the flow direction and Y-axis is perpendicular to the plate. The direction parallel to the trailing edge is taken as Z-axis. Pictures of the test-section and the traversing mechanism are shown in Fig. 2-4.

Measurements of mean- and fluctuating-velocities were made by hot-wire anemometers. The velocity component in the flow direction was measured by a single hot-wire placed parallel to the trailing edge. Components in Y- and Z-directions were measured by X-array wires. Hot-wire probes are shown in Fig. 2-5. The hot-wire is a tungsten wire of 3.8 microns in diameter and about 1 mm in length. Both ends of the wire are welded to steel supports. In constructing X-wires extra care was taken to match two wires and to place two wires as close as possible. The separation of two wires is about 0.1 mm.

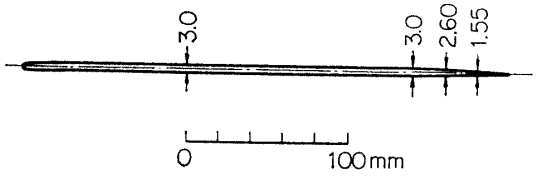

FIG. 2-2. Dimensions of wake-producing plate. All dimensions in millimeters.

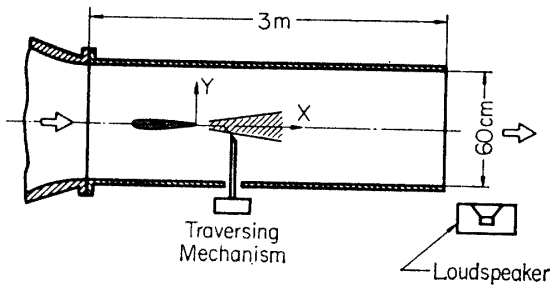

FIG. 2-3. Test-section arrangement and co-ordinate system.

This document is provided by JAXA.

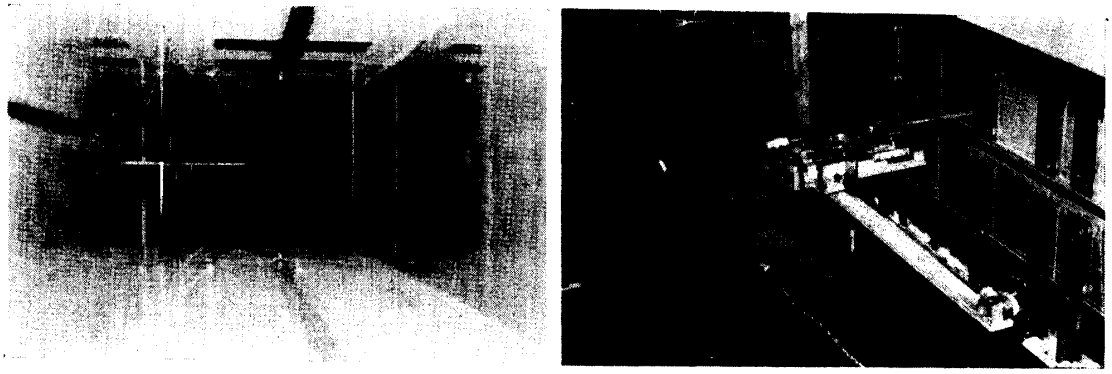

(A) (B)

FIG. 2-4. Pictures of test-section. (A) Interior of test-section taken from downstream end. (B) side wall and traversing mechanism.

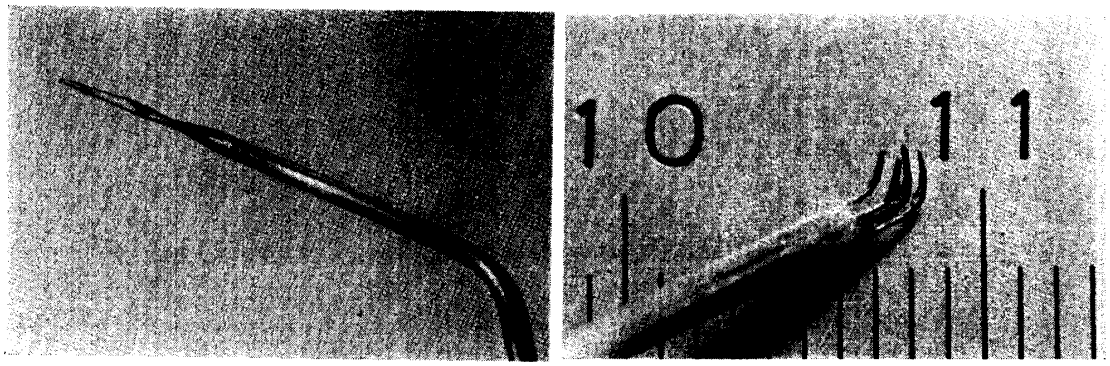

(A) (B)

FIG. 2-5. (A) Single hot-wire anemometer. (B) X-wire, scale in centimeters.

Hot-wire anemometers were operated in the constant-temperature mode. A block diagram of the electronic circuit is shown in Fig. 2-6. The hot-wire amplifiers were dc coupled. The signal from hot-wire was linearized by two square units. Two independent channels were used for X-wires. A wave analyzer (RC-feedback band-pass filter) was used for the spectral analysis. The bandwidth of the analyzer was proportional to the central frequency. Root-mean-square values of the output voltage were obtained by a square circuit and recorded on the Y-axis of an X-Y recorder. The position of the hot-wire anemometer in the wake was converted into a voltage by a potentiometer and fed to the X-axis of the recorder.

The static pressure was measured by a small static probe, 1 mm in diameter and 10 mm in length. Four holes are drilled on the cylindrical side of the probe. The reading of the static pressure is erroneous if there is a large-amplitude velocity fluctuation. A test was made on the effect of the side wind and the reading of the static pressure was insensitive to the angle of attack up to 6 degrees. This angle corresponds to the sidewise velocity component of 10% of the longitudinal velocity. Both mean- and fluctuation-values of lateral components in the present experiment are mostly within this limit. Therefore, no corrections were made to measured values of the static pressure.

This document is provided by JAXA.

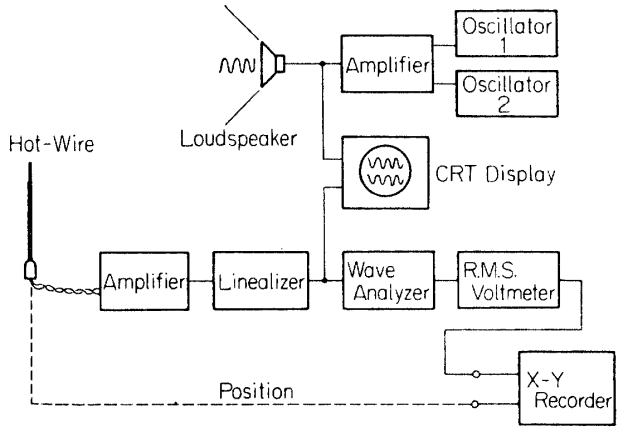

FIG. 2-6. Block diagram of hot-wire system.

All measurements were made at a fixed freestream velocity, 10 m/sec. The thickness of the boundary layer at the trailing edge with this wind speed is about 2 mm. The Reynolds number based on the length of the plate is 2×10^5 and the Reynolds number based on the thickness of the boundary layer at the trailing edge is about 1500.

Two turbulent wedges start from intersections of the leading edge of the wake-producing plate and the ceiling and the floor of the test-section. The expansion angle of this "transverse contamination" on the plate was found to be around 11 degrees. The width of the plate is 60 cm and we have a contamination-free region of more than 15 cm at the furthermost X-station in the experiment, 800 mm from the trailing edge. All data presented here may hot be influenced by the contamination.

The error of the measurement of the absolute value of $\overline{u^2}$ by a hot-wire anemometer may be less than 10%. Errors come mainly from the change of the calibration curve. Relative values are much more accurate. In measuring v- and w-fluctuations two wires must be matched and properly aligned. Besides errors due to mismatching and misalignment, the X-wires have a length of about 0.7 mm in Y-direction in which the distribution of $\overline{v^2}$ has a large gradient. The X-wires give averaged values. The error in $\overline{v^2}$ measurement may be around 20 percent. The same order-of-magnitude inaccuracy is inherent to the measurement of $\overline{w^2}$. When $\overline{w^2}$ is very small compared with $\overline{u^2}$ and $\overline{v^2}$, the error may be larger. Both mismatching and misalignment of X-wires lead to larger apparent values of $\overline{w^2}$.

The reproducibility of the flow field is not good in the natural transition. This may come from the run-to-run change of the background disturbance in the wind-tunnel. The intensity and the frequency of observed velocity fluctuations are not always the same, while relative values are maintained almost unchanged. With sound from the loudspeaker, the reproducibility is very much improved. It was noticed, however, that the sound with the same intensity does not produce the velocity fluctuation with the same amplitude on different days. In order to obtain

This document is provided by JAXA.

the best reproducibility the sound intensity was adjusted by measuring the amplitude of an induced velocity fluctuation at a monitoring point in the wake.

3. Natural Transition

First of all, the mean-velocity distribution of the boundary layer on the plate was measured. The distribution is of Blasius type on both sides of the plate and there are no velocity fluctuations in the boundary layer. In the wake, the velocity distribution near the trailing edge ($X=1$ mm) is still close to the Blasius distribution as shown in Fig. 3-1. At $X=40$ mm the velocity on the center-line is about 40 percent of the freestream velocity, U_0. The central velocity increases until $X=100$ mm, where it reaches about 0.85 U_0. It decreases fom $X=100$ mm to 150 mm and at larger X it increases downstream again. Distributions at various X-stations are almost similar but at $X=150$ mm, U/U_0 at around $Y=\pm 6$ mm exceeds unity. These results on the mean-velocity distribution have been already reported in the previous paper [5]. The streamwise variation of the mean velocity is clearly shown in Fig. 3-2 in which the non-dimensional central velocity, U_c/U_0, and the half-value breadth, b, are plotted against X. Both U_c and b increases until $X=80$ mm and then decreases. The half breadth at $X=0$ is about 1 mm. It stays almost constant until $X=30$ mm, reaches a maximum value, 3.5 mm at $X=80$ mm and then decreases down to 2.5 mm at $X=120$ mm. In Fig. 3-3 both U_c and b are shown in a wider range of X. The central velocity starts increasing at about $X=200$ mm and approaches to U_0 monotonically at larger X. Decreases of U_c and b near $X=100$ mm must be resulted from a nonlinear interaction with velocity fluctuations.

Lateral velocity components, V and W were measured and found to be small. The value of V does not exceed 3 percent of U_0 and W is less then that.

Distributions of the static pressure at various X-stations are shown in Fig. 3-4. The difference of pressures in the wake and in the free stream $p-p_0$ is non-dimensionalized by the dynamic pressure, $\rho U_0^2/2$. At $X=30$ mm the pressure in

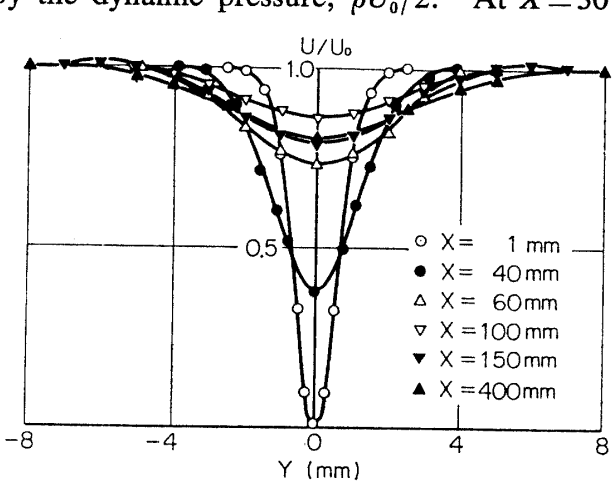

Fig. 3-1. Mean-velocity distribution in wake, natural transition, free-stream velocity, $U_0=10$ m/s.

This document is provided by JAXA.

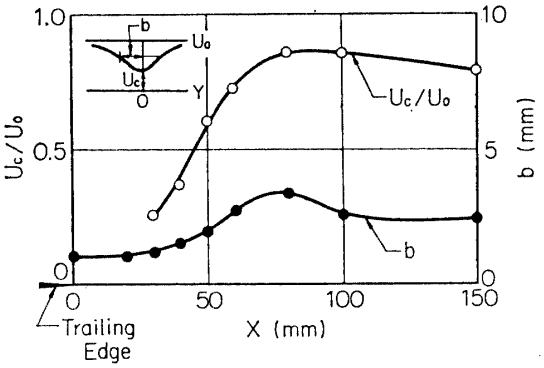

FIG. 3-2. Streamwise variations of non-dimensional velocity on the center line, U_c/U_0 (U_0: free-stream velocity) and Half-value breadth, b, natural transition.

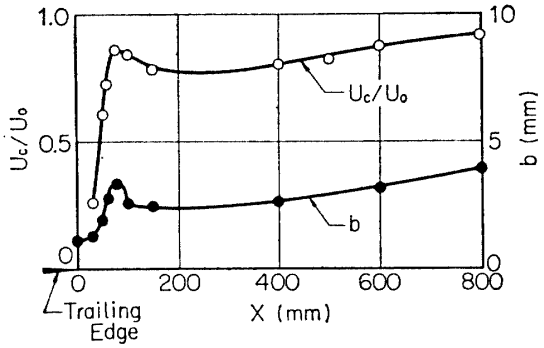

FIG. 3-3. Streamwise variations of non-dimensional velocity on the center line, U_c/U_0 (U_0: free-stream velocity) and half-value breadth, b natural transition.

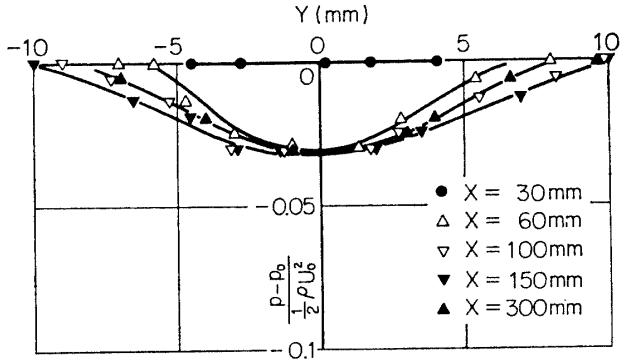

FIG. 3-4. Static-pressure distribution at five X-stations p: pressure in wake, p_0: pressure in free stream. Natural transition.

the wake is the same as the free-stream pressure. At $X=60$ mm the pressure in the wake is lower, the difference on the center line being about 3 percent of the dynamic pressure. The negative static pressure which persists until $X=300$ mm is not resulted from the dead-water region behind the plate.

No velocity fluctuations are observed in the boundary layer and just behind the plate. A small-amplitude fluctuation is found at around $X=20$ mm. The wave-form of the fluctuation is almost sinusoidal with the frequency of about 630 Hz. The amplitude increases in the flow direction. The behavior of the small-amplitude velocity fluctuation at small X has been thoroughly investigated and reported in reference 5. Experimental values on the wave-length, phase velocity and amplitude distribution in Y-direction agreed very well with results of linearized theory.

Wave-forms of u-fluctuations at various points in the wake are illustrated in Figs. 3-5 and 3-6 with two different sweep speeds. At $X=40$ mm, $Y=2$ mm, the wave-form is regular and sinusoidal, whereas on the center-line the fluctuation is composed of second harmonics (1260 Hz) and a slow, irregular fluctuation. The same is true at $X=60$ mm and 100 mm. The significance of the slow,

This document is provided by JAXA.

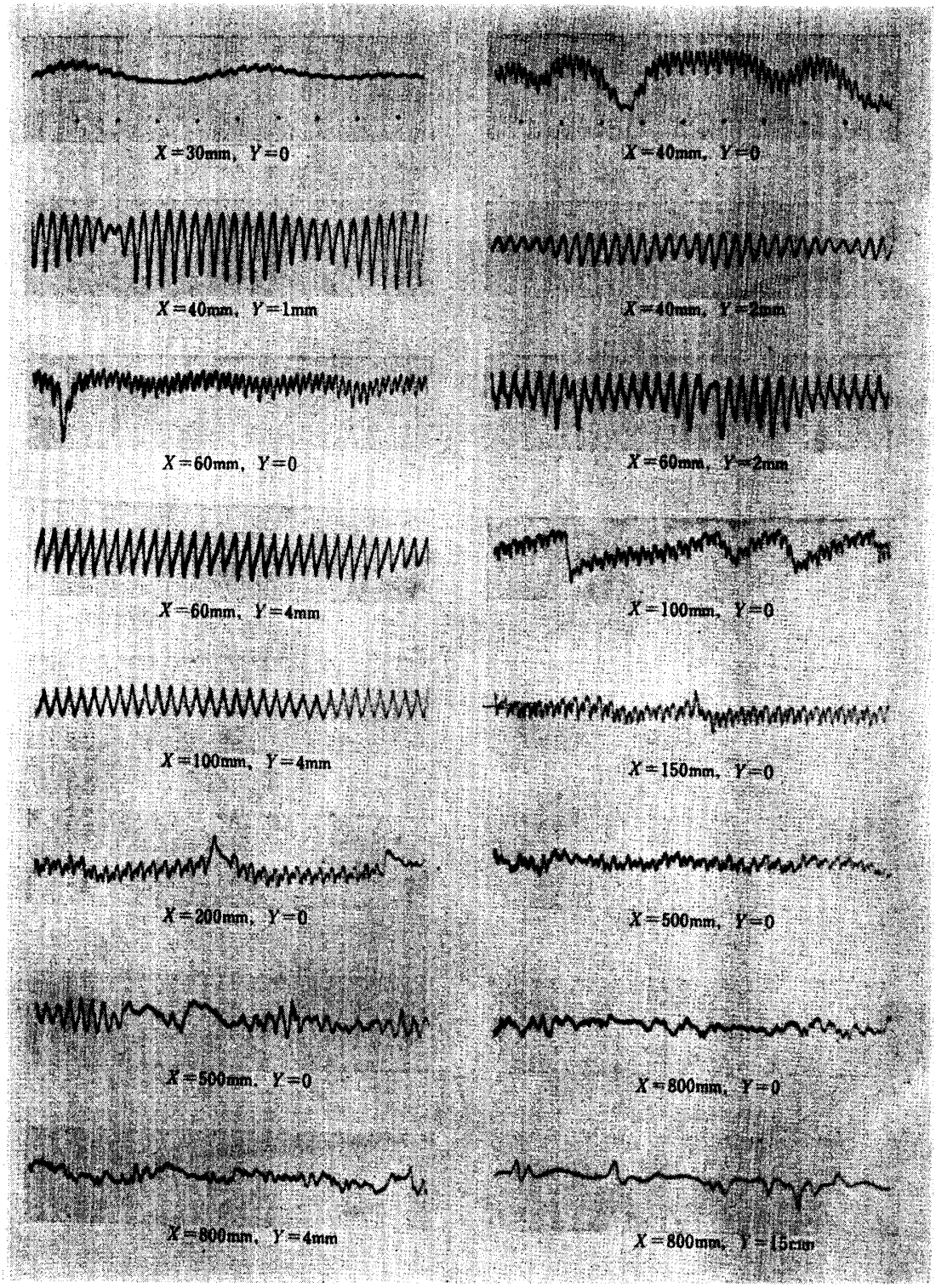

FIG. 3-5. Wave-forms of u-fluctuation, natural transition. Velocity increases upward. Time from left to right. Time interval between dots, 5 millisec.

This document is provided by JAXA.

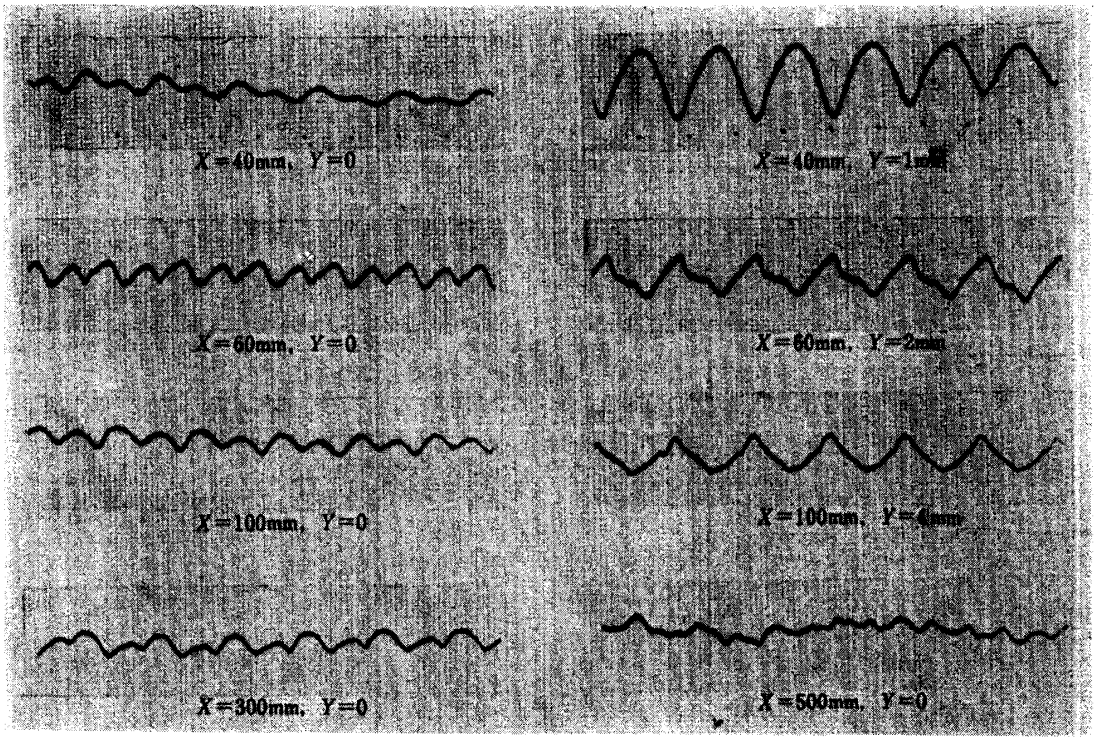

FIG. 3-6. Wave-forms of u-fluctuation, natural transition. Velocity increases upward. Time from left to right. Time interval between dots, 1 millisec.

irregular fluctuation will be discussed in Section 8 in connection with the randomization of regular fluctuations. Wave-forms change gradually into irregular patterns at large X. At $X=$ 500 mm, there are some remaining regularities but at $X=800$ mm wave-forms are completely irregular and turbulent. At the edge of the wake ($X=800$ mm, $Y=15$ mm) fluctuation signals are intermittent. In Fig. 3-6 with higher sweep speed details of fundamental and harmonic components (630 Hz and 1260 Hz) are clearly shown At $X=60$ mm and $X=100$, wave-forms are triangular. This implies the existence of several higher harmonics. In the transition process, higher harmonics seem to be generated from the fundamental component in a regular manner and low-frequency components are produced rather irregularly as observed in Fig. 3-5.

Wave-forms of v-fluctuation illustrated in Figs 3-7 and 3-8 are different from those of u-fluctuation. No irregular, slow fluctration is found near the center line. For instance, at $X=60$ mm, $Y=0$ the wave-form is quite regular. Although the fundamental component is distorted in various fashions, no decisive irregularity appears until $X=800$ mm. Distorted wave-forms of v-fluctuation are not necessarily the same as those of u. For instance, at $X=800$ mm, $Y=0$ the wave-form in Fig. 3-8 is like a square wave. We do not observe such a wave-form in u-fluctuation. The triangular wave-form at $X=100$ mm, $Y=4$ mm is similar to that of u at the same point in Fig. 3-6. The difference in wave-forms or u- and v-fluctuations is equivalent to the difference of distributions of various spectral components.

This document is provided by JAXA.

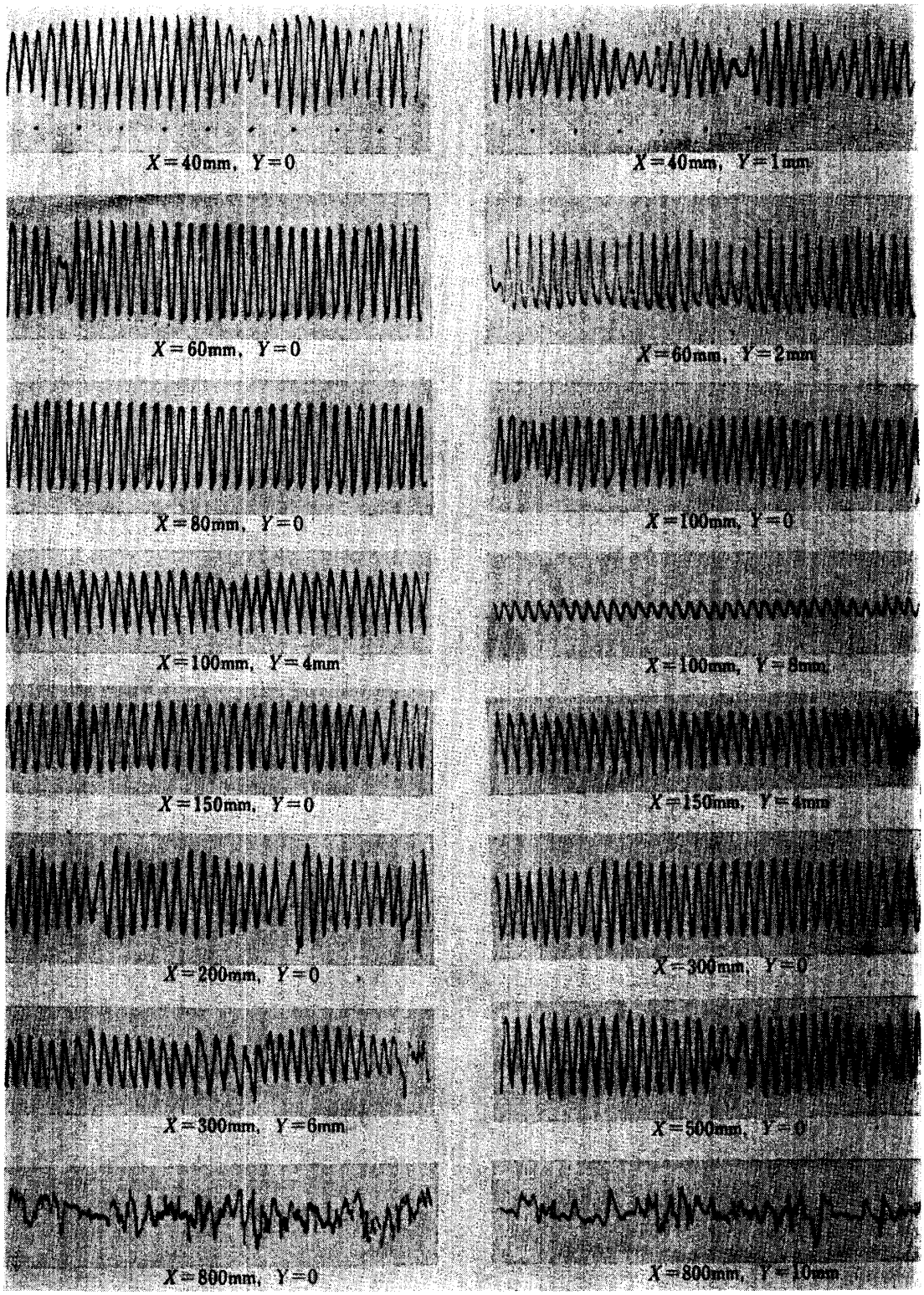

FIG. 3-7. Wave-forms of v-fluctuation, natural transition. Time interval between dots, 5 millisec.

This document is provided by JAXA.

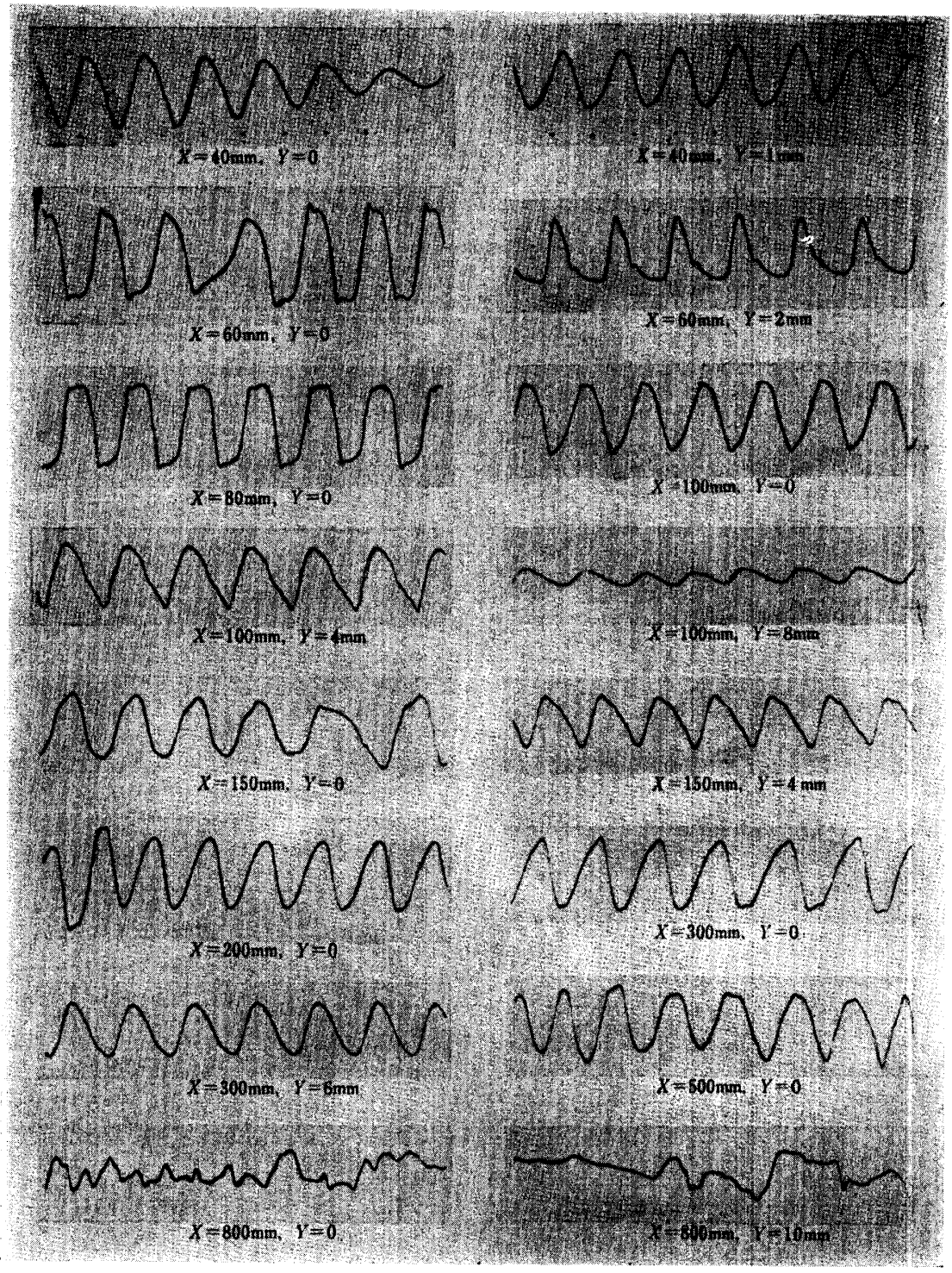

FIG. 3-8. Wave-forms of v-fluctuation, natural transition. Time interval between dots, 1 millisec.

This document is provided by JAXA.

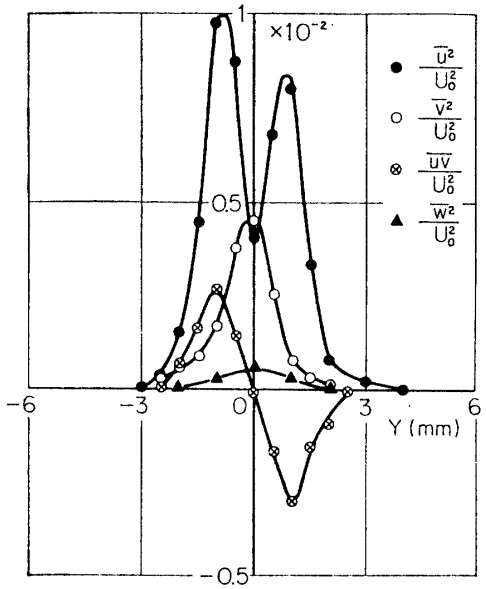

FIG. 3-9. Distributions of $\overline{u^2}$, $\overline{v^2}$, $\overline{w^2}$, and $\overline{uv}$, natural transition, $X=40$ mm.

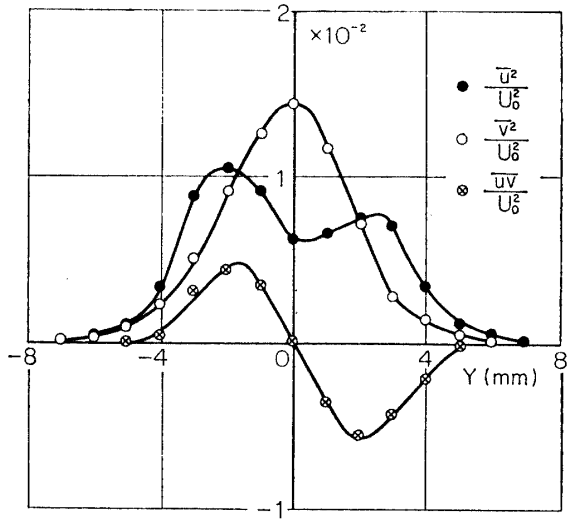

FIG. 3-10. Distributions of $\overline{u^2}$, $\overline{v^2}$ and $\overline{uv}$, natural transition, $X=60$ mm.

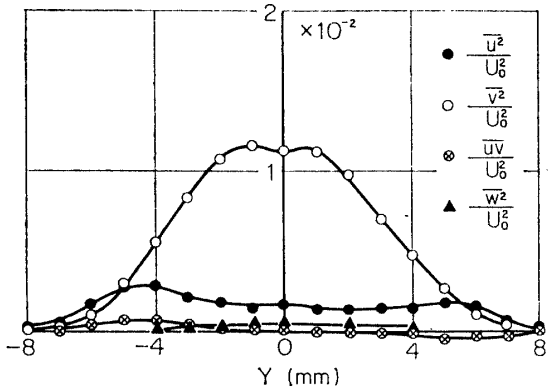

FIG. 3-11. Distributions of $\overline{u^2}$, $\overline{v^2}$, $\overline{w^2}$ and $\overline{uv}$, natural transition, $X=80$ mm.

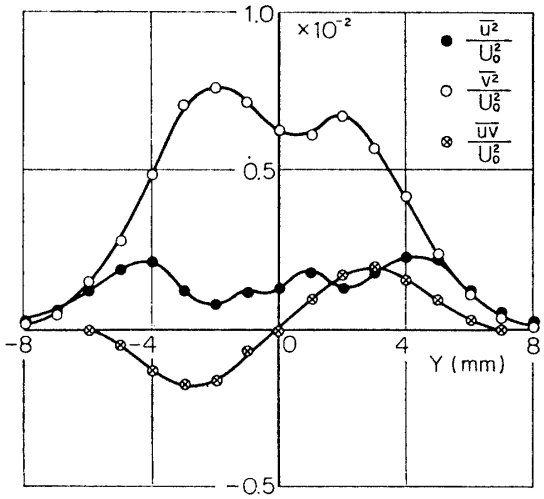

FIG. 3-12. Distributions of $\overline{u^2}$, $\overline{v^2}$ and $\overline{uv}$, natural transition, $X=100$ mm.

Mean-square values of three components $\overline{u^2}$, $\overline{v^2}$, $\overline{w^2}$, and the cross-correlation $\overline{uv}$ are shown in Figs. 3-9~3-16 at eight X-stations. They are all nondimensionalized by the free-stream velocity, U_0^2. Distributions of $\overline{u^2}$ have two peaks at small X ($X=40, 60, 80$ mm) and the intensity decreases from $X=40$ mm downstream. The breadth of the distribution increases in the flow direction monotonically. This is in contrast to the streamwise variation of the breadth of the meanvelocity distribution. At $X=100$ and 120 mm, distributions have four peaks. The distribution of $\overline{u^2}$ at $X=880$ mm has a maximum at $Y=0$. The overall u-fluctration is composed of several spectral components and distribution of $\overline{u^2}$ is made up by the superposition of distributions of various components. In that

This document is provided by JAXA.

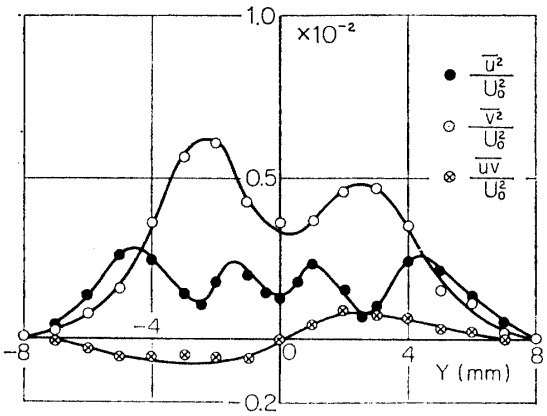

FIG. 3-13. Distributions of $\overline{u^2}$, $\overline{v^2}$ and $\overline{uv}$, natural transition, $X=120$ mm.

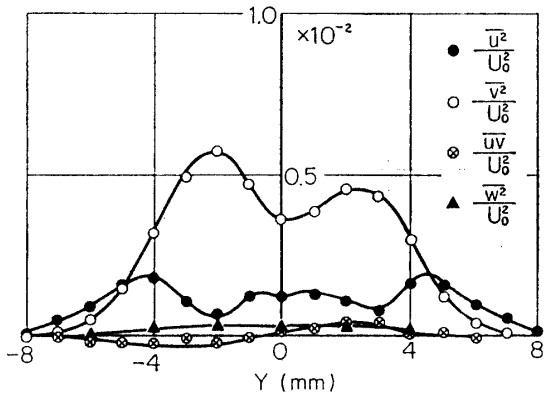

FIG. 3-14. Distributions of $\overline{u^2}$, $\overline{v^2}$, $\overline{w^2}$ and $\overline{uv}$, natural transition, $X=150$ mm.

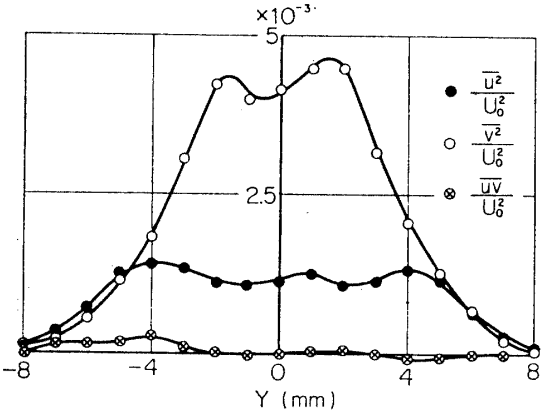

FIG. 3-15. Distributions of $\overline{u^2}$, $\overline{v^2}$ and $\overline{uv}$, natural transition, $X=400$ mm.

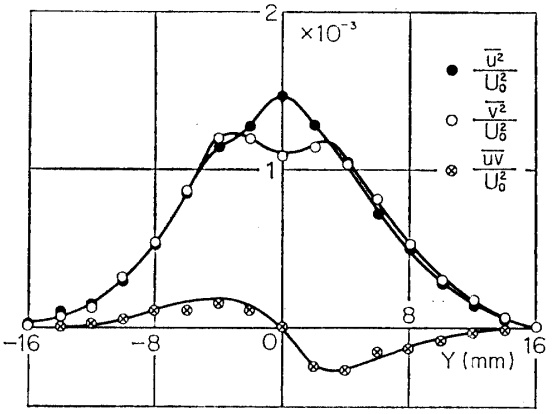

FIG. 3-16. Distributions of $\overline{u^2}$, $\overline{v^2}$ and $\overline{uv}$, natural transition, $X=800$ mm.

sense the distribution of each spectral component is of more fundamental importance. The lateral component, $\overline{v^2}$ is small compared with $\overline{u^2}$ at $X=40$ mm and the distribution has single peak at $Y=0$. At $X=60$ mm, $\overline{v^2}$ is larger than $\overline{u^2}$. At $X=120$ mm, the distribution of $\overline{v^2}$ has two off-centered peaks and at $X=800$ mm, $\overline{u^2}$ and $\overline{v^2}$ are almost equal. Distributions of $\overline{w^2}$ are shown in Figs. 3-9, 3-11 and 3-14. Comparing with other components $\overline{w^2}$ is small but not zero. Measured values of $\overline{w^2}$ might be larger than real ones, because a small misalignment of hot-wires leads to an apparently large value of $\overline{w^2}$.

The behavior of $\overline{uv}$ is peculiar. Since the flow is symmetrical, $\overline{uv}$ is zero on the center-line. At $X=40$ mm and 60 mm, $\overline{uv}$ is negative at $Y>0$, whereas at $X=100$ and 120 mm, the sign is reversed. At $X=800$ mm, $\overline{uv}$ is negative at $Y>0$ again. Experimental results at various X-stations indicate that the negative values of $\overline{uv}$ at $Y>0$ occur at positive $\partial U_c/\partial X$. The role of the Reynolds stress, $-\rho\overline{uv}$ in the momentum equation and the energy balance will be discussed in Section 7.

Figs. 3-17 and 3-18 show distributions of fundamental (630 Hz) and second harmonic (1260 Hz) components of u-fluctuation. Between $X=20$ mm and 150 mm, the amplitude of the fundamental component is almost zero on the

This document is provided by JAXA.

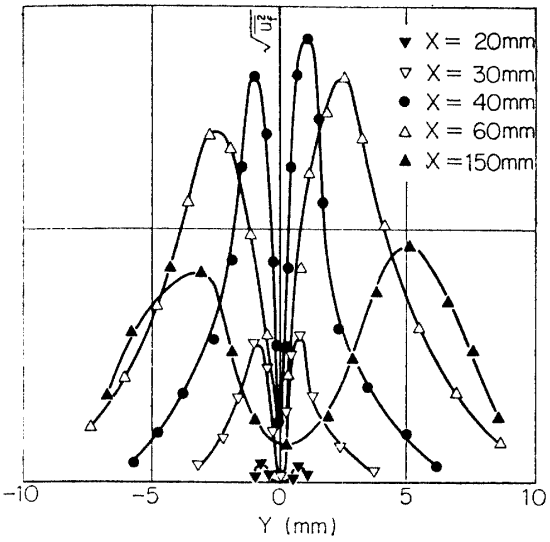

FIG. 3-17. Distribution of root-mean-square of fundamental component (630 Hz) of u-fluctuation, natural transition. Ordinate, arbitrary scale.

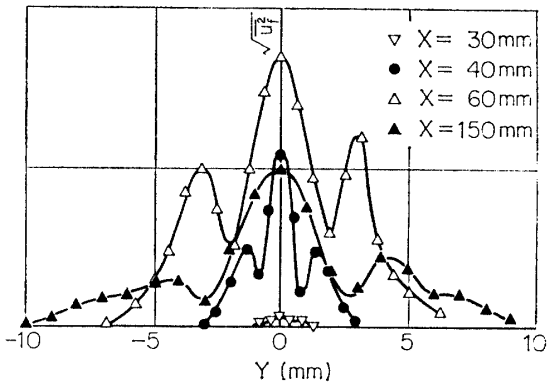

Fig. 3-18. Distribution of root-mean-square of second harmonics (1260 Hz) of u-fluctuation, natural transition. Ordinate, arbitrary scale.

center line and the phase is antisymmetrical, namely, the phase difference at two points symmetrical with respect to the center line is 180 degrees. Distributions of $\overline{u^2}$ in Fig. 3-9 and $\sqrt{\overline{u_f^2}}$ in Fig. 3-17 are similar except at $Y=0$. The slow fluctuation and harmonic components contribute to the finite value of $\overline{u^2}$ at $Y=0$. At $X=150$ mm, the distribution of $\overline{u^2}$ (Fig. 3-14) is rather flat, while there peaks in 630 Hz-component. Tht breadth of the distribution of fundamental component increases downstream monotonically. The second harmonic component has a maximum at $Y=0$ and two off-centered peaks. The phase is symmetrical al with respect to the center line. Distributions at various X-stations are almost similar. The streamwise development of fundamental and harmonic components are not the same and the relative magnitude of two components are different at different X and Y. Therefore, distributions of overall $\overline{u^2}$ are not similar at different X-stations and wave-forms at various points are different.

For v-fluctration, the 630 Hz-component has a maximum amplitude at $Y=0$ and the phase is symmetrical, while the phase of 1260 Hz-component is antisymmetrical.

4. Transition with Sound of Single Frequency

When a sound is introduced, a small-amplitude velocity fluctuation is induced in the wake. If the frequency of the fluctuation is in the unstable zone of the linear stability theory, the fluctuation grows exponentially. If the frequency is not proper, the induced fluctuation does not grow. The effect of the sound on the transition process depends on the intensity of sound. If the intensity is low, the amplitude of the induced velocity fluctuation is smaller than that of residual turbulence in the wind-tunnel and there is no noticeable effect of sound.

This document is provided by JAXA.

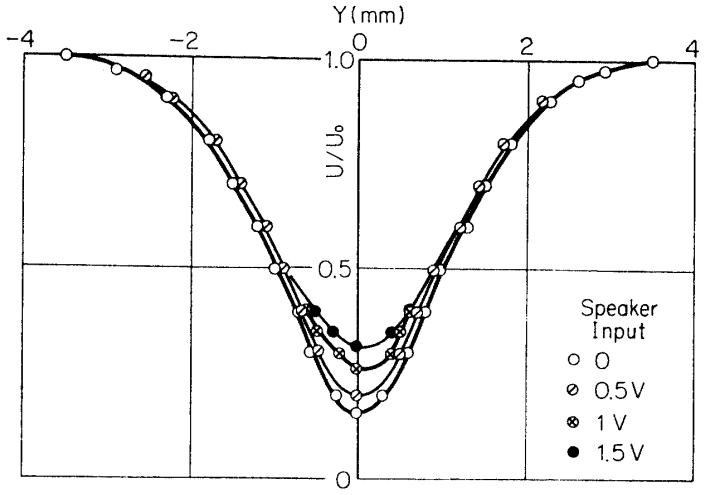

FIG. 4-1. Mean-velocity distribution with and without sound of 630 Hz, $X=20$ mm, $U_0=10$ m/s.

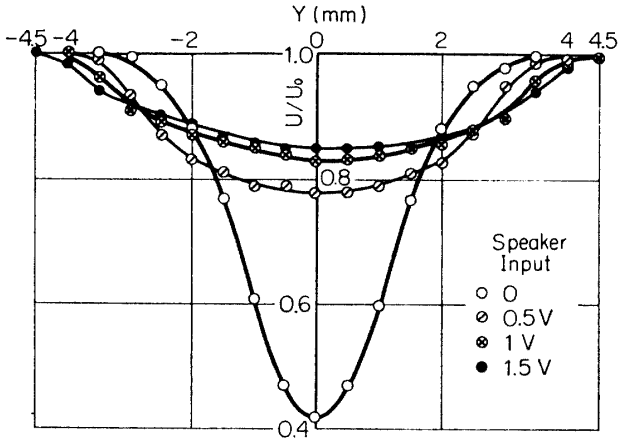

FIG. 4-2. Mean-velocity distribution with and without sound of 630 Hz, $X=40$ mm, $U_0=10$ m/s.

When the sound level exceeds a certain threshold, the effect is distinct. The wave-form of the velocity fluctuation becomes more regular than that in the natural transition. Even in this case, the amplitude of the fluctuation due to sound is still so small that we can observe only when it is amplified.

The effect of sound on the mean-velocity distribution is demonstrated in Figs. 4-1, 4-2, and 4-3 at three X-stations with three sound levels. The input voltage to the loudspeaker shown in those figures is propotional to the sound intensity in the wake. The frequency of sound is 630 Hz. This frequency is the same as that of the natural fluctuation and the fluctuation with the frequency has a large theoretical linear-growthrate. Sound with different frequency has less effect and if the frequency is too high or too low, no effect is observed. The effect on the mean velocity is not observed at $X<20$ mm. At $X=20$ mm, the effect is to increase the velocity on the center-line. The stronger sound has more effect. The breadth of the wake is not affected. Remarkable effects are shown

This document is provided by JAXA.

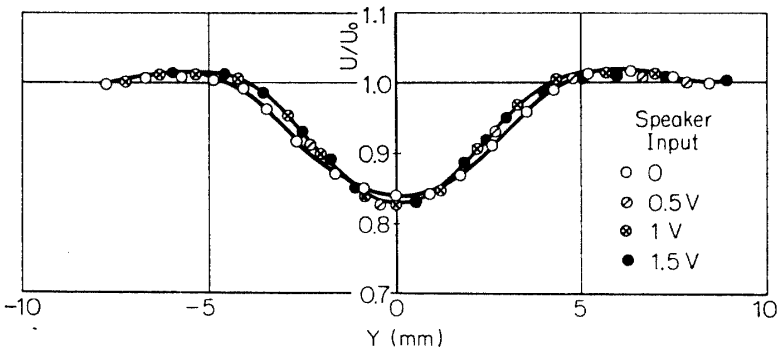

FIG. 4.3. Mean-velocity distribution with and without sound of 630 Hz, $X=150$ mm, $U_0=10$ m/s.

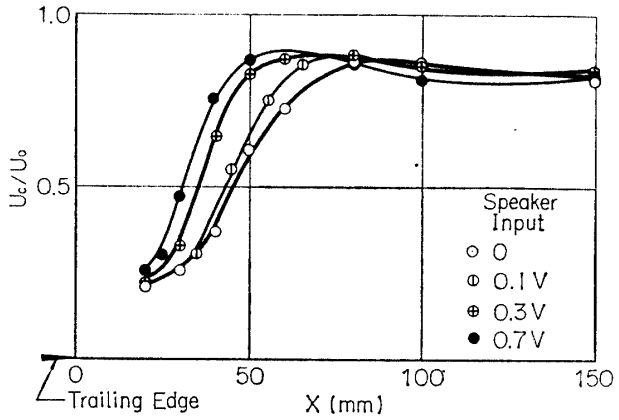

FIG. 4-4. Streamwise variation of velocity on the center line, U_c, with and without sound 630 Hz. $U_0=10$ m/s.

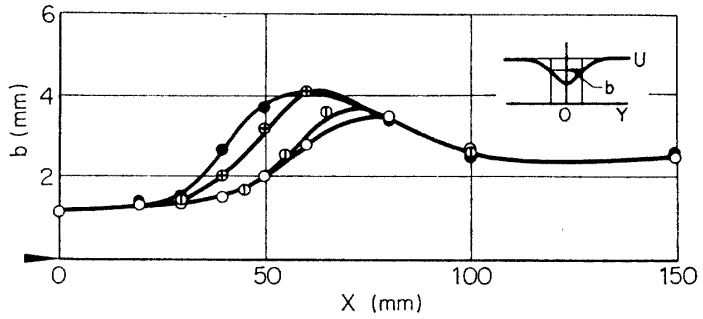

FIG. 4-5. Streamwise variation of half-value breadth, b, with and without sound of 630 Hz. $U_0=10$ m/s. For legend, see figure 4-4.

in Fig. 4-2 ($X=40$ mm). Distributions with and without around are entirely different. Not only the central velocity but also the breadth of the distribution is very much affected. The 0.5 V-sound is very effective and higher sound levels (1 V and 1.5V) do not result in much difference. At X=150 mm (Fig. 4-3) the effect of sound is very small again.

The streamwise variation of tht central velocity U_c is shown in Fig. 4-4 at three sound levels. Between $X=20$ mm and 70 mm U_c increases as the sound

This document is provided by JAXA.

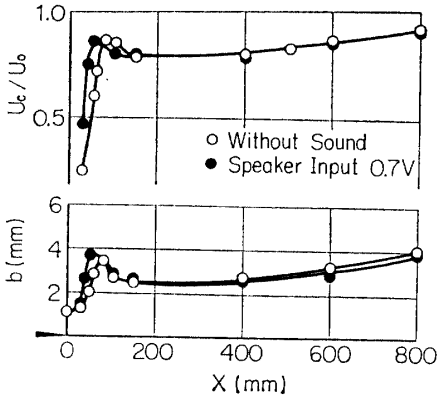

FIG. 4-6. Streamwise variation of velocity on the center line, U_c, and half-value breadth, b, with and without sound of 630 Hz.

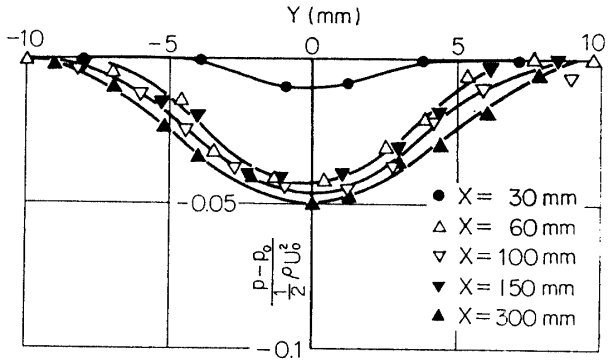

FIG. 4-7. Static-pressure distribution with sound of 630 Hz. p: pressure in wake, p_0: pressure in free stream. U_0=10 m/s.

level is increased. At X=100 mm the effect is reversed, that is, the higher sound level results in the smaller U_c. And at X=150 mm, effects are very small. The effect is localized bttween X=20 mm and 100 mm and the sound, roughly speaking, shifts the X-axis. The variation of the half-breadth, b, is plotted in Fig. 4-5. Here again the increase of b takes place at smaller X for higher sound level. At X=100 mm and 150 mm there are no effects. In Fig. 4-6 U_c and b are plotted in a wider range of X and the effect of sound at large X is shown to be extremely small. The effect of sound on the mean velocity should be indirect. The sound induces velocity fluctuations, and changes in the mean velocity is modified through an interaction with fluctuations.

The distribution of tht static pressure in presence of 630 Hz-sound is shown in Fig. 4-7. The lowest static-pressure coefficient with sound is about −0.05 at X=60 mm in contrast to −0.03 in the natural transition. The low-pressure region starts at X=30 mm. In the natural transition the region starts around X=40 mm. The decrease of the static pressure should be also a result of the nonlinear interaction.

Wave-forms of u-fluctuation in presence of sound are illustrated in Figs. 4-8 and 4-9 with two different sweep speeds. At the top of each column, the wave-form of sound is shown. Both figures indicate that wave-forms of velocity fluctuations at X <500 mm are very regular. The slow irregular wave-form of u near Y=0 observed in the natural transition (Fig. 3-5) is not present in Fig. 4-8. Although harmonics are produced in various fashions, the fluctuation is periodic. At X=500 mm, Y=0 a slow, irregular component appears. At X=800 mm, the wave-form becomes irregular but there are still some periodic components. This is in contrast to the natural transition in which at X=800 mm the fluctuation is entirely turbulent. The randomization is delayed by the presence of sound. The distortion of the wave-form shown in Fig. 4-9 takes place in a complicated manner. The amplitude and phase of harmonic components have different distributions in X- and Y-directions.

This document is provided by JAXA.

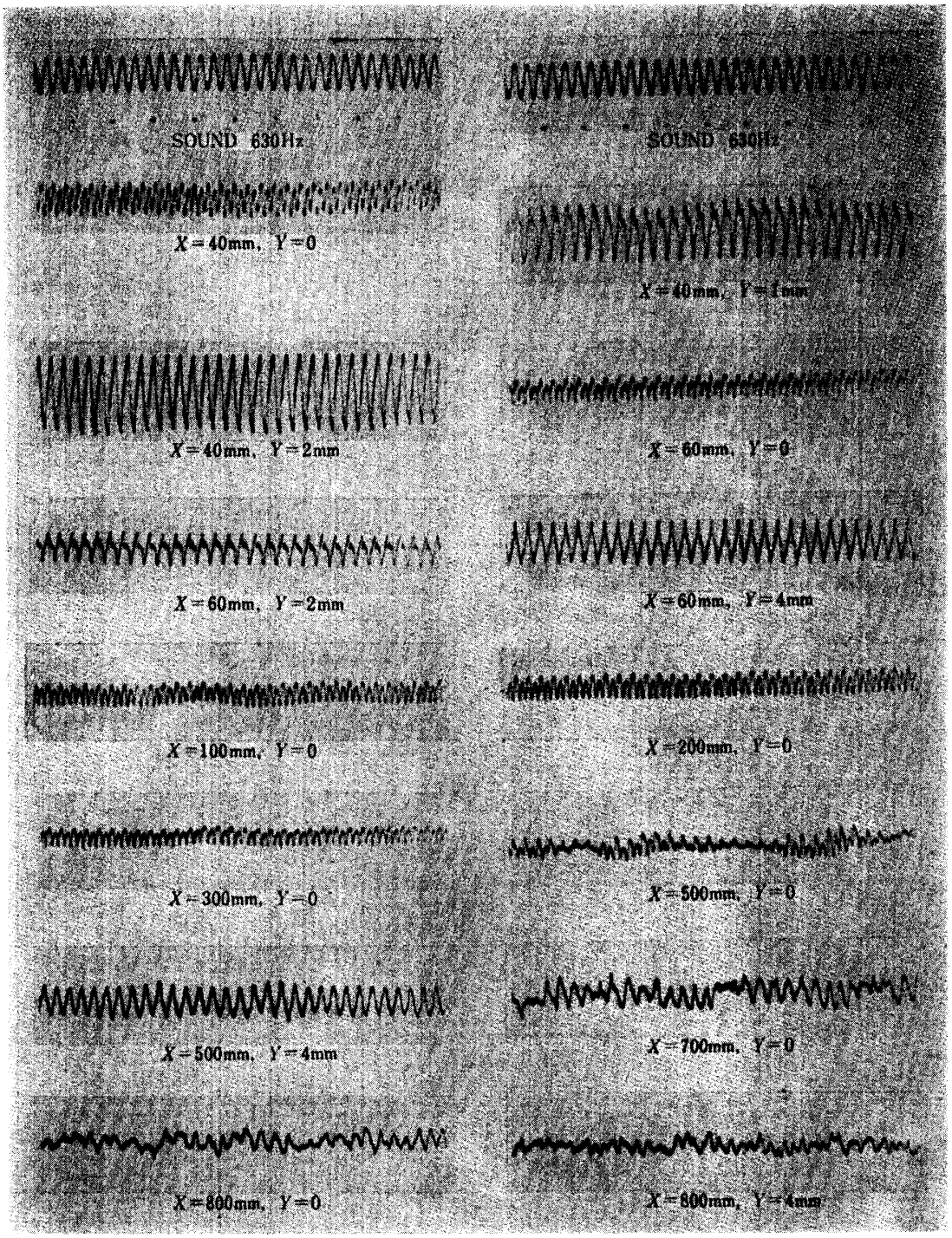

FIG. 4-8. Wave-forms of u-fluctuation with sound of 630 Hz. Time from left to right. Time interval between dots, 5 millisec. Velocity increases upward.

This document is provided by JAXA.

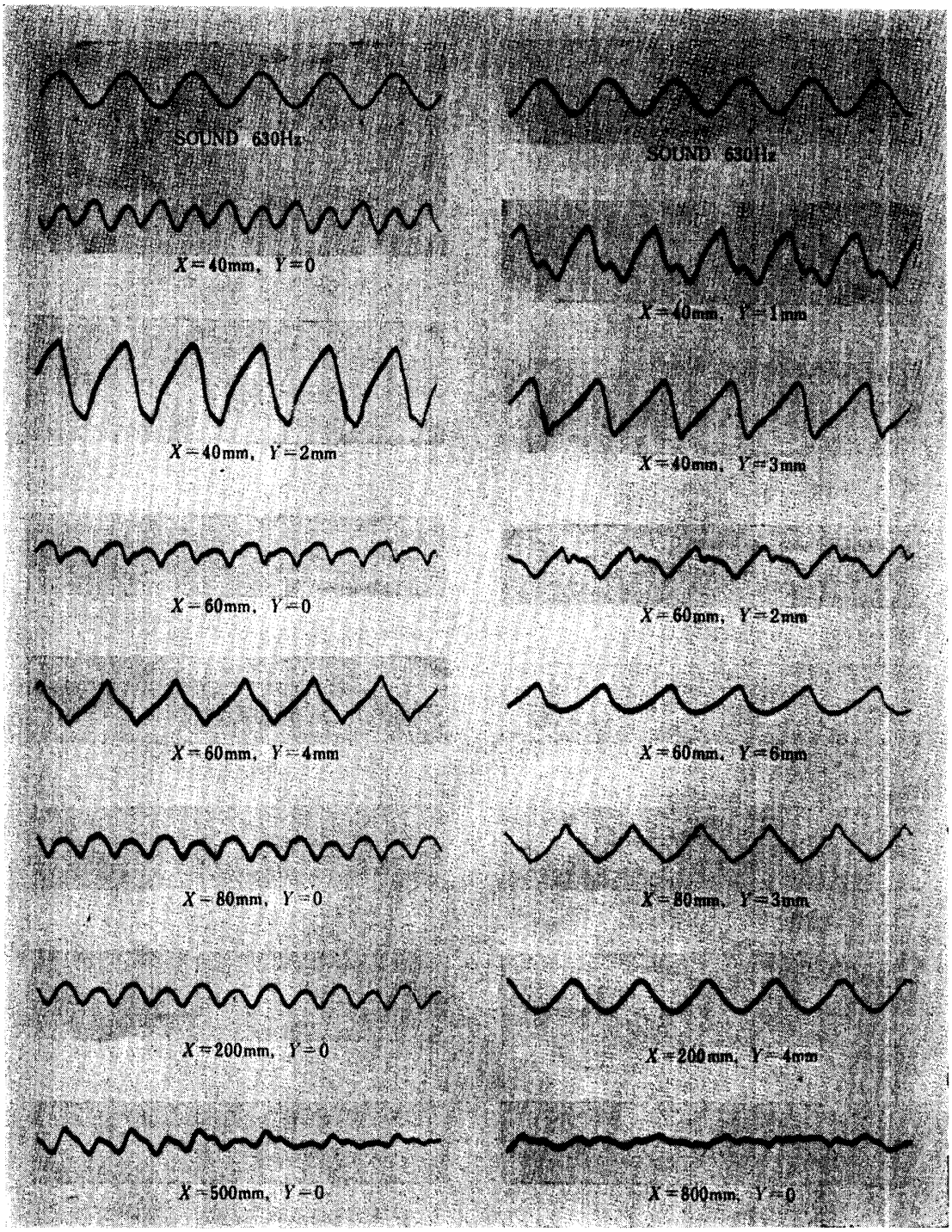

FIG. 4-9. Wave-forms of u-fluctuation with sound of 630 Hz. Time interval between dots, 1 millisec.

This document is provided by JAXA.

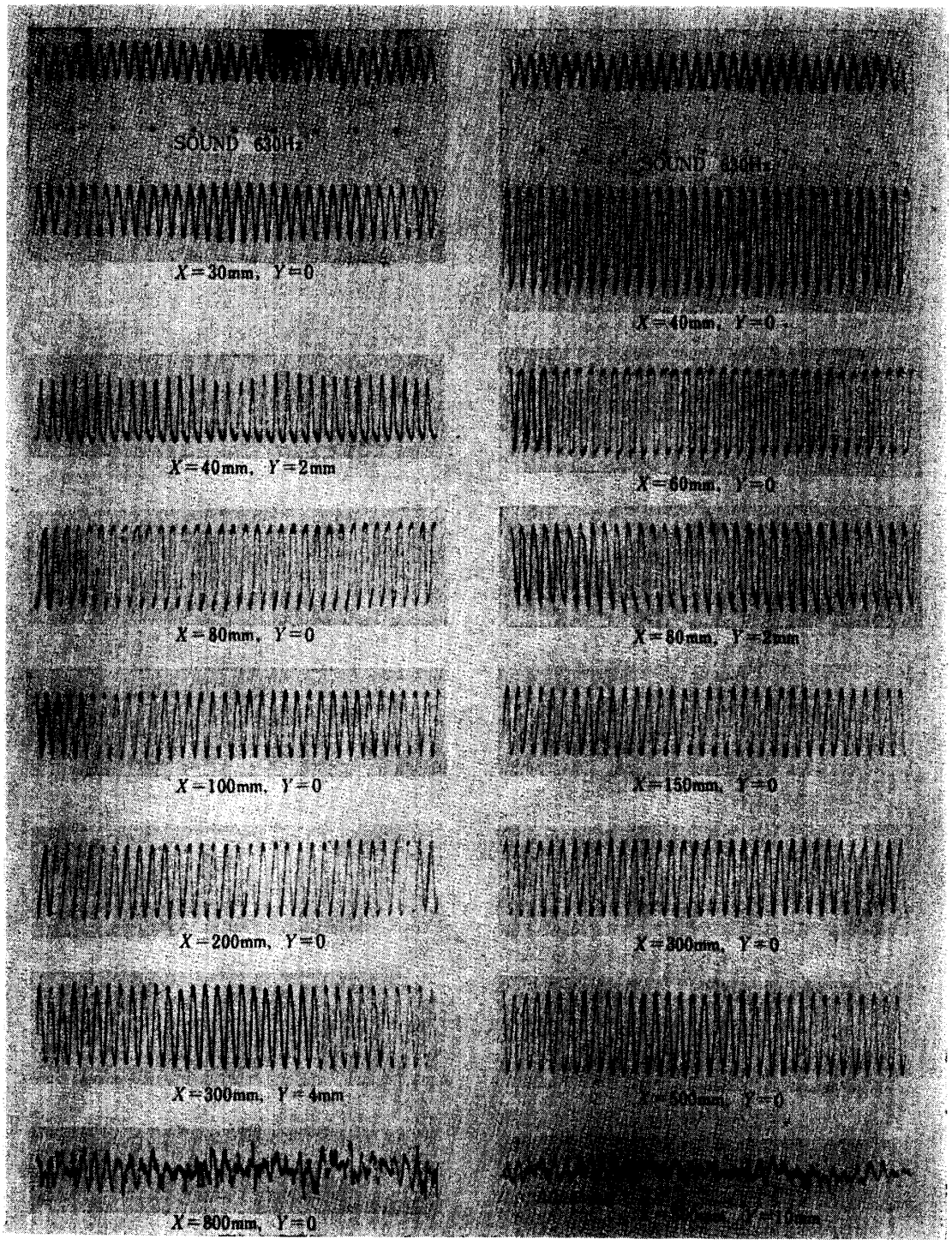

FIG. 4-10. Wave-forms of v-fluctuation with sound of 630 Hz. Time interval between dots, 5 millisec.

This document is provided by JAXA.

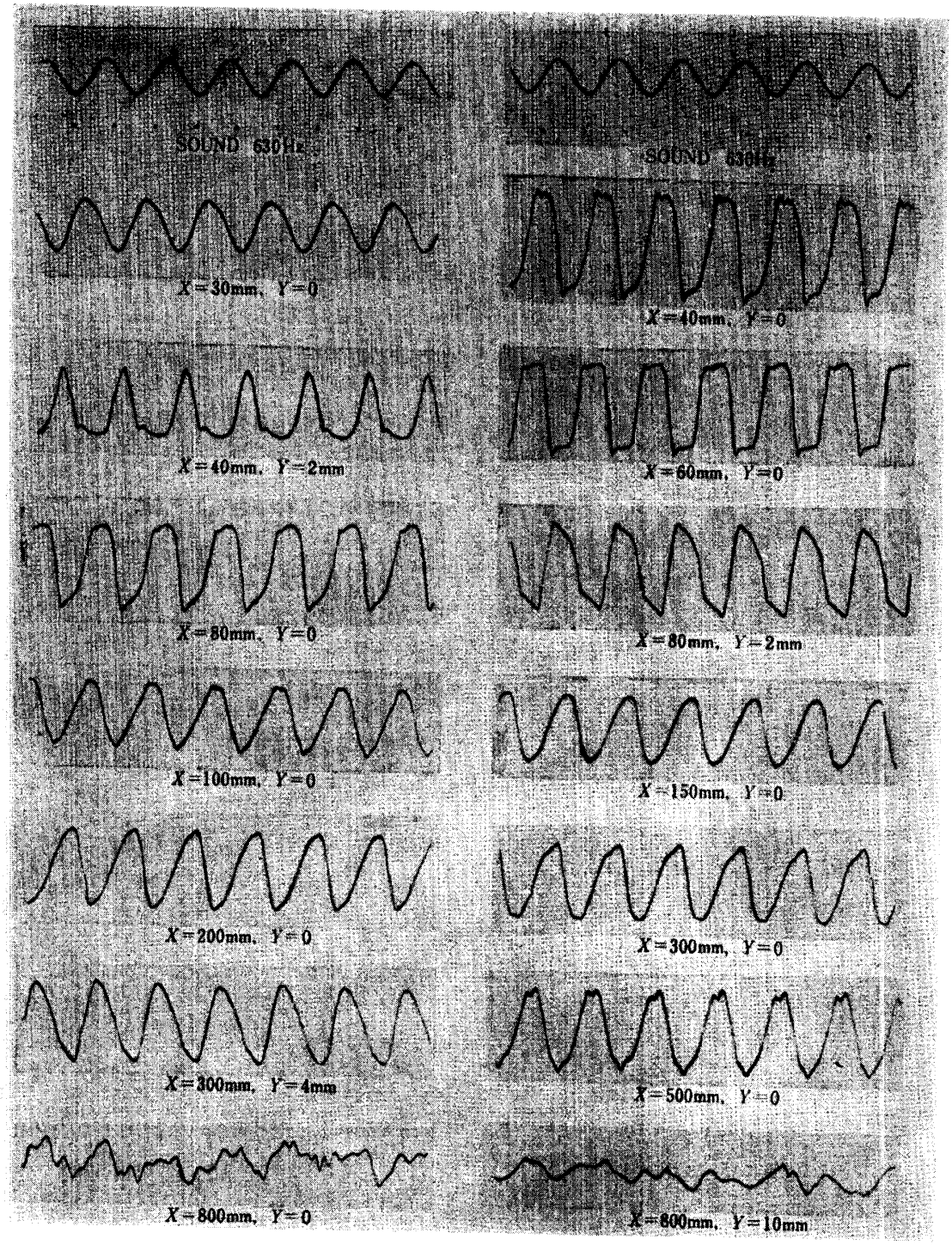

FIG. 4-11. Wave-forms of v-fluctuaton with sound of 630 Hz. Time interval between dots, 1 millisec.

This document is provided by JAXA.

In Figs. 4-10 and 4-11 wave-forms of v-fluctuation are shown. They are regular and periodic until $X=500$ mm. No slow, irregular fluctuations are found in Fig. 4-10. This lack of low-frequency component in v-fluctuation coincides with that in the natural transition. Distortions of 630 Hz-component in u- and v-fluctuations are different. Wave-forms of u (Fig. 4-9) are almost triangular and those of v (Fig. 4-11) are like square waves. This difference exists also in the natural transition (Fig. 3-6 and 3-8).

The effect of sound on the amplitude of u-fluctuation is illustrated in Figs. 4-12, and 4-13. At $X=40$ mm, $\sqrt{\overline{u^2}}$ at large Y is larger in presence of sound. Values at two off-centered peaks are maximum at the speaker input of 0.3 V, not at the maximum sound intensity. At $Y=0$, $\sqrt{\overline{u^2}}$ with the highest sound level is the

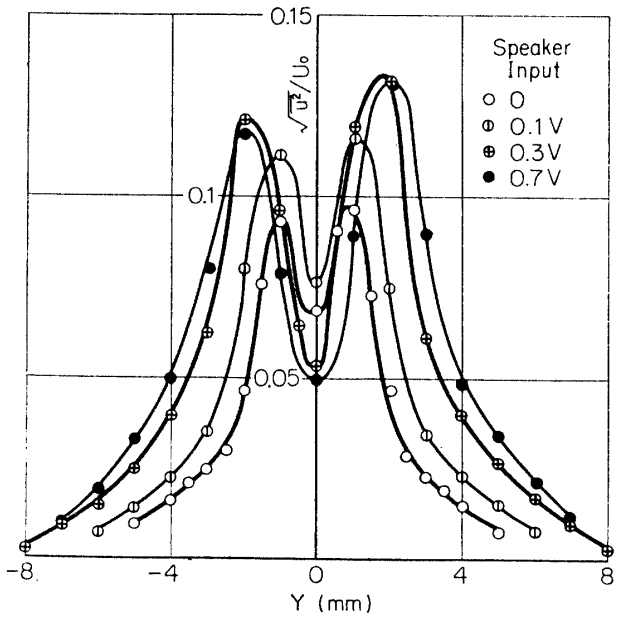

FIG. 4-12. Distribution of root-mean-square of u-fluctuation with and without sound of 630 Hz, $X=40$ mm.

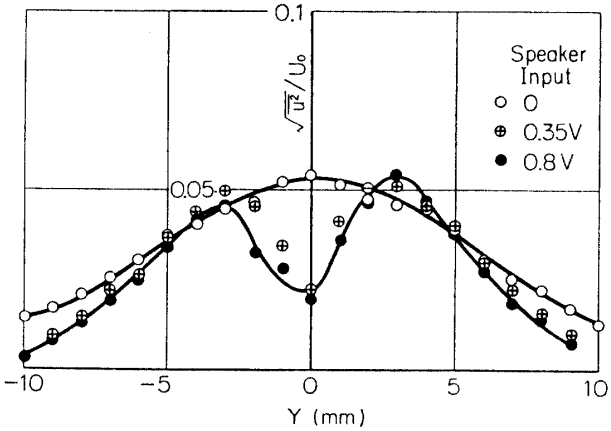

FIG. 4-13. Distribution of root-mean-square of u-fluctuation with and without sound of 630 Hz, $X=600$ mm.

This document is provided by JAXA.

smallest. These facts might be due to the difference in the streamwise development of $\sqrt{\overline{u^2}}$ for different sound levels. For higher sound level, the maximum value in the streamwise variation of $\sqrt{\overline{u^2}}$ might occur at smaller X. The apparent decrease of $\sqrt{\overline{u^2}}$ at $X=40$ mm is due to the fact that the maximum of $\sqrt{\overline{u^2}}$ occurs at X smaller than 40 mm. At $X=600$ mm (Fig. 4-13) the effect of sound is not to increase the fluctuation amplitude but to change the distribution. Experimental results indicate that the dip at $Y=0$ in the distribution of $\sqrt{\overline{u^2}}$ at $X=40$ mm persists until $X=600$ mm in presence of sound. The distribution with a dip at $Y=0$ is typical for the spectral component of 630 Hz. Wave-forms of u-fluctuation indicate that the 630 Hz-component still exists at $X=600$ mm. On the other hand, in the natural transition the distribution of $\sqrt{\overline{u^2}}$ is flat. It suggests that the 630 Hz-component is no more predominant.

Figs. 4-14 and 4-15 show distributions of $\sqrt{\overline{u^2}}$ at various X-stations for two loudspeaker inputs, 0.1 V and 0.7 V, respectively. At $X=25$ mm $\sqrt{\overline{u^2}}$ with 0.1 V sound (Fig. 4-14) is smaller than that with 0.7 V sound (Fig. 4-15) but distributions are similar. The dip at $Y=0$ for higher sound level is more pronounced. The maximum value of $\sqrt{\overline{u^2}}$ occurs at $X=45$ mm for 0.1 V sound and at $X=30$ mm for 0.7 V sound. We find again that the sound shifts the X-axis. The 630 Hz-component of u-fluctuation is antisymmetrical ard vanishes at $Y=0$. The finite value of $\sqrt{\overline{u^2}}$ at $Y=0$ is mainly due to the second harmonics, 1260 Hz-component, which has a maximum value on the center line.

Distributions of $\overline{u^2}$, $\overline{v^2}$ and $\overline{uv}$ at various X-stations are shown in Figs. 4-16～4-21. At $X=40$ mm, the distribution of $\overline{u^2}/U_0^2$ has two off-centered peaks, whereas that of $\overline{v^2}/U_0^2$ has one maximum on the center-line. The peak value of $\overline{u^2}$ is larger than that of $\overline{v^2}$. The distribution of $\overline{uv}$ is antisymmetrical with respect to the center

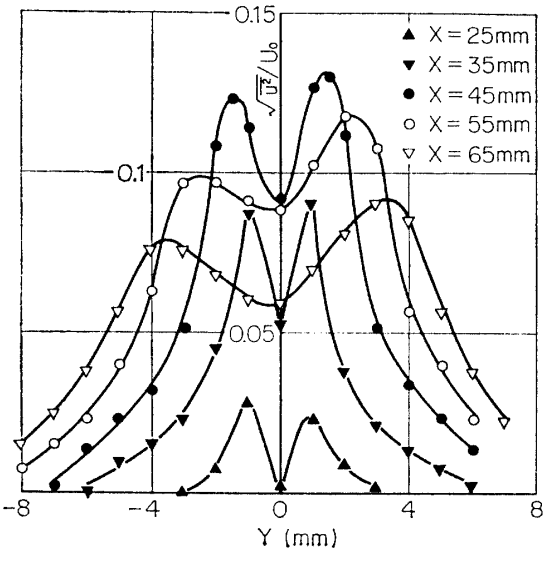

FIG. 4-14. Distribution of root-mean-square of u-fluctuation with sound of 630 Hz. Input to loudspeaker, 0.1 V.

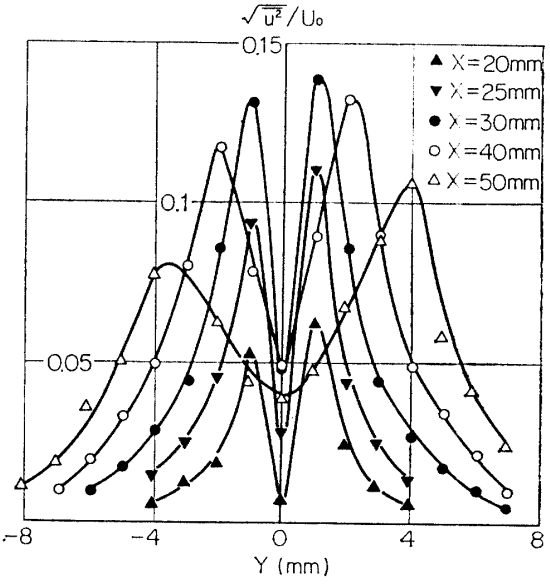

FIG. 4-15. Distribution of root-mean-square of u-fluctuation with sound of 630 Hz. Input to loudspeaker, 0.7 V.

This document is provided by JAXA.

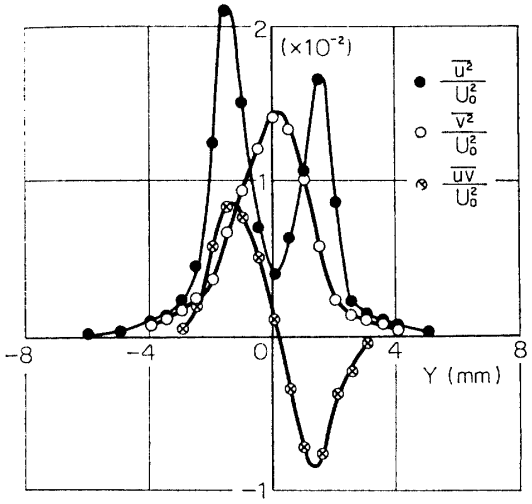

FIG. 4-16. Distributions of $\overline{u^2}$, $\overline{v^2}$ and $\overline{uv}$ with sound of 630 Hz. X=40 mm.

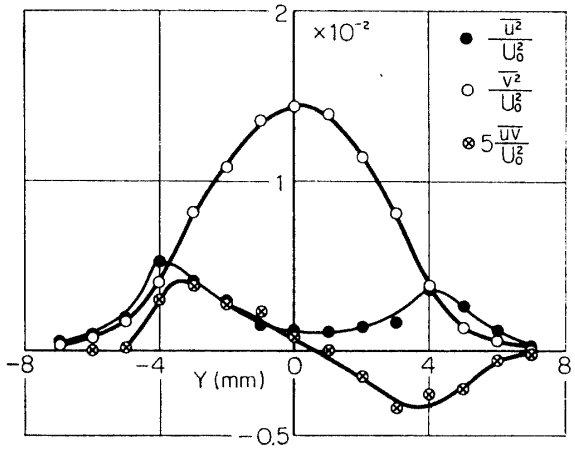

FIG. 4-17. Distributions of $\overline{u^2}$, $\overline{v^2}$ and $\overline{uv}$ with sound of 630 Hz. X=60 mm.

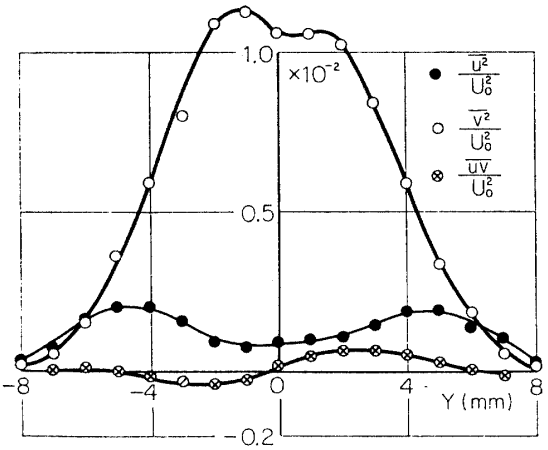

FIG. 4-18. Distributions of $\overline{u^2}$, $\overline{v^2}$ and $\overline{uv}$ with sound of 630 Hz. X=80 mm.

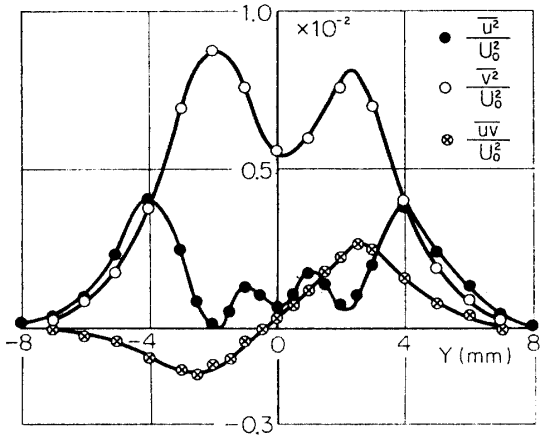

FIG. 4-19. Distributions of $\overline{u^2}$, $\overline{v^2}$ and $\overline{uv}$ with sound of 630 Hz. X=100 mm.

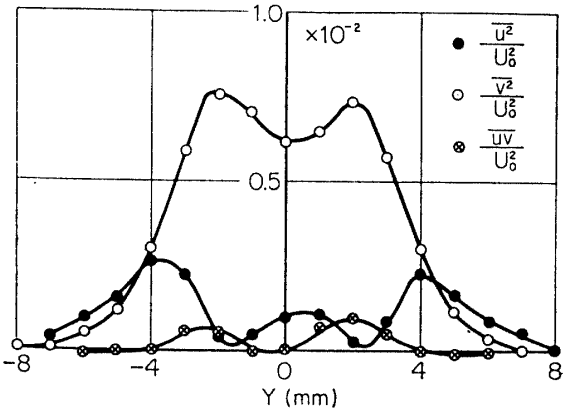

FIG. 4-20. Distributions of $\overline{u^2}$, $\overline{v^2}$ and $\overline{uv}$ with sound of 630 Hz. X=150 mm.

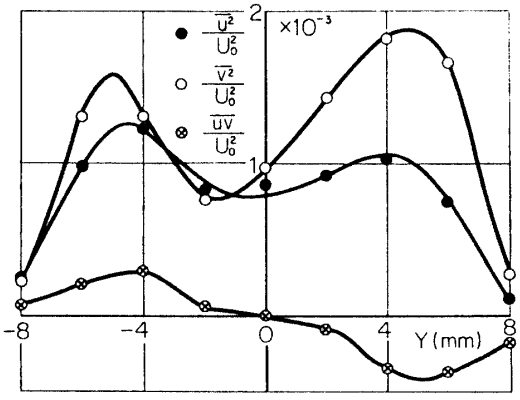

FIG. 4-21. Distributions of $\overline{u^2}$, $\overline{v^2}$ and $\overline{uv}$ with sound of 630 Hz. X=800 mm.

This document is provided by JAXA.

line, and is negative at $Y>0$. At $X=60$ mm (Fig. 4-17), $\overline{v^2}$ is much larger than $\overline{u^2}$ and $\overline{uv}$ is smaller than that at $X=40$ mm. At $X=80$ mm, $\overline{u^2}$ is much smaller than $\overline{v^2}$ and the sign of $\overline{uv}$ is reversed. From $X=40$ mm to 80 mm, $\overline{v^2}$ decreases only a little whereas $\overline{u^2}$ decays down to 10 percent. At $X=100$ mm, the distribution of $\overline{u^2}$ has four peaks and that of $\overline{v^2}$ shows a minimum at $Y=0$. These streamwise variations of various statistical quantities are similar to those in the natural transition. The production of fluctuation energy is given by $-\rho\overline{uv}\,\partial U/\partial y$. It is positive between $X=40$ mm and 60 mm and negative between $X=80$ mm and 100 mm. At $X=150$ mm the production is very small and at $X=800$ mm it is slightly positive again.

5. Transition with Sound of Two Frequencies

The interaction of two velocity fluctuations in the wake can be investigated by introducing two sounds and inducing two fluctuations. If frequencies of both sounds are properly chosen, both fluctuations may grow independently as long as amplitudes are small. When amplitudes of two fluctuations reach certain values, they will interact each other. In the present experimental conditions, the frequency of the natural, selfinduced fluctuation is 630 Hz and the frequency of first sound was chosen to be the same frequency. The frequency of the second sound was varied from 400 Hz to 900 Hz. The effect of the second fluctuation on the first was observed by recording the r. m. s. of 630 Hz-component while the frequency of second sound was changed. Results with various levels of second sound are shown in Fig. 5-1. The input of the first sound to the loudspeaker was fixed at 0.5 V and the input of second sound,

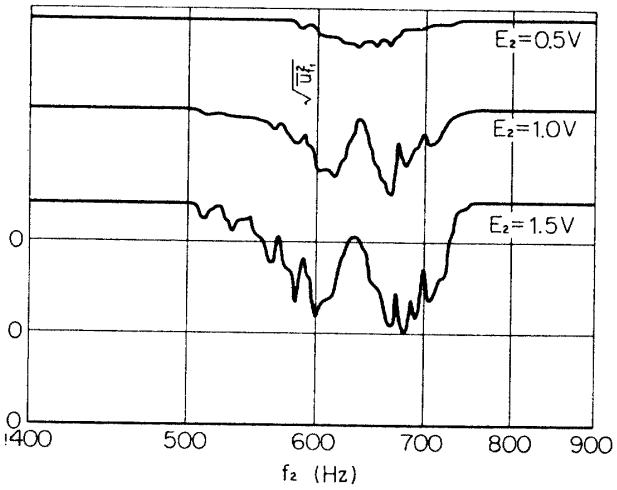

Fig. 5-1. Root-mean-square value of 630 Hz-component, $\sqrt{\overline{u^2_{f_1}}}$, with second sound of various frequencies. $X=40$ mm, $Y=2$ mm, $U_0=10$ m/s.
First sound: frequency, $f_1=630$ Hz and input voltage $E_1=0.5$ V.
Second sound: frequency, f_2 and input voltage E_2.

This document is provided by JAXA.

E_2 was changed from 0.5 to 1.5 V. Actually, two "sounds" were mixed in the electrical circuit before they were fed to the loudspeaker and we created one sound with two frequencies. But for smplicity, we may describe, as if there are two sounds in the test-section.

The amplitude of the 630 Hz-velocity-fluctuation decreases when the second sound is present. This fact was already described in reference 5 as the "suppression effect". When the level of the second sound is 0.5 V, the effect exists in the frequency range of second sound between 580 and 720 Hz. At the second sound of 630 Hz, there is actually one sound. The r. m. s. of 630 Hz-component decreases, because of the increased sound level of that frequency. With second sound of 1.5 V, the nonlinear interaction is more pronounced and the second sound between 500 and 750 Hz is effective. In this frequency range the induced velocity fluctuation has an appreciable linear growth-rate. Outside this range the growth rate is small and the induced velocity fluctuation may not attain enough amplitude for the nonlinear interaction with the first fluctuation. Small peaks and valleys in Fig. 5-1 may be resulted from the resonance of sound in the test-section.

Detailed measurements of the nonlinear interaction were made with the first and second sound of the frequency, 630 Hz and 700 Hz, respectively. Experimental results at different frequencies were almost the same. The nature of the nonlinear interaction depends heavily on the relative amplitudes of two fluctuations. In the present experiment, two amplitudes were made equal. Since growth rates of two

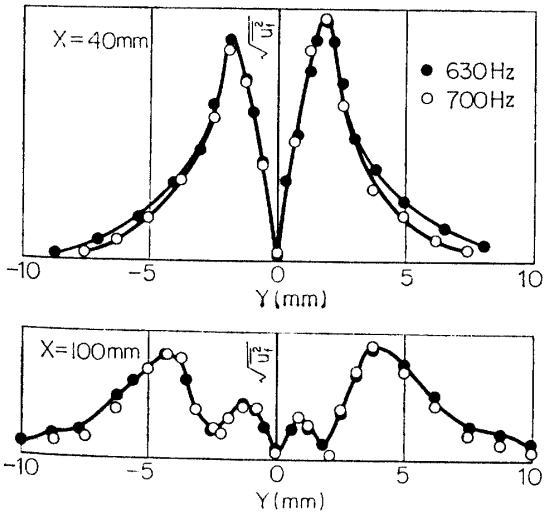

FIG. 5-2. Distributions of root-mean-square values of 630 Hz- and 700 Hz-fluctuation with sound of single frequency. Ordinate scale is arbitrary. X=4mm and 100mm.

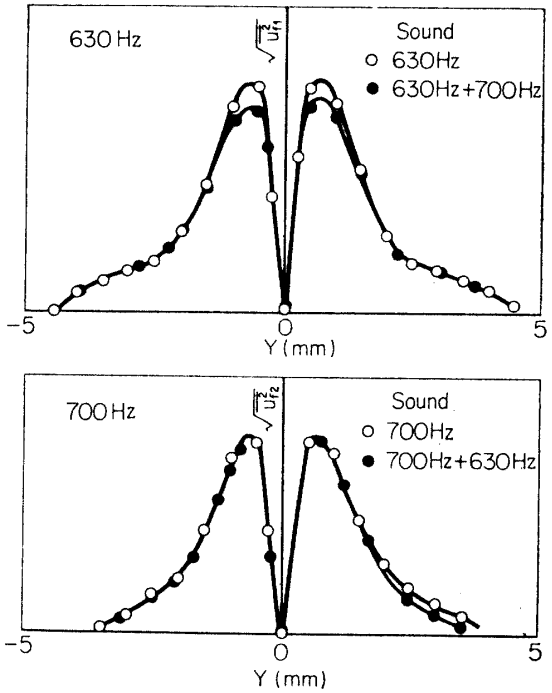

FIG. 5-3. Distributions of root-mean-square of 630 Hz-, $\sqrt{\overline{u_{f_1}^2}}$, and 700 Hz-fluctuation, $\sqrt{\overline{u_{f_2}^2}}$, with sound of single frequency and two frequencies. X=20 mm.

This document is provided by JAXA.

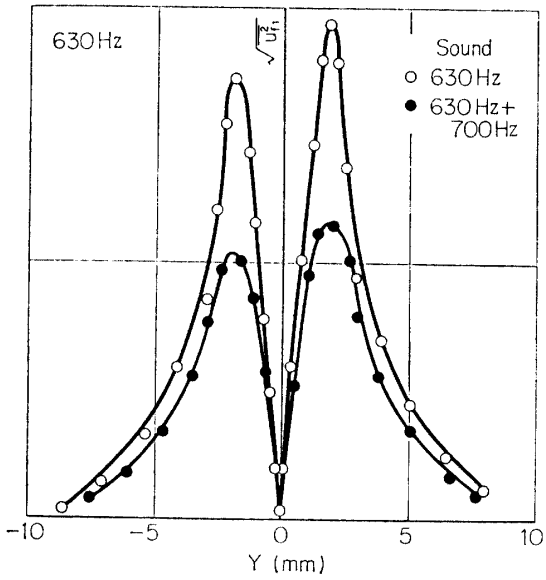

FIG. 5-4. Distribution of root-mean-square of 630 Hz-fluctuation with sound of single frequency (630 Hz) and two frequencies (630 Hz+700 Hz). $X=40$ mm. Ordinate scale is arbitrary.

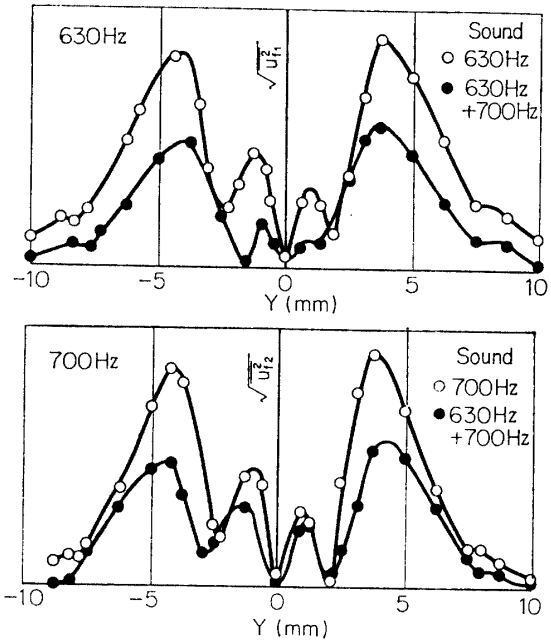

FIG. 5-5. Distributions of root-mean-squares of 630 Hz-, $\sqrt{\overline{u_{f_1}^2}}$, and 700 Hz-fluctuation, $\sqrt{\overline{u_{f_2}^2}}$, with sound of single frequency and two frequencies. $X=100$ mm.

components in the linear region are different, levels of two sounds have to be adjusted so that amplitudes of two velocity fluctuations were equal. Before introducing two sounds, the nature of each velocity fluctuation was observed in presence of single sound. Fig. 5-2 is an example of the distribution of amplitude of each component at various X-stations. The ordinate is arbitrary but relative magnitudes of two components are expressed correctly. Distributions in Y-direction and streamwise variations of two components are very much alike.

When two sounds are introduced, two velocity fluctuations interact each other and the amplitudes of fluctuations are modified as shown in Figs. 5-3, 5-4 and 5-5. Distributions in the absence and in the presence of the other component are compared in those figures. At $X=20$ mm (Fig. 5-3) the interaction of both components (630 Hz and 700 Hz) is very small. This means this X-station is in the linear region and both components grow almost independently. At $X=40$ mm (Fig. 5-4) on the other hand, the 630 Hz-component is suppressed by the presence of the 700 Hz-component. The same is true for 700 Hz-component. At this X-station, distributions are still similar to the one in the linear region (e.g. at $X=20$ mm). At $X=100$ mm, the distribution has four peaks (Fig. 5-5) and there is a distinct mutual interaction. The amplitude is reduced to about 60 percent of the original value. Experimental results at various X-stations indicate that the reduction of the amplitude is mutual and equal in amount for both fluctuations when the starting amplitudes of the two are the same.

This document is provided by JAXA.

The mean-velocity distribution is not modified much by the addition of the second sound. Streamwise variations of the central velocity, U_c, and the half breadth, b, are shown in Figs. 5-6, 5-7 and 5-8 with two sounds U: reaches a maximum. At about $X=300$ mm, U_c is a minimum and increases downstream. The at $X=50$ mm. value of U_c at small X is close to that with single sound. At large X, U_c is closer to that of natural transition (Fig. 5-8). The variation of

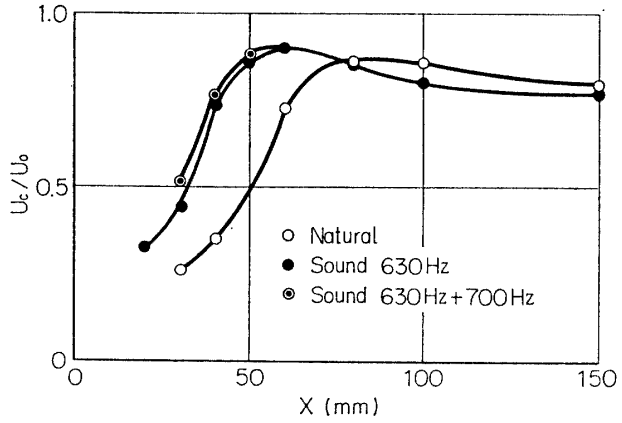

FIG. 5-6. Streamwise variation of velocity on the center line, U_c, in three cases. $U_0=10$ m/s.

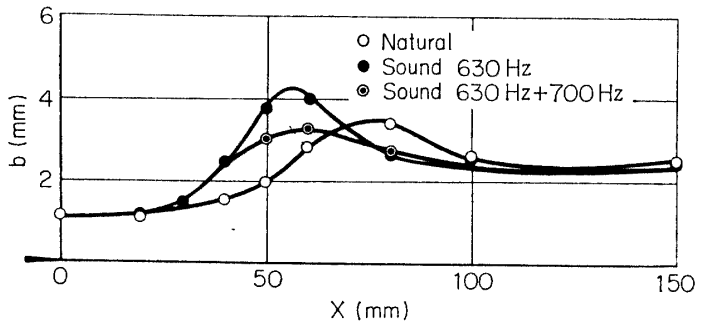

FIG. 5-7. Streamwise variation of half-value breadth, b, in three cases. $U_0=10$ m/s.

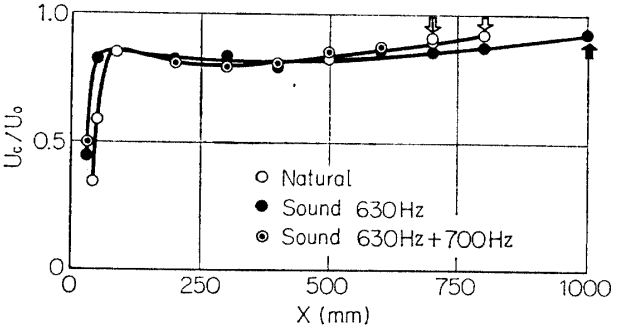

FIG. 5-8. Streamwise variation of velocity on the center line, U_c in three cases. $U_0=100$ m/s. Arrows indicate X-stations where wave-forms of velocity fluctuations become random.

This document is provided by JAXA.

b at small X shows a difference from both natural and single-sound cases. An abrupt increase in U_c or b is an indication of the onset of the nonlinear interaction. It takes place at around $X=30$ mm.

The distribution of the static pressure with two sounds, is almost the same as that with single sound. The negative pressure on the centerline is at most 5 percent of the dynamic pressure of the free stream.

Wave-forms of velocity fluctuations are illustrated in Figs. 5-9~5-12. At the top of each column the wave-form of sound is shown. The sound has a beat of 70 Hz (=700 Hz−630 Hz) but this does not mean the presence of 70 Hz-sound. The beat is a result of the linear superposition. The wave-form of u-fluctuation at $X=20$ mm, $Y=0$ (Fig. 5-9) consists of 70 Hz-component and fluctuations with much higher frequencies. At $X=30$ mm, $Y=0$ the 70 Hz-component is a little distorted, round at the top and spiky at the bottom. This suggests the existence of harmonics of 70 Hz-component. At $Y=1$ mm and 2 mm on the same X-station wave-forms are entirely different. The frequency of highfrequency component at $Y=0$ is around 1300 Hz. At $Y\neq 0$ the frequency is about 650 Hz. At $X=40$ mm, $Y=0$ the 70 Hz component is like a pulse train and at $Y\neq 0$ wave-forms are very much different. At $X=60$ mm, $Y=0$ the 70 Hz-component is like a saw-tooth wave and this regular form is distorted at larger X. At $X=200$ mm, $Y=0$ the saw-tooth wave is no longer regular. Irregularities appear especially at the top of the wave-form (large value of u). At $X=500$ mm, $Y=0$ saw-teeth have all disintegrated. At $X=800$ mm wave-forms are irregular and random. These various wave-forms at various points in the wake indicate that by several spectral components with different distributions and streamwise developments are superposed.

Details of high-frequency components are shown in Fig. 5-10. Fundamental components (630 Hz and 700 Hz) are distorted in various fashions and no systematic description is possible on the change of wave-forms.

Wave-froms of v-fluctuation show considerable differences. Apparently, at $X=30$ mm, $Y=0$ (Fig. 5-11) there is 70 Hz-component but actually, the component is just a beat. A spectral analysis revealed that the 70 Hz-component in v-fluctuation is extremely small. In the wave-form at $Y\neq 0$, we observe 630 Hz- and 700 Hz-components and no harmonics. This is another contrast to the u-fluctuation. At larger X the apparent 70 Hz-component is less and fundamental components are distorted (for instance at, $X=60$ mm, $Y=2$ mm). The wave-form is quite regular until $X=500$ mm and suddenly becomes turbulent at $X=800$ mm. This is another difference from the u-fluctuation. The wave-from of v at $X=500$ mm is more regular than u. These differences seem to be essential in the transition process. A detailed discussion on this point will be made in Section 8. Fig. 5-12 with a faster sweep speed shows details of high-frequency components. Generally speaking, wave-forms in the figure are alike to those in Fig. 4-11 with single sound.

The effect of two sounds on the intensity of u-fluctuation is shown in Figs. 5-13,

This document is provided by JAXA.

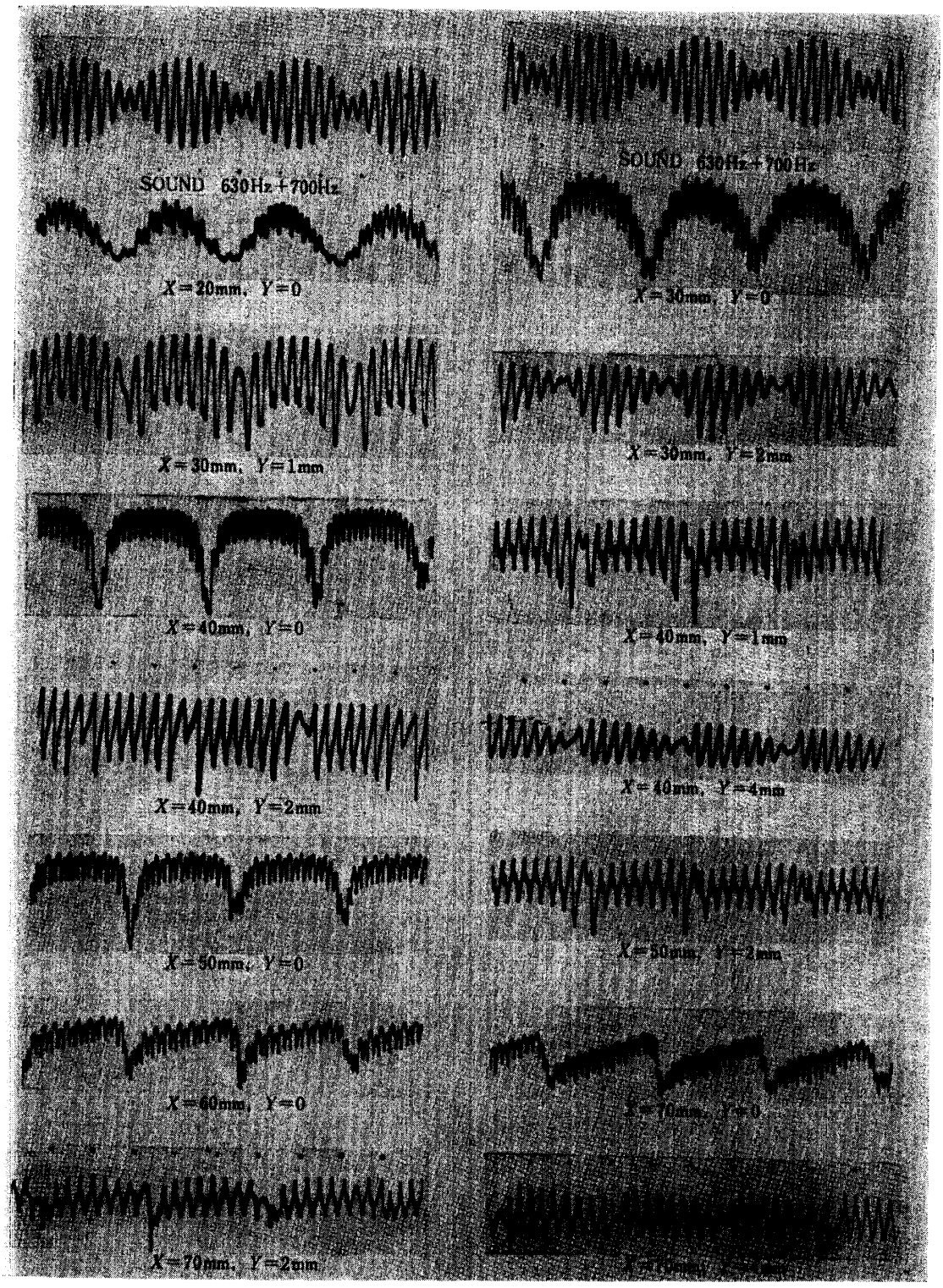

FIG. 5-9(1). Wave-forms of u-fluctuation with sound of 630 Hz and 700 Hz. Velocity increases upward. This from left to right. Time interval between dots, 5 millisec.

This document is provided by JAXA.

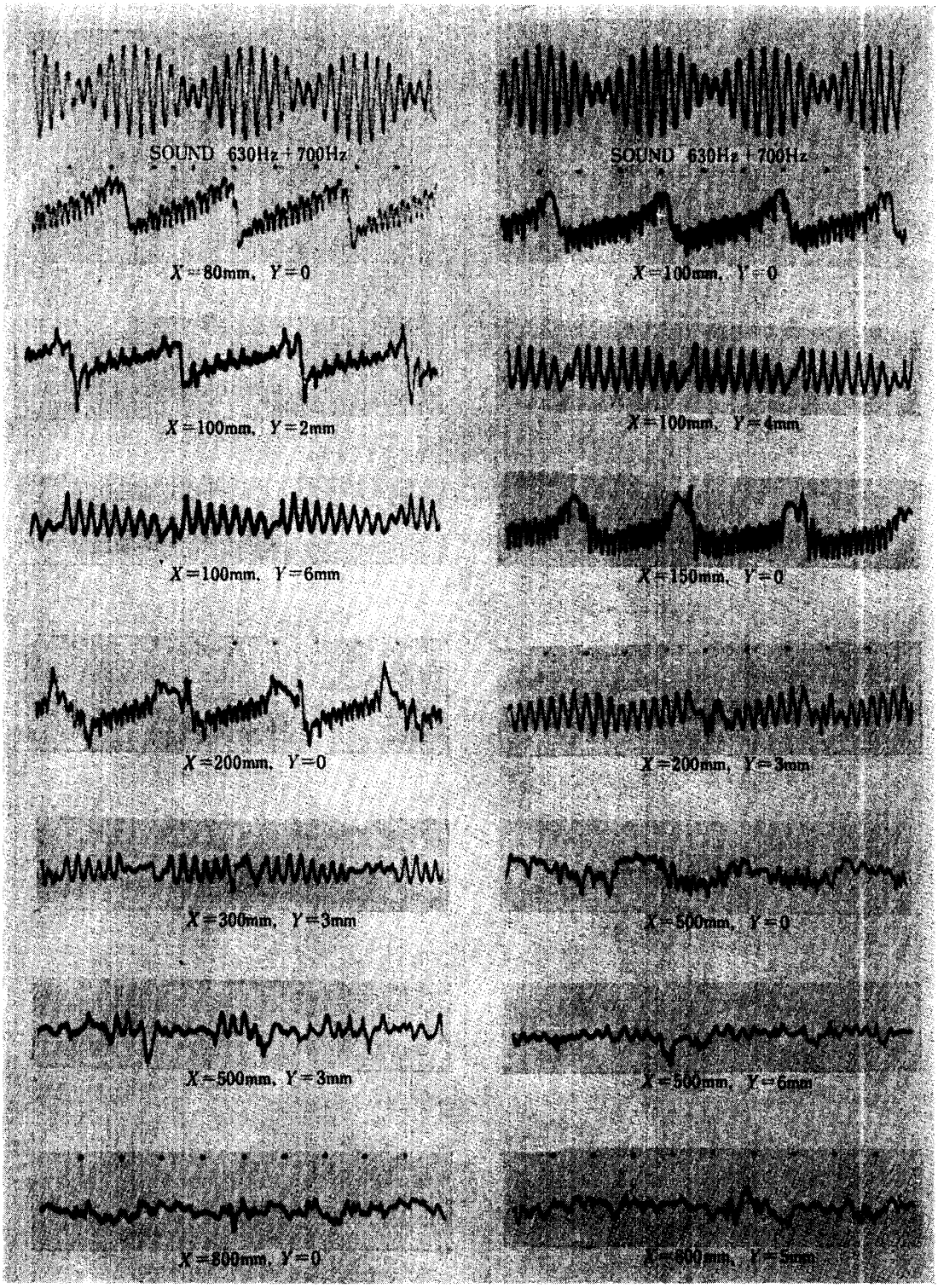

FIG. 5-9(2).

This document is provided by JAXA.

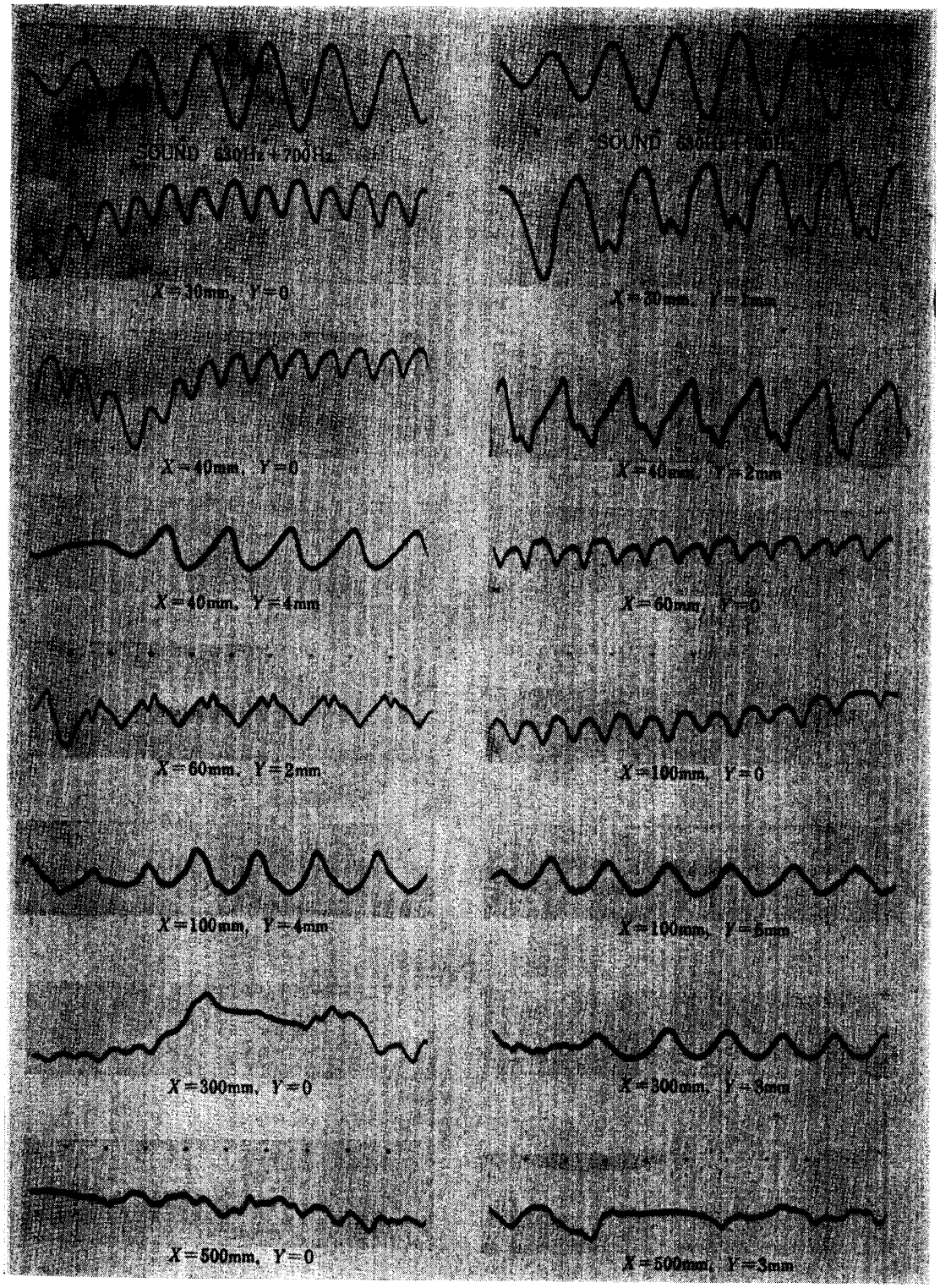

FIG. 5-10. Wave-forms of u-fluctuation with sound of 630 Hz and 700 Hz. Time interval between dots, 1 millisec.

This document is provided by JAXA.

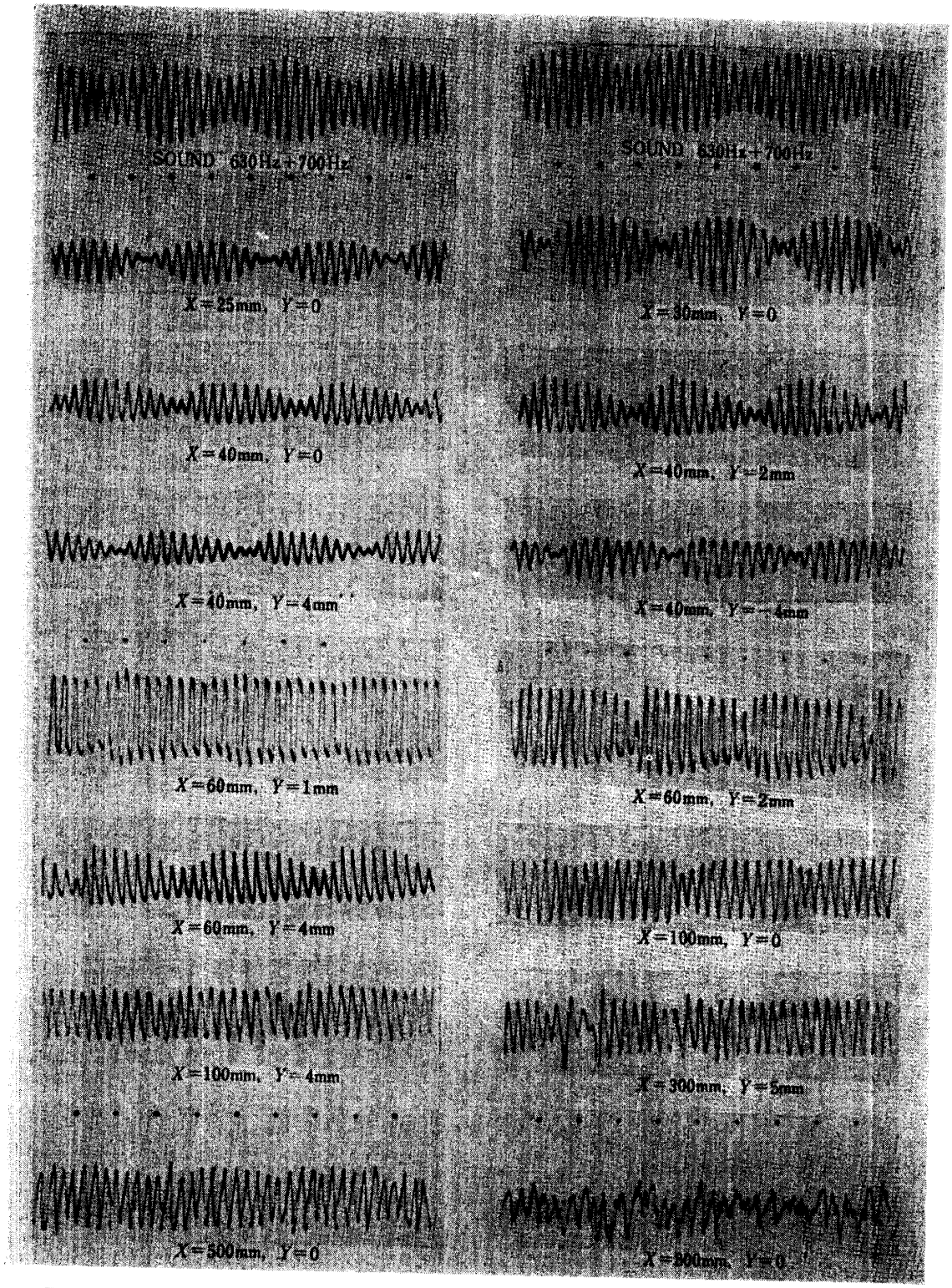

FIG. 5-11. Wave-forms of v-fluctuation with sound of 630 Hz and 700 Hz. Time interval between dots, 5 millisec.

This document is provided by JAXA.

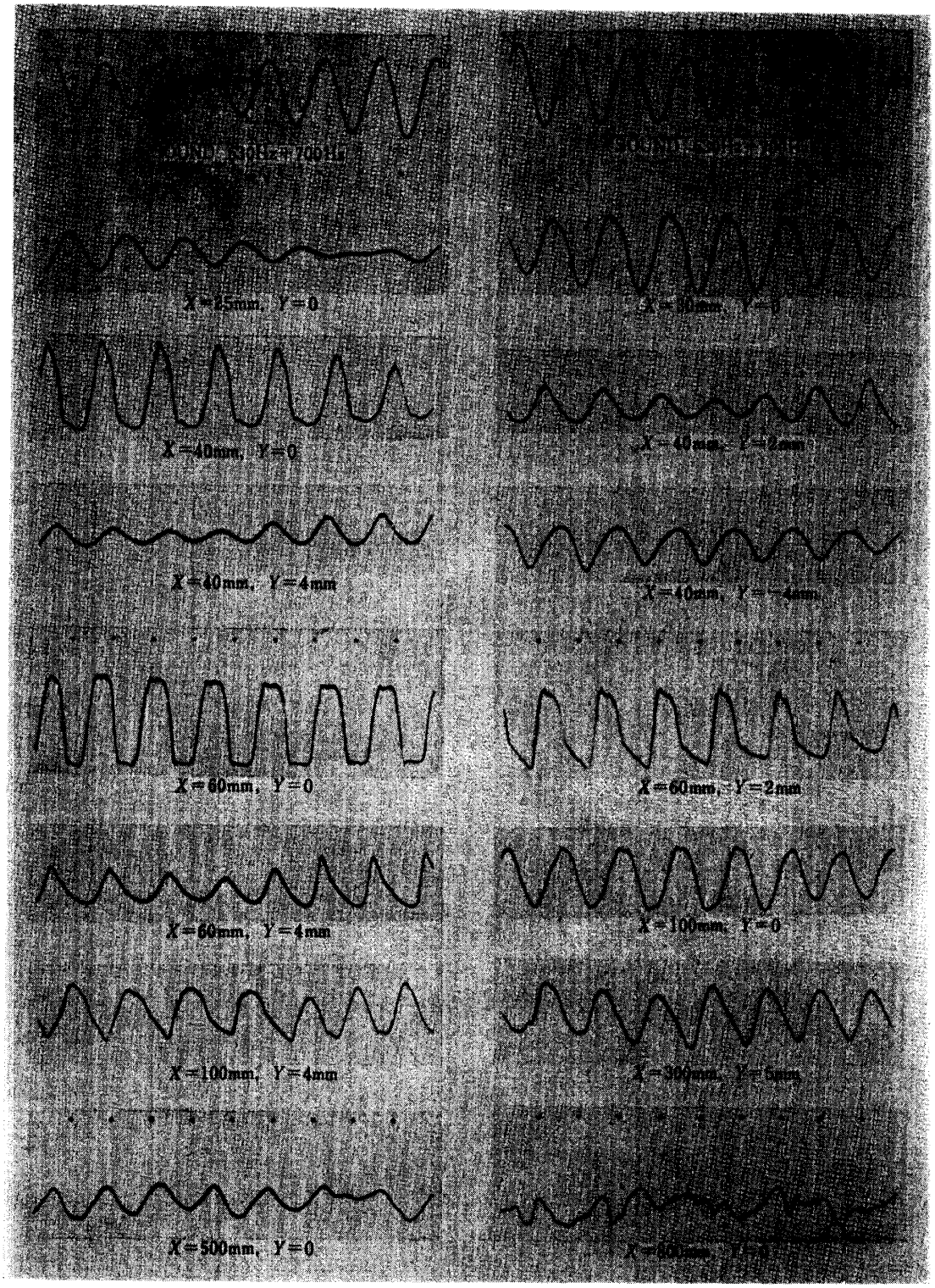

FIG 5-12. Wave-forms of v-fluctuation with sound of 630 Hz and 700 Hz. Time interval between dots, 1 millisec.

This document is provided by JAXA.

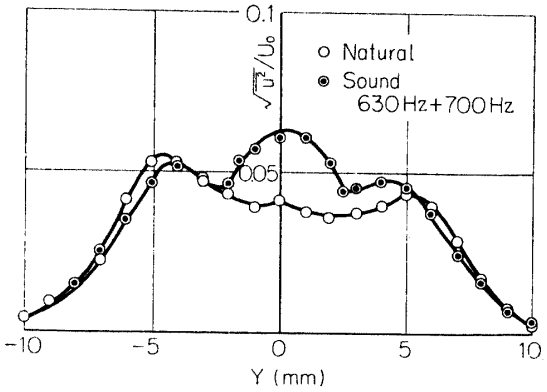

FIG. 5-13. Distribution of root-mean-square of u-fluctuation, natural and with two sounds. $X=80$ mm.

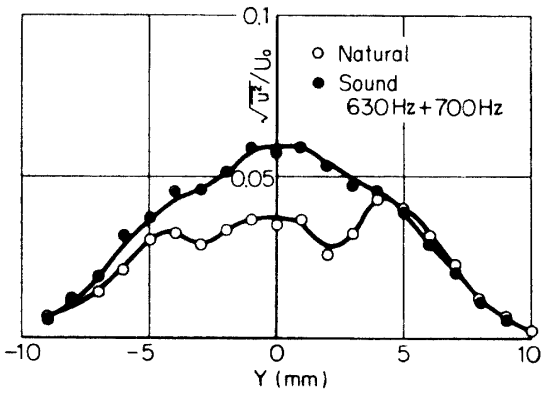

FIG. 5-14. Distribution of root-mean-square of u-fluctuation, natural and with two sounds. $X=150$ mm.

5-14 and 5-15. At $X=80$ mm (Fig. 5-13), $\sqrt{\overline{u^2}}$ near the axis increases remarkably when two sounds are present. Values at $|Y|>5$ mm remain almost unchanged. At $X=150$ mm (Fig. 5-14), distributions with and without sound are different near $Y=0$. At $X=600$ mm (Fig. 5-15), no effect of sound is observed. The increase of $\sqrt{\overline{u^2}}$ near $Y=0$ at $X=80$ mm and 150 mm is mainly due to the generation of 70 Hz-component and its harmonics. At $X=600$ mm, 70 Hz-component is no longer predonimant and $\sqrt{\overline{u^2}}$ is not affected by sounds.

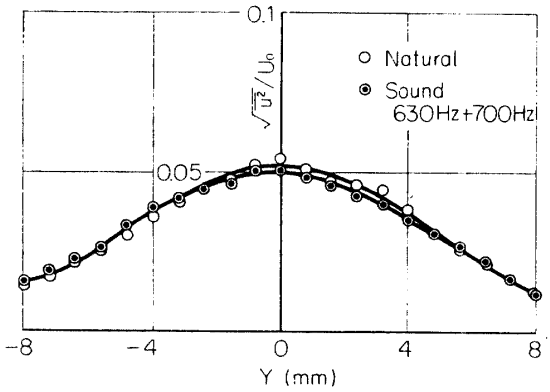

FIG. 5-15. Distribution of root-mean-square of u-fluctuation, natural and with two sounds. $X=600$ mm.

Spectra of u-fluctuations at points from $X=40$ mm to 300 mm are shown in Fig. 5-16. On the center line, the 70 Hz-component and its harmonics are very large. Even fifth harmonics (350 Hz) are found at $X=40$ mm. At $X=60$ mm, $Y=0$ harmonics of 70 Hz are relatively large in magnitude. This corresponds to the distorted wave-form in Fig. 5-9. The 1330 Hz-component (sum of 630 Hz and 700 Hz) is present in most of the spectra at $Y=0$. On the other hand, both 630 Hz- and 700 Hz-components are very small because distributions of these two fundamental components are antisymmetrical with respect to the center line. At $X=150$ mm, harmonics of 70 Hz-component become small and at $X=300$ mm third and fourth harmonics are larger than second harmonics. At two off-centered points ($X=40$ mm, $Y=2.5$ mm and $X=100$ mm, $Y=3$ mm) 630 Hz- and 700 Hz-components dominate. Thus the u-fluctuation consists of spectral components with frequencies of 70 Hz, 140 Hz, 210 Hz, $\cdots$, 630 Hz, 700 Hz and 1330 Hz. Harmonics of 1330 Hz-component must be present but their amplitudes are small. These spectral components have different distributions in X- and Y- direction.

This document is provided by JAXA.

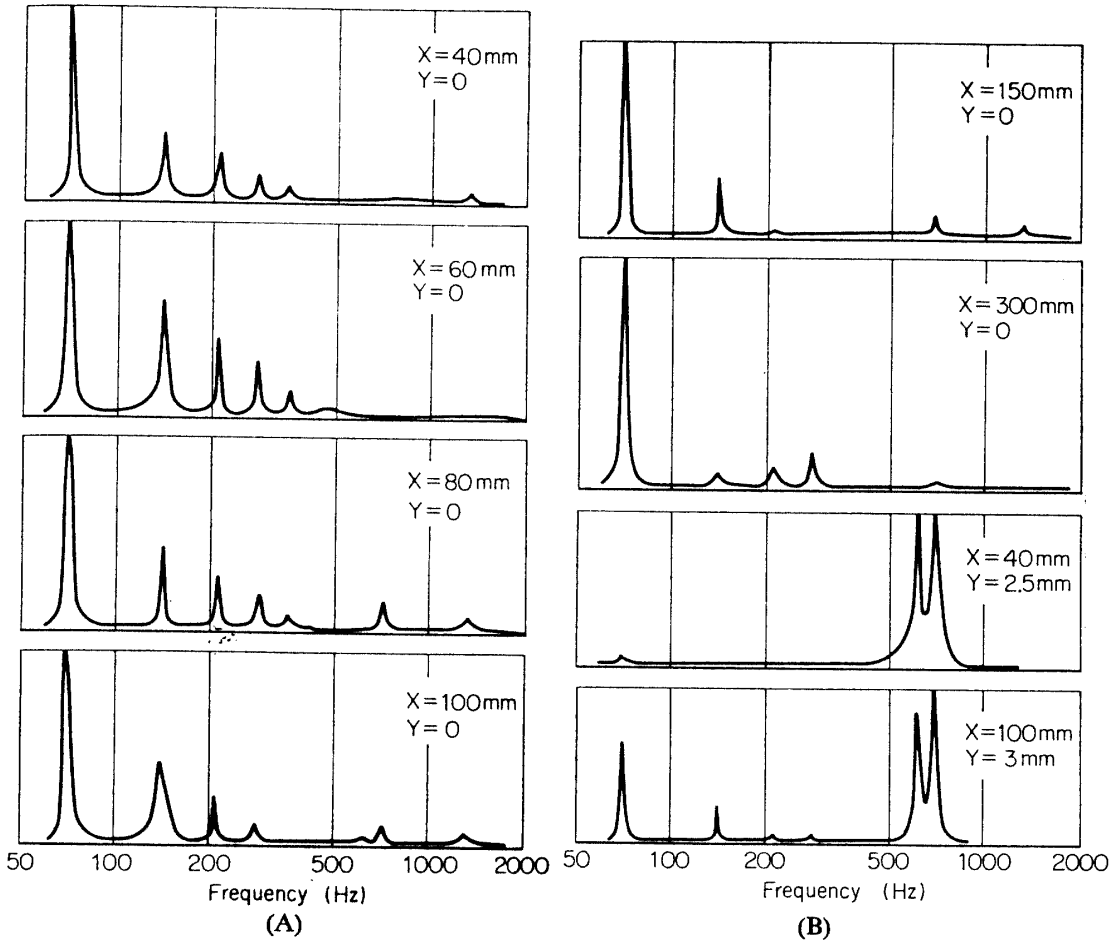

FIG. 5-16. Spectra of u-fluctuation with sound of 630 Hz and 700 Hz. Normalized by maximum values.

Spectra of v-fluctution lack 70 Hz-component and its harmonics and consist mostly of 630 Hz, 700 Hz-and 1300 Hz-components.

Distributions of low-frequency components of u-fluctuation in Y-direction are shown in Figs. 5-17～5-20. Distributions of 70 Hz-component (Fig. 5-17) are symmetrical with respect to the centerline at all X-stations. The component starts growing at $X=20$ mm, becomes maximum at about $X=30$ mm and then decreases. Between $X=20$ mm and 40 mm the distribution has a peak on the axis and two side peaks of which positions shift outward as X increases. It is now clear that the central peak of $\sqrt{\overline{u^2}}/U_0$ in Fig. 5-13 is mainly due to the 70 Hz-component. There are about 180 phase shifts at two dips between central and side peaks. Locations of two side peaks roughly coincide with the position of the maximum shear in the mean-velocity distribution. At $X=60$ mm, the distribution is entirely different and another equilibrium distribution seems to be established in the region $X=80$～120 mm. A phase reversal in this distribution takes place at around $Y=\pm 4$ mm. At $X=300$ mm the central peak becomes large again. At larger X, the distribution is broad and flat without any clear phase change. At $X=800$ mm, the wake is turbulent and there is no distinct 70 Hz-component in the velocity fluctuation.

This document is provided by JAXA.

The behaviour of the second harmonic component (140 Hz) is very much alike to that of 70 Hz-component as shown in Fig. 5-18. The distribution at small X has three peaks and at $X=80\sim100$ mm another equilibrium distribution is established with a phase reversal at about $Y=\pm4$ mm. At $X=800$ mm the distribution has a minimum on the axis and there is no definite phase relation in Y-direction. This behaviour is the same for third (210 Hz) and fourth (280 Hz)

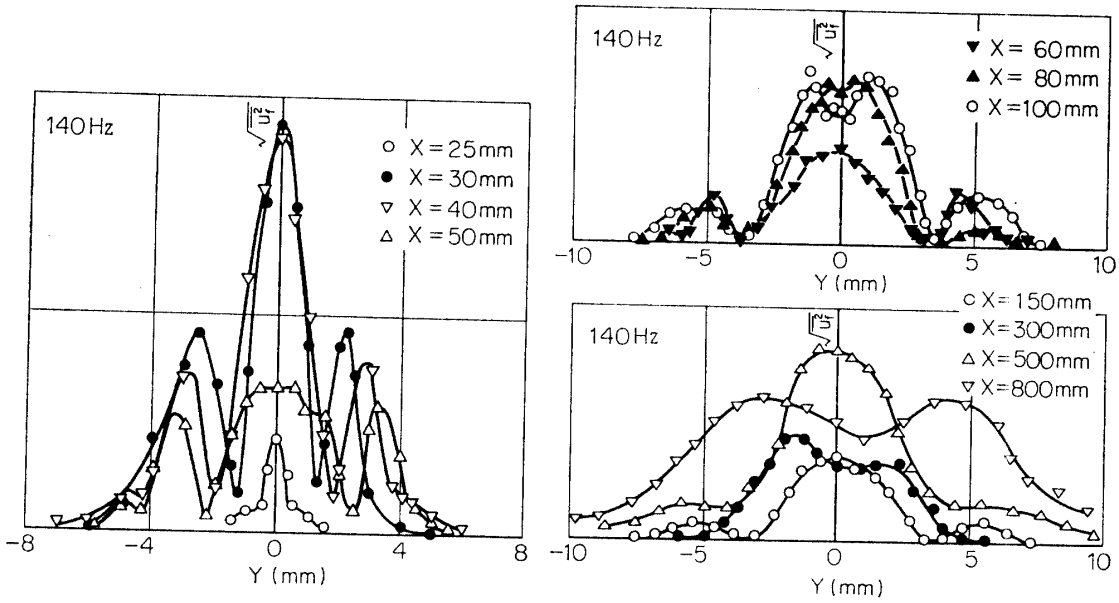

FIG. 5-18. Distribution of 140 Hz-component with sound of 630 Hz and 700 Hz. Ordinate scale is arbitrary. Relative values are expressed correctly.

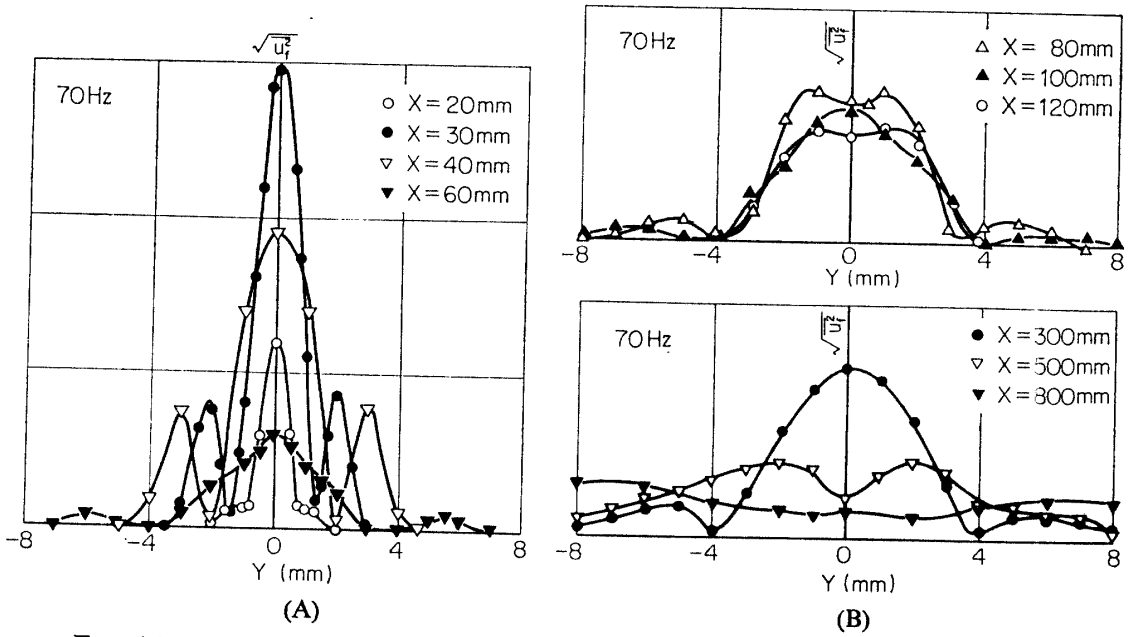

FIG. 5-17. Distribution of 70 Hz-component with sound of 630 Hz and 700 Hz. Ordinate scale is arbitraty. Relative values are expressed correctly.

This document is provided by JAXA.

harmonics as shown in Figs. 5-19 and 5-20. Streamwise developments of these harmonic components are alike except that higher harmonics start growing at larger X. For instance, 70 Hz-component has a maximum at around $X=30$ mm, whereas 280 Hz-component reaches a maximum value at around $X=40$ mm.

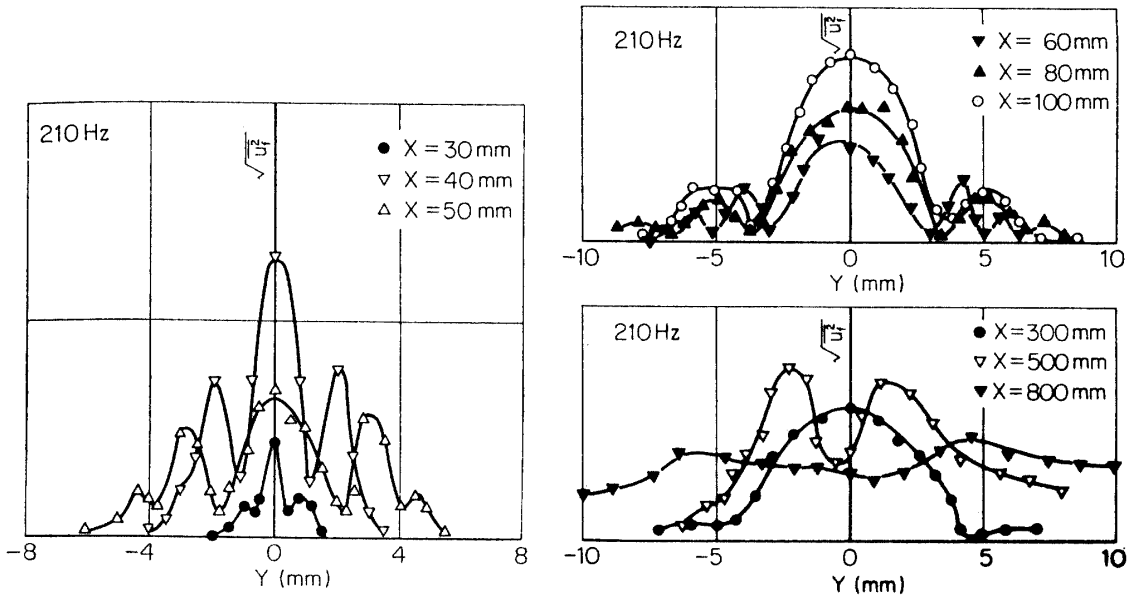

(A) (B)

FIG. 5-19. Distribution of 210 Hz-component with sound of 630 Hz and 700 Hz. Ordinate scale is arbitrary. Relative values are expressed correctly.

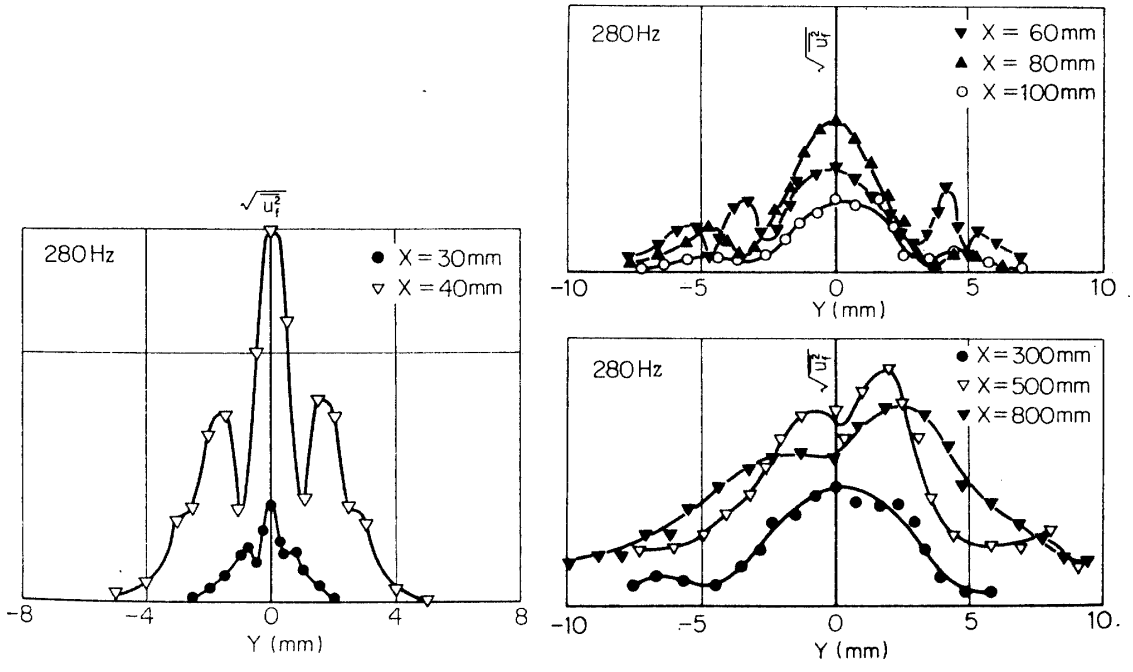

(A) (B)

FIG. 5-20. Distribution of 280 Hz-component with sound of 630 Hz and 700 Hz. Ordinate scale is arbitrary. Relative values are expressed correctly.

This document is provided by JAXA.

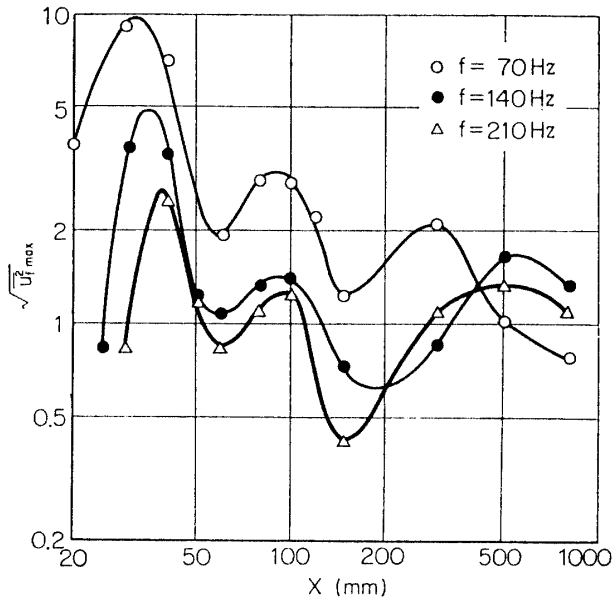

FIG. 5-21. Streamwise variations of three low-frequency components of u-fluctuation with sound of 630 Hz and 700 Hz. $\sqrt{\overline{u_f^2}}_{max}$: maximum of $\sqrt{\overline{u_f^2}}$ at each X-station. Ordinate scale is arbitrary. Relative values are expressed correctly.

Fig. 5-21 shows streamwise variations of maximum value of $\sqrt{\overline{u_f^2}}$ at each X-station. Three curves for three components show a similar trend. There are first peaks at $X=30\sim40$ mm. Second peaks are found at $X=80\sim100$ mm. This corresponds to the establishment of single-peak distribution of $\sqrt{\overline{u_f^2}}$ at $X=80\sim100$ mm. Third peaks appear at $X=300\sim500$ mm. This corresponds to the formation of the double-peak distribution.

Now we can distinguish at least three regions in the process of development of the low-frequency fluctuations. The first region is characterized by a fast growth due to the non-linear interaction of two fundamental components. In the second region ($X=40\sim60$ mm) the slow fluctuation loses energy due to the energy transfer to other spectral components or the mean motion. The viscous effect is very small for these low-frequency (long wave-length) fluctuations. Another growth takes place between $X=60$ mm and 100 mm. This growth should be due to a different mechanism with that in the first region, because the amplitude distribution in Y-direction is entirely different. The mechanism of growth and decay at larger X is not known.

Distributions of fundamental components (630 Hz and 700 Hz) are shown in Figs. 5-22 and 5-23.

They grow between $X=20$ mm and 30 mm with distributions antisymmetrical with respect to the center-line. A 180-degree phase jump takes place at $Y=0$. From $X=40$ mm the amplitude decreases downstream. The decrease is so remarkable that it can not be explained by the viscous dissipation. Since low-frequency components also decreases in this region, the energy of fluctuations may be transfered to the mean motion. A detailed discussion on this point will be

This document is provided by JAXA.

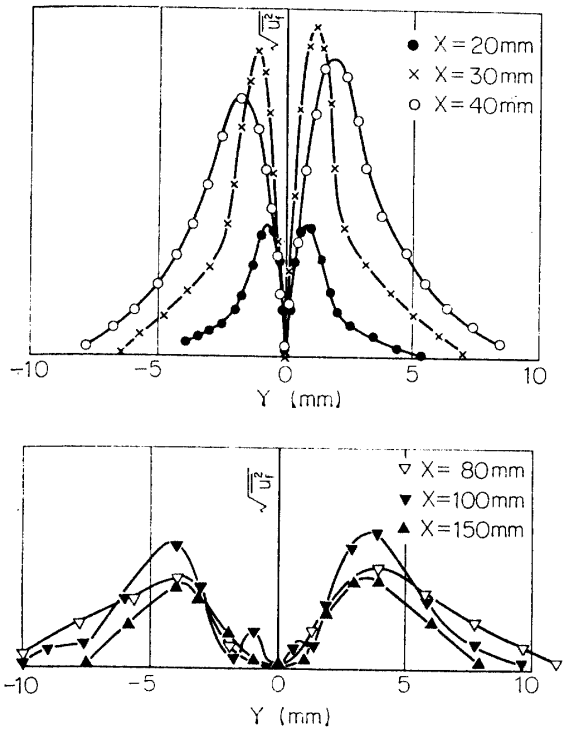

FIG. 5-22. Distribution of 630 Hz-component of u-fluctuation with sound of 630 Hz and 700 Hz. Ordinate scale is arbitrary.

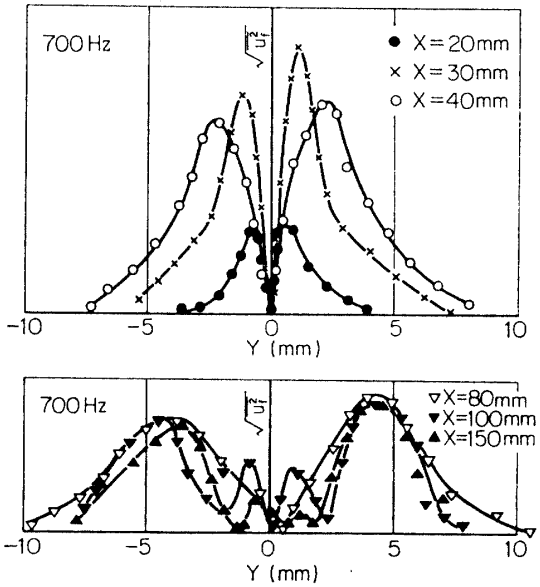

FIG. 5-23. Distribution of 700 Hz-component of u-fluctuation with sound of 630 Hz and 700 Hz. Ordinate scale is arbitrary.

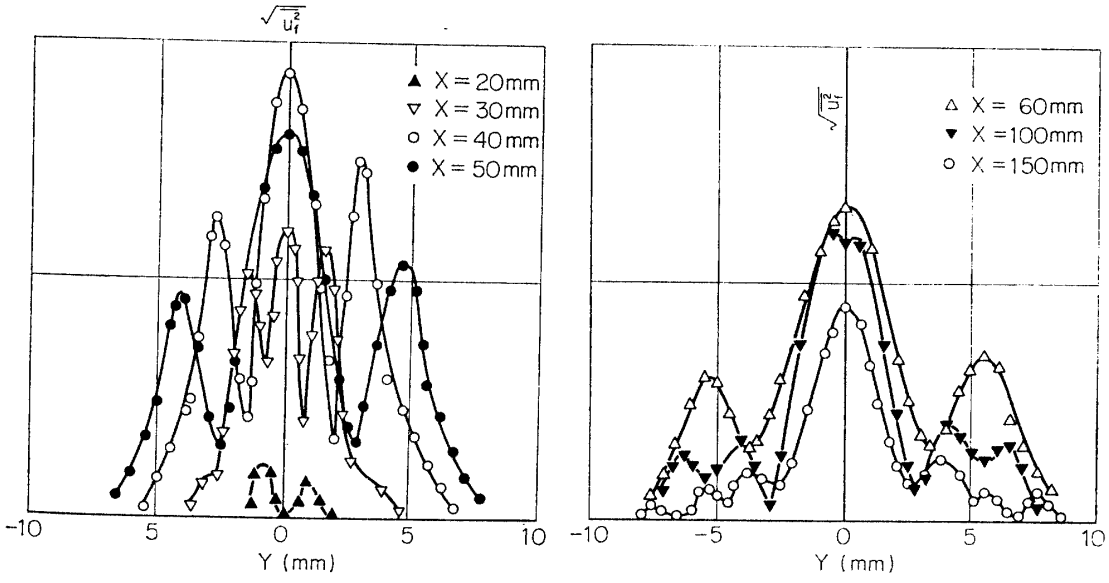

FIG. 5-24. Distribution of 1330 Hz-component of u-fluctuation with sound of 630 Hz and 700 Hz. Ordinate scale is arbitrary.

This document is provided by JAXA.

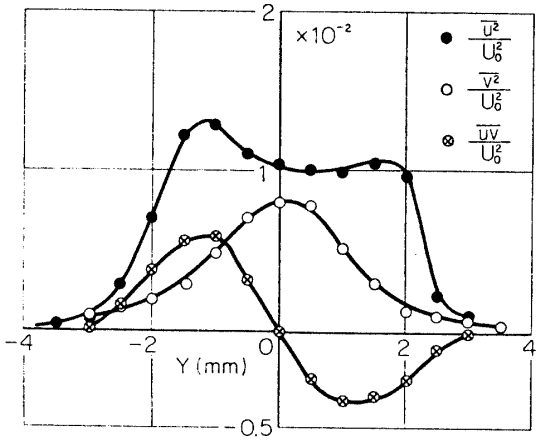

FIG. 5-25. Distributions of $\overline{u^2}$, $\overline{v^2}$ and $\overline{uv}$ with sound of 630 Hz and 700 Hz. $X=30$ mm.

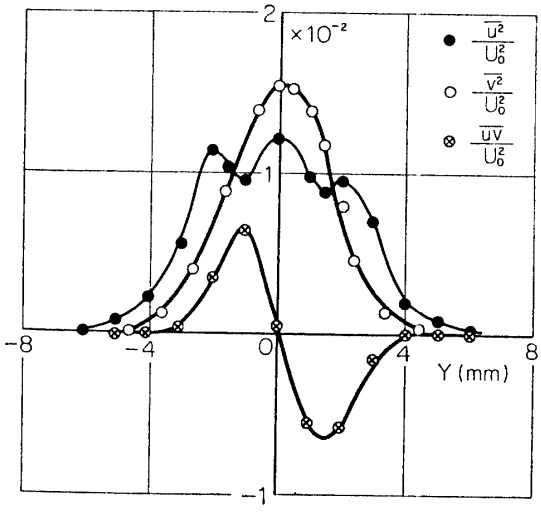

FIG. 5-26. Distributions of $\overline{u^2}$, $\overline{v^2}$ and $\overline{uv}$ with sound of 630 Hz and 700 Hz. $X=40$ mm.

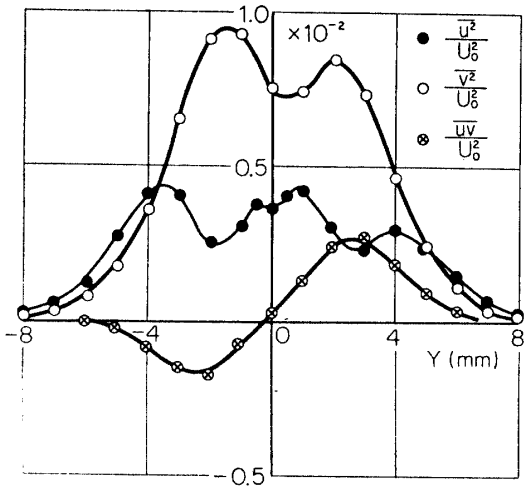

FIG. 5-27. Distributions of $\overline{u^2}$, $\overline{v^2}$ and $\overline{uv}$ with sound of 630 Hz and 700 Hz. $X=80$ mm.

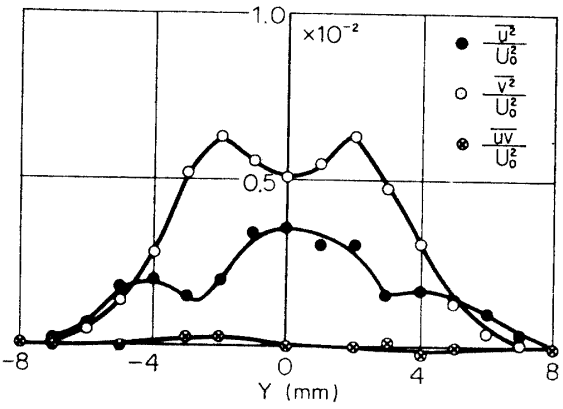

FIG. 5-28. Distributions of $\overline{u^2}$, $\overline{v^2}$ and $\overline{uv}$ with sound of 630 Hz and 700 Hz. $X=120$ mm.

found in the next section. At $X=150$ mm an entirely different distribution is established.

The distribution of 1330 Hz-component is symmetrical with respect to the center-line as shown in Fig. 5-24. The amplitude increases in the flow direction between $X=20$ mm and 40 mm and then gradually decreases downstream. The decrease is monotonic and there are no repeated growth and decay as low-frequency components. Distributions between $X=30$ mm and 60 mm have a central peak and two side peaks. In this respect, this component is similar to the 70 Hz-component. One difference is that the 70 Hz-component grows at smaller to the 70 Hz-component. One difference is that the 70 Hz-component grows at smaller X than 1330 Hz-component. Locations of two side peaks shift outward

This document is provided by JAXA.

until $X=60$ mm. At $X=100$ mm four side peaks and at $X=150$ mm six side peaks are found. This feature is also different from that of 70 Hz-component.

Distributions of lateral velocity fluctuations are shown in following several figures. Fig. 5-25 shows $\overline{u^2}$, $\overline{v^2}$, and $\overline{uv}$ at $X=30$ mm. They are nondimensionalized by the free-stream velocity, U_0. The distribution of $\overline{u^2}$ has two peaks and $\overline{v^2}$ is a little smaller than $\overline{u^2}$. The cross product $\overline{uv}$ is negative for $Y>0$ and the magnitude is comparable with $\overline{u^2}$ and $\overline{v^2}$. This means that a large amount of energy is transfered from the mean motion to the fluctuation. The lateral component $\overline{v^2}$ at $X=40$ mm is larger than that at $X=30$ mm as shown in Fig. 5-26. The longitudinal component $\overline{u^2}$ neither increases nor decreases. The apperance of a central peak in the distribution of $\overline{u^2}$ at $X=40$ mm is due to the generation of the 70 Hz-component as described before. Two side peaks consist of 630 Hz- and 700 Hz-components. The value of $\overline{uv}$ is almost the same as that at $X=30$ mm. Another lateral component $\overline{w^2}$ is small. This figure is to be compared with Fig. 4-16 with sound of single frequency. Both figures are alike except a central peak of $\overline{u^2}$ in Fig. 5-26. At $X=80$ mm (Fig. 5-27) the sign of $\overline{uv}$ is reversed. Both $\overline{u^2}$ and $\overline{v^2}$ are smaller than those at $X=40$ mm. Since the effect of viscosity is small, the decay of the total fluctuation energy $(\overline{u^2}+\overline{v^2}+\overline{w^2})$ must be due to the energy transfer. The decrease of energy is more remarkable in $\overline{u^2}$ than in $\overline{v^2}$. The energy transfer to the mean motion might take place more in $\overline{u^2}$ than $\overline{v^2}$. At $X=120$ mm (Fig. 5-28) $\overline{uv}$ is almost zero. At $X=80$ mm and 120 mm $\overline{v^2}$ is definitely larger than $\overline{u^2}$. At $X=800$ mm, $\overline{u^2}$ and $\overline{v^2}$ are almost equal and $\overline{uv}$ is small, the production of fluctuation energy being slightly positive. The wake is turbulent at $X=800$ mm and distributions in Fig. 5-29 are similar to those found in a usual fully-developed turbulent wake.

These quantities, $\overline{u^2}$, $\overline{v^2}$, $\overline{w^2}$ and $\overline{uv}$ are composed of various spectral components. Important components are with frequencies of 70 Hz, 630 Hz, 700 Hz and 1330 Hz. The 70 Hz-component has a very large u-fluctuation as shown in Figs. 5-30, 5-31 and 5-32. At all three X-stations $\overline{v_f^2}$ and $\overline{(uv)_f}$ are extremely small. This fact

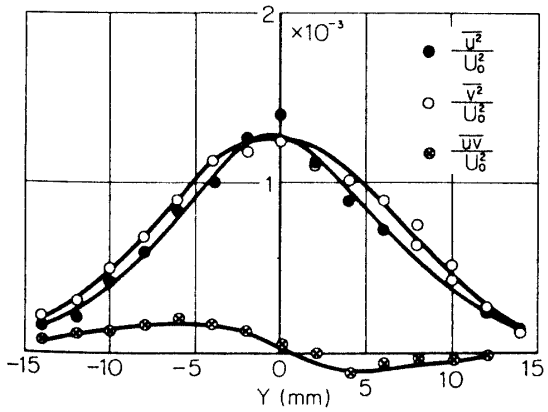

FIG. 5-29. Distributions of $\overline{u^2}$, $\overline{v^2}$ and $\overline{uv}$ with sound of 630 Hz and 700 Hz. $X=800$ mm.

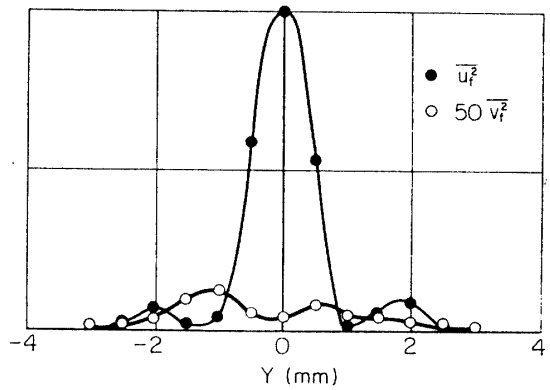

FIG. 5-30. Distributions of 70 Hz-components, $\overline{u_f^2}$ and $\overline{v_f^2}$ with sound of 630 Hz and 700 Hz. $X=30$ mm. Ordinate scale is arbitrary.

This document is provided by JAXA.

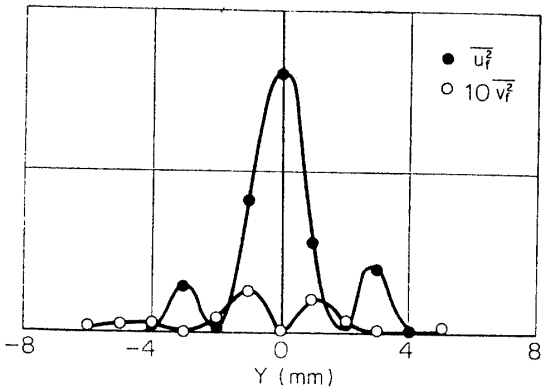

FIG. 5-31. Distributions of 70 Hz-components, $\overline{u_f^2}$ and $\overline{v_f^2}$ with sound of 630 Hz and 700 Hz. $X=40$ mm. Ordinate scale is arbitrary.

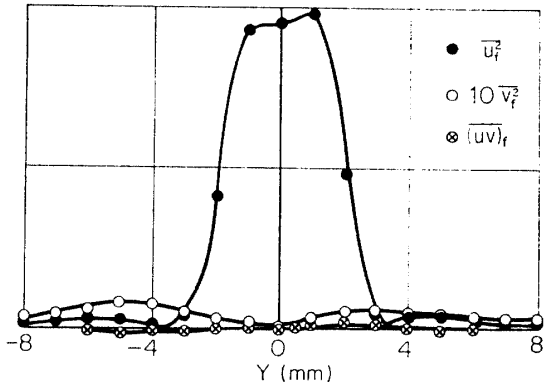

FIG. 5-32. Distributions of 70 Hz-components, $\overline{u_f^2}$, $\overline{v_f^2}$ and $\overline{(uv)_f}$ with sound of 630 Hz and 700 Hz. $X=80$ mm. Ordinate scale is arbitrary.

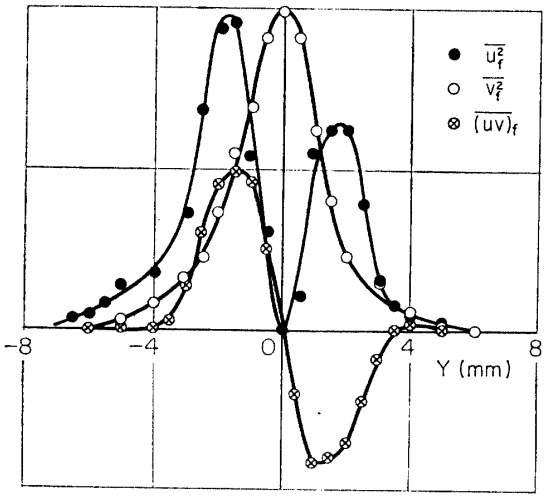

FIG. 5-33. Distributions of 700 Hz-components, $\overline{u_f^2}$, $\overline{v_f^2}$ and $\overline{(uv)_f}$ with sound of 630 Hz and 700 Hz. $X=40$ mm. Ordinate scale is arbitrary.

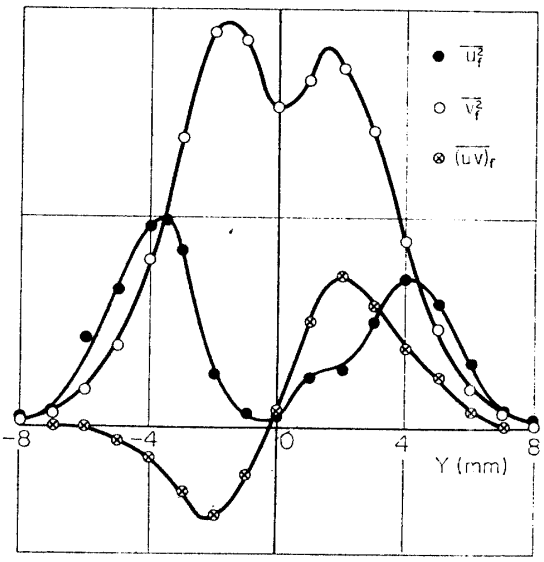

FIG. 5-34. Distributions of 700 Hz-components, $\overline{u_f^2}$, $\overline{v_f^2}$ and $\overline{(uv)_f}$ with sound of 630 Hz and 700 Hz. $X=80$ mm. Ordinate scale is arbitrary.

indicates that the 70 Hz-component is almost a longitudinal wave. In Figs. 5-30 and 5-31, $\overline{(uv)_f}$ is too small to be plotted. At $X=30$ mm and 40 mm distributions of $\overline{u_f^2}$ have three peaks, one on the center line and other two at around $Y=\pm 2\sim 3$ mm. The 700 Hz-component at $X=40$ mm (Fig. 5-33) has nearly equal amount of $\overline{u_f^2}$, $\overline{v_f^2}$, and $\overline{(uv)_f}$. The distribution of $\overline{u_f^2}$ has a minimum at $Y=0$ and the phase is antisymmetrical with respect to the center line. The sign of $\overline{(uv)_f}$ is different at $X=40$ mm and $X=80$ mm (Fig. 5-34). Moreover, $\overline{v_f^2}$ at $X=80$ mm is much larger than $\overline{u_f^2}$. The nature of 630 Hz-component is the same as 700 Hz-component. These features coincide with those of overall $\overline{u^2}$, $\overline{v^2}$, and $\overline{uv}$.

Distributions of 1330 Hz-component are shown in Figs. 5-35 and 5-36. At $X=40$ mm, $\overline{v_f^2}$ is zero on the center-line and the maximum value is a little smaller

This document is provided by JAXA.

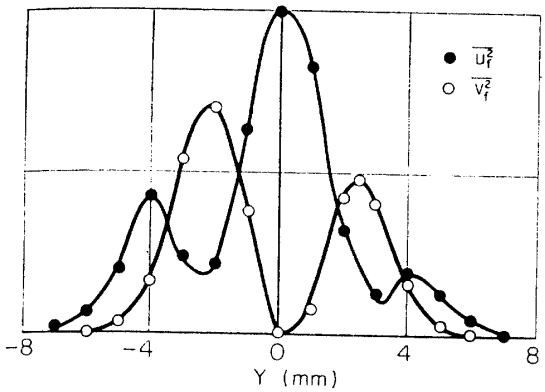

FIG. 5-35. Distributions of 1330 Hz-components, $\overline{u_f^2}$ and $\overline{v_f^2}$ with sound of 630 Hz and 700 Hz. $X=40$ mm. Ordinate scale is arbitrary.

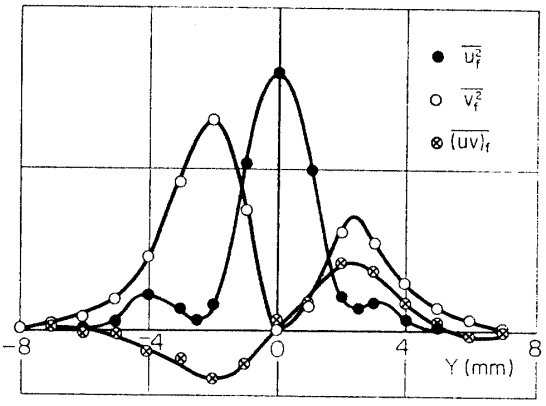

FIG. 5-36. Distributions of 1330 Hz-components, $\overline{u_f^2}$, $\overline{v_f^2}$ and $\overline{(uv)_f}$ with sound of 630 Hz and 700 Hz. $X=80$ mm. Ordinate scale is arbitrary.

than $\overline{u_f^2}$. Distributions of $\overline{u_f^2}$ and $\overline{v_f^2}$ of 1330 Hz-component are alike to those of 70 Hz-component except the relative magnitude of $\overline{u_f^2}$ and $\overline{v_f^2}$. At $X=80$ mm, the production of fluctuation energy due to 1330 Hz-component is negative. In most points in the wake the energy of 1330 Hz-component is small compared with other spectral components.

These experimental results indicate that overall values $\overline{v^2}$ and $\overline{uv}$ include mainly fundamental components, 630 Hz and 700 Hz. On the other hand, $\overline{u^2}$ consists mostly of fundamental and low-frequency components.

6. Nonlinear Interaction of Spectral Components

When there are two velocity fluctuations, the growth of each fluctuation is suppressed by the nonlinear interaction. If amplitudes of two fluctuations are not the same, the component with smaller amplitude experiences more suppression. When two sounds (frequencies f_1 and f_2) are introduced into the wake and sound levels are adjusted so that two induced velocity fluctuations have same amplitudes, the mutual interaction results in the equal amount of suppression and the production of spectral components with frequencies, f_1-f_2, $2(f_1-f_2)$, . . . and f_1+f_2, $2(f_1+f_2)$ . . . . The wave length corresponding to high-frequency components —f_1+f_2, $2(f_1+f_2)$, . . . —is short and the viscous effect reduces amplitudes of these components. There fore, roles of high-frequency components in the transition process may be insignificant. The energy contained in low-frequency components—f_1-f_2, $2(f_1-f_2)$, . . . —is appreciable and it is important is the energy balance in the nonlinear development of velocity fluctuations.

The onset of the nonlinear interaction is characterized by a rapid expansion of the wake and a non-exponential growth of velocity fluctuation. Theoretically, both take place when higher-order terms in the equation of motion becomes large. Streamwise variations of the central velocity, U_c and the half-value breadth, b are shown in Figs. 5-6, 5-7 and 5-8. An unusual feature is the decrease of both U_c

This document is provided by JAXA.

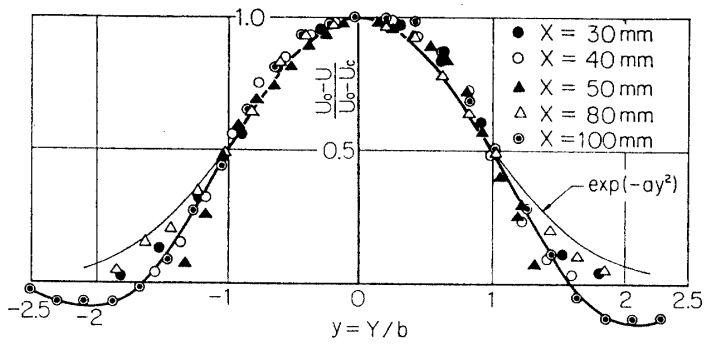

FIG. 6-1. Non-dimensional plot of mean-velocity distribution with sound of 630 Hz. U_0: freestream velocity, U_c: velocity on the center line, b: half-value breadth. Thin full line represents $(U_0-U)/(U_0-U_c)=\exp(-ay^2)$.

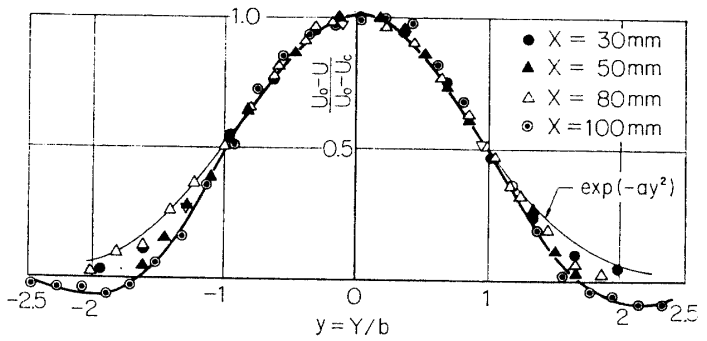

FIG. 6-2. Non-dimensional plot of mean-velocity distribution with sound of 630 Hz and 700 Hz.

and b between $X=60$ mm and 120 mm. This occurs in all transition processes including natural, with sound of single frequency and with sound of two frequencies. The physical process taking place in those three cases must be the same. The nondimensional mean-velocity distribution at various X-stations are shown in Figs. 6-1 and 6-2 for sound of single frequency and for two frequencies, respectively. The distribution is nondimensionalized by U_c and b. Thin solid lines in two Figs. indicate the distribution given by,

$$\frac{U_0-U}{U_0-U_c}=\exp(-ay^2)$$

in which $a=0.69315$ and $y=Y/b$. Distributions at small X are almost similar. In general, experimental points in the nonlinear region lie a little above the solid line for $|Y|>1$ and below for $|Y|<1$. At about $X=100$ mm points at large Y lies below abcissa. In other words, the mean-velocity of the wake edge exceeds the free-stream velocity. This fact was already pointed out in reference 5 and this over-shoot must be a result of the nonlinear interaction.

The streamwise variations of quantities concerning distributions of two spectral components, 630 Hz and 70 Hz are shown in Fig. 6-3. The 630 Hz-component

This document is provided by JAXA.

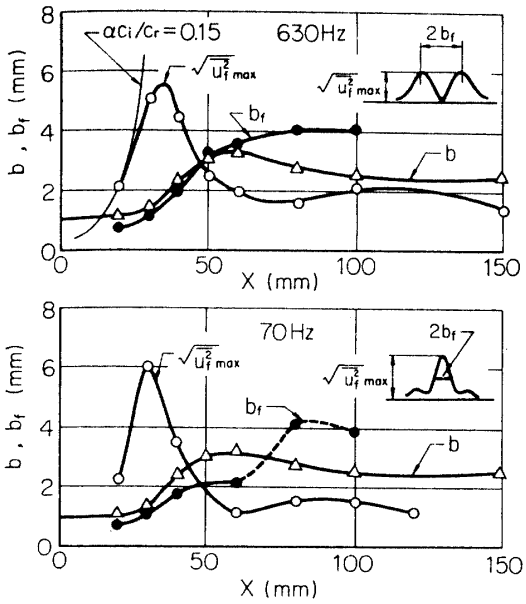

FIG. 6-3. Streamwise variations of maximum root-mean-square of spectral components at each X-station, $\sqrt{\overline{u_f^2}}_{max}$ and of breadth of distributions, b_f. b: half-value breadth of mean-velocity distribution.

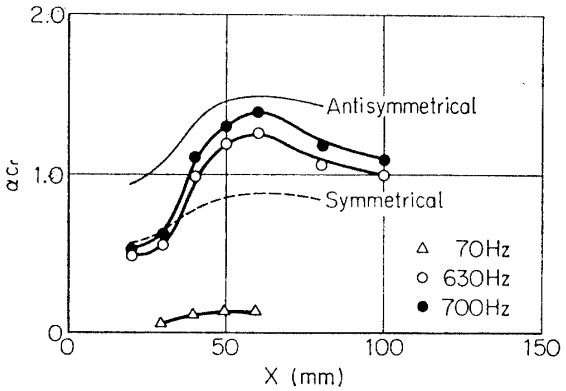

FIG. 6-4. Streamwise variations of non-dimensional frequency of three spectral components (70 Hz, 630 Hz and 700 Hz) with sound of 630 Hz and 700 Hz. Thin solid line, neutral frequency for antisymmetrical fluctuation and broken line, symmetrical fluctuation. Both by linear theory with local equilibrium.

of u-fluctuation has two peaks in Y-distribution. The peak value at each X-station is denoted by $\sqrt{\overline{u_f^2}}_{max}$ and the separation of two peaks is denoted by $2b_f$. In the upper part of the figure, these two quantities and the half-breadth of the wake, b based on the mean-velocity distribution are plotted against X. At $X=35$ mm $\sqrt{\overline{u_f^2}}_{max}$ reaches a maximum value and decreases downstream. A thin solid line indicate the exponential growth of the amplitude with the maximum growth rate in the linear theory ($\alpha c_i/c_r=0.15$). Apparently, the growth of $\sqrt{\overline{u_f^2}}_{max}$ at $X>25$ mm is less than this exponential growth. The amplitude $\sqrt{\overline{u_f^2}}_{max}$ shows two maximum at around $X=35$ mm and 100 mm, while b_f increases monotonically. The variation of b_f is similar to that of b until $X=50$ mm and at larger X, b decreases while b_f increases. The distribution of 70 Hz-component has a maximum on the center-line. The half-value breadth of $\sqrt{\overline{u_f^2}}_{max}$ was taken as $2b_f$. At around $X=30$ mm, $\sqrt{\overline{u_f^2}}_{max}$ is largest. The increase of b_f is again monotonic. As far as $\sqrt{\overline{u_f^2}}_{max}$ and b_f are concerned, both 630 Hz- and 70 Hz-components change in X-direction in a similar manner.

The streamwise variation of the nondimensional frequency expressed as $\beta_r=2fb/U_0-U_c$ is shown in Fig. 6-4. Although the frequency, f does not change in X-direction, b and U_c do change. Therefore, β_r changes in X-direction as indicated. The uppermost thin solid line indicates the theoretical nondimensional frequency of antisymmetrical u-fluctuation at neutral stability ($c_i=0$). At around

This document is provided by JAXA.

$X=60$ mm, the 700 Hz-component is close to the curve. In other words, the component may not grow so much if the linear theory is valid at the X-station. The experimental fact is that the fluctuation decays at $X=60$ mm as shown in Fig. 6-3. A thin broken line indicates β_r of the neutral symmetrical u-fluctuation according to the linear theory.* Since the 70 Hz-component is symmetrical, triangles showing 70 Hz-component are to be compared with the broken line. The comparison fails to explain the decay of the 70 Hz-component. If the linear theory is applicable in the nonlinear region all these three components should grow in X-direction but actually they decay. It is concluded that the growth or decay of spectral components in the nonlinear region can not be predicated by the linear theory, even if it is modified by the nondimensionalization with local values of b and U_c.

The nondimensional wave number, $\alpha=2\pi b/\lambda$, λ being the wave-length of the velocity fluctuation is shown in Fig. 6-5. The wave-length was obtained experimentally by measuring the phase change in X-direction. The wave-length of u-fluctuation was the same as that of v-fluctuation. The phase speed of 630 Hz-component is around $0.7\sim0.8\ U_0$ almost independent of X, while the phase speed of 70 Hz-component is around $0.5\sim0.6\ U_0$ and increases in X-direction. Although precise

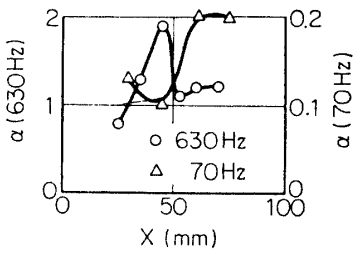

FIG. 6-5. Streamwise variations of non-dimensional wave number, α, of two spectral components (70 Hz and 630 Hz) with sound of 630 Hz and 700 Hz.

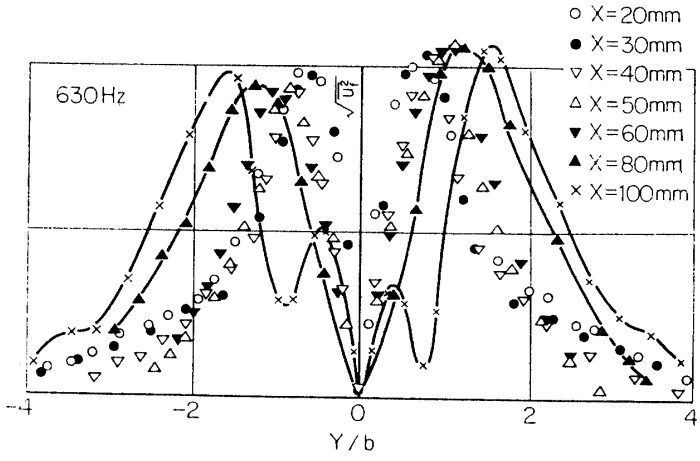

FIG. 6-6. Non-dimensional plot of distribution of 630 Hz-component with sound of 630 Hz. Abcissa is non-dimensionalized by half breadth, b and ordinate is normalized by mean of two peak values.

* The calculation of linear equation for a symmetrical fluctuation in $\exp(-ay^2)$-type flow was made recently by K. Tanaka of our group.

This document is provided by JAXA.

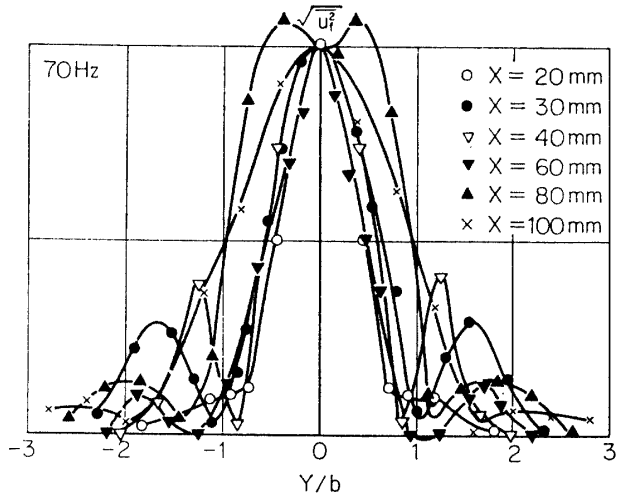

FIG. 6-7. Non-dimensional plot of distribution of 70 Hz-component, with sound of 630 Hz and 700 Hz.

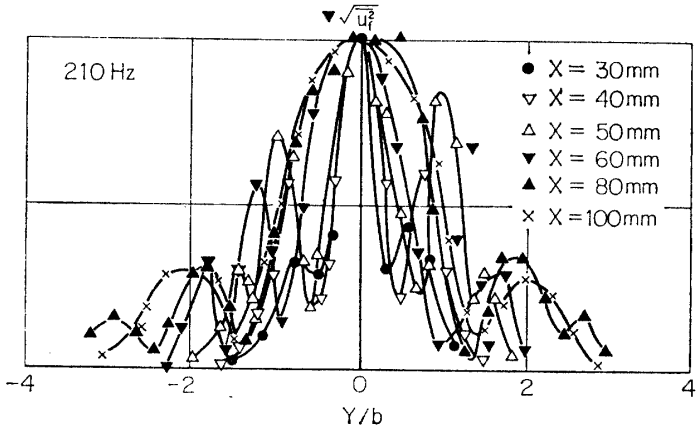

FIG. 6-8. Non-dimensional plot of distribution of 210 Hz-component with sound of 630 Hz and 700 Hz.

measurements of the phase speed in the nonlinear region are difficult due to the distortion of the wave-form, the phase speed of 70 Hz-component seems to be less than that of 630 Hz-component.

Amplitude distributions in Y-direction are normalized by the maximum value and shown in Figs. 6-6～6-10. The Y-axis is nondimensionalized by the half-breadth, b. With a sound of single-frequency the distribution of 630 Hz-component (Fig. 6-6) is almost similar from $X=20$ mm to 60 mm. At $X=80$ mm the distribution becomes broader and at $X=100$ mm an entirely different distribution with two small peaks around $|Y/b|=\pm 0.4$ is established. The 70 Hz-component (Fig. 6-7) shows a similarity until $X=60$ mm at small Y/b. At $1<|Y/b|<2$, small peaks grow until $X=40$ mm and gradually decay thereafter. The distribution at $X=100$ mm is entirely different. Distributions of 210 Hz-component (Fig. 6-8) are similar to those of 70 Hz-component except at large Y/b. At $X=50$ mm and 60 mm, 210 Hz-component has two side peaks at around $Y/b=1$ and 1.5.

This document is provided by JAXA.

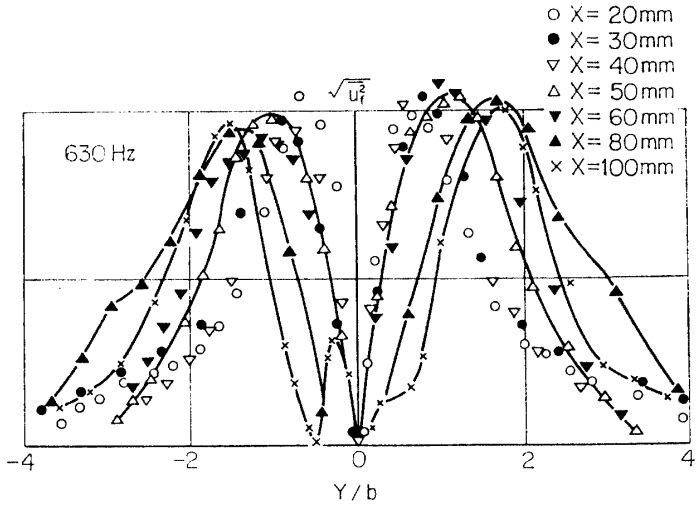

FIG. 6-9. Non-dimensional plot of distribution of 630 Hz-component with sound of 630 Hz and 700 Hz.

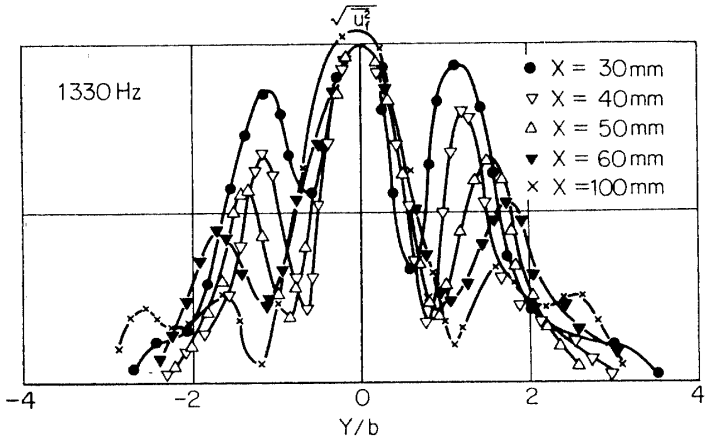

FIG. 6-10. Non-dimensional plot of distribution of 1330 Hz-component with sound of 630 Hz and 700 Hz.

At $X=80$ mm they are slifted outward and at $X=100$ mm only one side peak is found. The similarity of distributions of 630 Hz-component with sound of two frequencies (Fig. 6-9) is not as good as that with single-frequency sound, but the general tendency is almost the same. At $X=100$ mm we again find a distribution with a pair of small peaks near $Y/b=+0.3$. The 1330 Hz-component in Fig 6-10 shows a gradual outward shift of positions of side peaks at large X. From these experimental results we conclude that fundamental components (630 Hz and 700 Hz) exhibit a similar distribution in the nonlinear region until $X=60$ mm and components produced by the nonlinear effect show less similarity. At $X=100$ mm, all similarities are lost.

Experimental results on w-fluctuation were shown in several figures in preceding Sections. Generally speaking, $\overline{w^2}$ is small compared with $\overline{u^2}$ and $\overline{v^2}$ and distributions in Y-direction are similar to those of $\overline{v^2}$ rather than $\overline{u^2}$. Streamwise variations

This document is provided by JAXA.

of three velocity components are summarized in Fig. 6-11. Ratios of the maximum amplitudes of two components at each X-station are shown. Although the shape of Y-distribution is different, the ratio may roughly represent the relative magnitude. In natural transition $\overline{w^2}$ is extremely small (at $X=40$ mm, $\sqrt{\overline{w^2}}_{max}$ is less than 5% of $\sqrt{\overline{u^2}}_{max}$) and the ratio $\sqrt{\overline{w^2}}_{max}/\sqrt{\overline{u^2}}_{max}$ gradually increases in the nonlinear region. Since $\sqrt{\overline{u^2}}_{max}$ itself decreases in the flow direction, the increase of the ratio does not mean the increase of the absolute value of $\overline{w^2}$. When two sounds are present, $\overline{w^2}$ is about half of $\sqrt{\overline{u^2}}_{max}$ at $X=40$ mm. This is reasonable because the nonlinear region starts at smaller X. The ratio $\sqrt{\overline{w^2}}_{max}/\sqrt{\overline{u^2}}_{max}$ increases in the flow direction and reaches about 70% at $X=150$ mm. When $\overline{v^2}$ is very large, the measured values of $\overline{w^2}$ may be larger than real ones. An extremely small misalignment of X-type hot-wire results in an apparent increase of $\overline{w^2}$. At small X, $\sqrt{\overline{v^2}}$ is smaller than $\sqrt{\overline{u^2}}$ but at around $X=50$ mm $\sqrt{\overline{v^2}}$ exceeds $\sqrt{\overline{u^2}}$ and becomes twice at around $X=60\sim80$ mm. And then decreeses at larger X.

Relative magnitudes of spectral components are shown in Fig. 6-12, which shows ratios of maximum amplitudes of spectral components of u, v and w at each X-station in presence of the sounds. The 70 Hz-components of v and w are extremely small, whereas v-fluctuation of 630 Hz-component is large. The 70 Hz-component is composed of only u-fluctuation and $\overline{v^2}$ and $\overline{w^2}$ are mostly made up with 630 Hz- and 700 Hz-components.

The phase distribution of u-fluctuation in Z-direction was measured by traversing a single hot-wire in Z-direction. The sound was used as a phase standard. Experimental results indicate a phase variation in Z-direction. As mentioned earlier, the present flat plate was carefully mechined and aligned to the flow. And still, the phase difference of 630 Hz-component at $X=40$ mm, $Y=5$ mm is as high as 0.8π in Z between $+80$ mm and -80 mm. This value is almost the same as that reported in reference 5. At $X=120$ mm we observe nearly the same

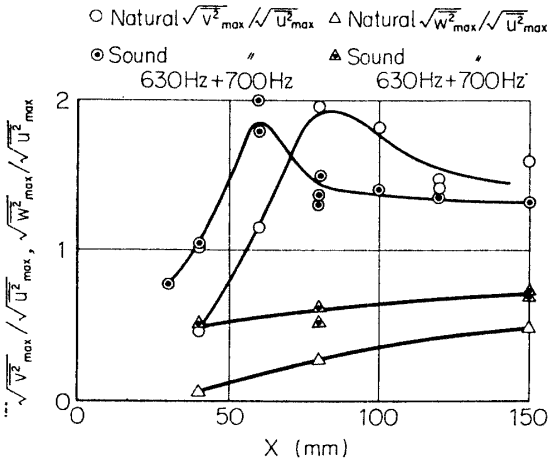

FIG. 6-11. Relative magnitudes of maximum values of $\sqrt{\overline{u^2}}$, $\sqrt{\overline{v^2}}$, and $\sqrt{\overline{w^2}}$ at each X-station. Natural transition and with sound of 630 Hz and 700 Hz.

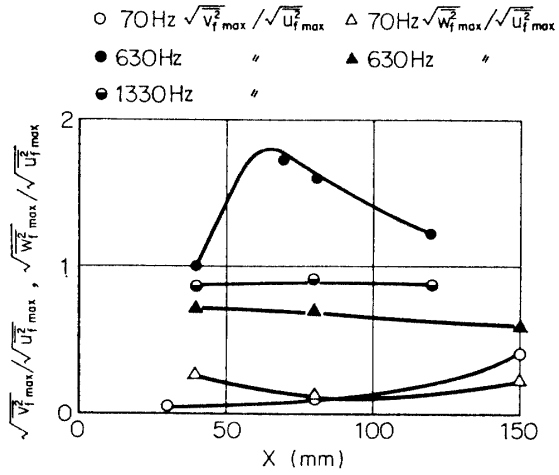

FIG. 6-12. Relative magnitudes of maximum values of spectral components (70 Hz, 630 Hz and 1330 Hz) at each X-station with sound of 630 Hz and 700 Hz.

This document is provided by JAXA.

amount of phase difference. There is no periodicity in the phase distribution in Z. The phase variation may be due to the residual small spanwise irregularity of the flow in the wind-tunnel. The magnitude of $\overline{u^2}$ is constant in Z-direction. This indicates that the process of three-dimensionalization in the transition region of the wake is different from that in the boundary layer. The non-uniform distribution of $\overline{u^2}$ in Z-direction characterizes the nonlinear region of the boundary layer. In the wake there is no "peak" or "valley" section. Moreover, there are no adrupt "breakdowns".

7. Balance of Momentum and Energy

The continuity equation for the mean motion is, neglecting W,

$$\frac{\partial U}{\partial X}+\frac{\partial V}{\partial Y}=0 \tag{7-1}$$

Using this equation we can estimate V from experimental data of U. Since the wake is symmetrical, $V=0$ at $Y=0$ and the maximum of V is found around $Y=b$. Therefore, a rough estimate of $V_{\max}$ at each X-station is given by $-b(\partial U_c/\partial X)$. The largest value of $\partial U_c/\partial X$ in the present experiment is about 0.3 m/sec/mm. Then $V_{\max}$ is 0.6 m/s. This is only 6 percent of the free-stream Velocity. The mean flow can be considered parallel. This is in contrast to the jet, of which inclination of the flow near the edge is very large and the mean flow is far from being parallel.

The velocity fluctuation in the region, 20 mm$<X<$150 mm, is decomposed as

$$u=\sum_j u_j(X, Y)\sin(\alpha_j X+\omega_j t+\theta_j) \tag{7-2}$$

$$v=\sum_j v_j(X, Y)\sin(\alpha_j X+\omega_j t+\phi_j) \tag{7-3}$$

in which j denotes each spectral component, α_j and ω_j are the wave number and the frequency, respectively, u_j and v_j are amplitude distribution as functions of X and Y. Phase angles θ_j and ϕ_j are assumed to be constant. Since w-fluctuation is small, it can be neglected. Each spectral component of u and v must satisfy the continuity equation as

$$\left(\frac{\partial u_j}{\partial X}\right)^2+\alpha_j^2 u_j^2-\left(\frac{\partial v_j}{\partial Y}\right)^2=0 \tag{7-4}$$

$$\phi_j=\theta_j+\tan^{-1}\left[\frac{\alpha_j u_j}{\partial u_j/\partial X}\right] \tag{7-5}$$

In general, large α_j corresponds to large ω_j because the phase speed, ω_j/α_j is in the order of the free-stream velocity. For fluctuations with large α_j the second term in equation (7-4) is larger than the first term and

This document is provided by JAXA.

$$\frac{\partial v_f}{\partial Y} \simeq \alpha_f u_f \simeq \frac{\omega_f}{U_0} u_f$$

This means that v_f is large for high-frequency components.

When α_f is small, the second term is small and the first term dominates. Then $\partial u_f/\partial X = -\partial v_f/\partial Y$. These simple relations agree with experimental results on amplitudes of spectral components. For instance, $\overline{v_f^2}$ of 70 Hz-component (α_f and ω_f, small) is much smaller than $\overline{u_f^2}$. Since $\overline{(uv)_f}$ can not exceed $\sqrt{\overline{u_f^2}} \cdot \sqrt{\overline{v_f^2}}$, $\overline{(uv)_f}$ is also small compared with $\overline{u_f^2}$. On the other hand, $\overline{v_f^2}$ and $\overline{(uv)_f}$ of 1330 Hz-components (α_f and ω_f, large) are comparable with $\overline{u_f^2}$.

The equation of motion of a two-dimensional flow with fluctuation is given by

$$U\frac{\partial U}{\partial X} + V\frac{\partial U}{\partial Y} + \frac{\partial \overline{u^2}}{\partial X} + \frac{\partial \overline{uv}}{\partial Y} = -\frac{1}{\rho}\frac{\partial P}{\partial X} + \nu\left(\frac{\partial^2 U}{\partial X^2} + \frac{\partial^2 U}{\partial Y^2}\right) \tag{7-6}$$

$$U\frac{\partial V}{\partial X} + V\frac{\partial V}{\partial Y} + \frac{\partial \overline{uv}}{\partial X} + \frac{\partial \overline{v^2}}{\partial Y} = -\frac{1}{\rho}\frac{\partial P}{\partial Y} + \nu\left(\frac{\partial^2 V}{\partial X^2} + \frac{\partial^2 V}{\partial Y^2}\right) \tag{7-7}$$

Since there is no solid boundary in the flow, the Reynolds stress might be larger than the viscous stress everywhere in the flow. This may be true not only in the fully developed turbulent wake but also in the region with fluctuations of appreciable amplitude. Neglecting viscous terms, equation (7-7) becomes

$$U\frac{\partial V}{\partial X} + \frac{\partial \overline{uv}}{\partial X} + \frac{\partial}{\partial Y}\left(\frac{V^2}{2} + \overline{v^2} + \frac{P}{\rho}\right) = 0 \tag{7-8}$$

Integrating this equation between $Y=0$ and ∞, we have

$$\frac{P_c}{\rho} = -\overline{v_c^2} \tag{7-9}$$

where subscript c denotes the value on the center line and the static pressure at $Y=\infty$ is taken to be zero. Dividing both sides by $1/2 \cdot U_0^2$

$$C_{pc} \equiv \frac{P_c}{1/2 \cdot \rho U_0^2} = -2\frac{\overline{v_c^2}}{U_0^2} \tag{7-10}$$

Experimental values for the static pressure coefficient c_{pc} and $2\overline{v_c^2}/U_0^2$ in natural transition are shown in fig. 7-1. They agree well for $X<60$ mm but at larger X they show an appreciable discrepancy.

Equation (7-6) at $Y=0$ is, neglecting viscous terms,

$$\frac{\partial}{\partial X}\left(\frac{U_c^2}{2} + \overline{u_c^2} + \frac{P_c}{\rho}\right) + \left(\frac{\partial}{\partial Y}\overline{uv}\right)_{Y=0} = 0 \tag{7-11}$$

Substituting $\frac{P_c}{\rho} = -\overline{v_c^2}$

This document is provided by JAXA.

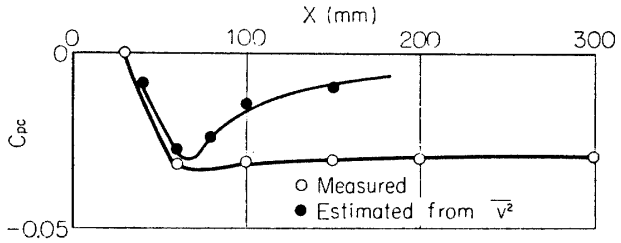

FIG. 7-1. Static-pressure coefficient on the center line, direct measurement and estimate from V^2. Natural transition.

$$U_c\frac{\partial U_c}{\partial X}+\frac{\partial}{\partial X}(\overline{u_c^2}-\overline{v_c^2})+\left(\frac{\partial}{\partial Y}\overline{uv}\right)_{Y=0}=0 \tag{7-12}$$

Since $\overline{u_c^2}$ is close to $\overline{v_c^2}$, this becomes approximately,

$$U_c\frac{\partial U_c}{\partial X}=-\left(\frac{\partial}{\partial Y}\overline{uv}\right)_{Y=0} \tag{7-13}$$

This is one of the most important relation in the region of nonlinear interaction, where $\partial U_c/\partial X$ can be either positive or negative as shown in, for example, fig. 5-6. Experimental values for both terms in (7-13) are shown in Table 7-1. Both have the same sign, in other words, at the X-station where U_c increases in flow direction the derivative of $\overline{uv}$ is negative. The calculated values of the second term are, smaller than those of the first term. It may due to an experimental error because both terms include graphical differentiations. The validity of (7-13) is

TABLE 7-1.

X (mm)	$\frac{U_c}{U_0}\left(\frac{\partial U_c/U_0}{\partial X}\right)$ ($\times 10^{-2}$/cm)	$-\frac{\partial}{\partial Y}\left(\frac{\overline{uv}}{U_0^2}\right)$ ($\times 10^{-2}$/cm)
Natural transition		
40	4.8	3.0
60	8.0	3.4
80	0.6	≤ 0
100	−0.6	−0.9
120	−0.9	−0.5
150	−0.4	−0.2
400	0.05	≤ 0
With sound of 630 Hz and 700 Hz		
30	11	6
40	12	7
80	− 2.7	−1.2
120	$\lesssim$ 0	≤ 0
800	0.2	0.06

Stress balance on the center line. Natural transition and with sound of 630 Hz and 700 Hz.

This document is provided by JAXA.

approcimately verified. The intergration of equation (7-6) in Y direction from 0 to ∞ gives

$$-\frac{d\theta}{dX}+2\frac{d}{dX}\int_0^\infty \frac{\overline{u^2}}{U_0^2}dY+\frac{d}{dX}\int_0^\infty C_p dY=0 \tag{7-14}$$

where θ is the half momentum thickness defined as

$$\theta\equiv\int_0^\infty \frac{U}{U_0}\left(1-\frac{U}{U_0}\right)dY$$

An integration of (7-14) in X direction gives the conservation of the momintum flux as,

$$\theta-2\int_0^\infty \frac{\overline{u^2}}{U_0^2}dY-\int_0^\infty C_p dY=\text{const.} \tag{7-15}$$

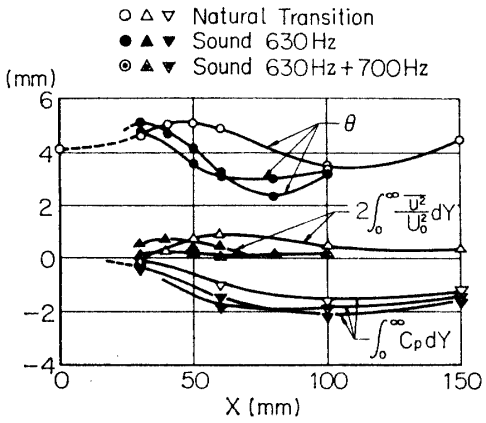

FIG. 7-2. Three terms of momentum flux calculated from experimental date. Natural transition, with sound of 630 Hz and with sound of 630 Hz and 700 Hz.

Each term in this equation can be calculated from experimental data as shown in fig. 7-2 for three cases. In all cases θ is largest and the streamwise variation of θ is almost balanced by the pressure term. The normal stress is very small and the total momentum flux is nearly constant. It is obvious that the negative static pressure in the wake should be properly taken in account in understanding the mechanism of the nonlinear interaction. This decrease of the static pressure was observed also in the transition process of a jet (reference 6).

The energy equation for the fluctuations is, neglecting w and $\partial/\partial z$, expressed as

$$U\frac{\partial\overline{q^2}}{\partial X}+V\frac{\partial\overline{q^2}}{\partial Y}+2\overline{uv}\frac{\partial U}{\partial Y}+2\overline{u^2}\frac{\partial U}{\partial X}+2\overline{v^2}\frac{\partial V}{\partial Y}+\frac{\partial\overline{q^2u}}{\partial X}+\frac{\partial\overline{q^2v}}{\partial Y}$$
$$+\frac{2}{\rho}\frac{\partial\overline{pu}}{\partial X}+\frac{2}{\rho}\frac{\partial\overline{pv}}{\partial Y}-\nu\frac{\partial^2\overline{q^2}}{\partial X^2}-\nu\frac{\partial^2\overline{q^2}}{\partial Y^2}+\Phi=0 \tag{7-16}$$

where Φ denotes the viscous dissipation due to the velocity fluctuation and $\overline{q^2}=\overline{u^2}+\overline{v^2}$. The viscous dissipation due to the mean motion is neglected. Derivatives of fluctuating quantities in X-direction is small and can be neglected, that is,

$$\frac{\partial q^2u}{\partial X}+\frac{2}{\rho}\frac{\partial\overline{pu}}{\partial X}-\nu\frac{\partial^2\overline{q^2}}{\partial X^2}=0$$

This document is provided by JAXA.

Integrating remaining terms in Y-direction from $-\infty$ to $+\infty$ we obtain in a non-dimensional form

$$-\frac{\partial}{\partial X}\int_{-\infty}^{\infty}\frac{\overline{u^2}+\overline{v^2}}{U_0^2}\cdot\frac{U}{U_0}dY-2\int_{-\infty}^{\infty}\left[\frac{\overline{uv}}{U_0^2}\frac{\partial U}{\partial Y}\frac{1}{U_0}+\frac{\overline{u^2}-\overline{v^2}}{U_0^2}\frac{\partial U}{\partial X}\frac{1}{U_0}\right]\partial Y=\frac{1}{U_0^3}\int_{-\infty}^{\infty}\Phi dY$$

The first term corresponds to the convection of the fluctuation energy by U, the second term is the production of fluctuation energy and the right-hand side is the viscous dissipation. Two terms in the left-hand side can be calculated from experimental data as shown in Fig. 7-3. The difference of two terms is the dissipation which was not measured. The negative production is clearly shown between $X=6$ mm and 120 mm. The positive production is maximum at about $X=30$ mm and the convection term varies almost parallel with the production. At $X=40$ mm, the convection seems to be larger than the production. This might be due to an experimental error. The dissipation is always small and the production and convection are almost in balance. In other words, the produced energy is convected with little loss. The production between $X=60$ mm and 120 mm is negative, namely the fluctuation energy is transfered to the mean motion. In the is convected with little loss. The production between $X=60$ mm and 120 mm is region, the convection is also negative. The negative convection means that the energy is convected to that X-station. Since the dissipation is small, most of the convected energy is given back to the mean motion.

The Reynolds stresses in the momentum equation are composed of spectral components. Experimental results indicate that contributions of fundamental components (f_1 and f_2) are always dominant. For low-frequency components (f_1-f_2, $2(f_1-f_2)$, $\cdots$) $\overline{uv}$ is almost zero. High-frequency components (f_1+f_2, $2(f_1+f_2)$, $\cdots$) have small values of $\overline{uv}$, which are not significant in the overall stress balance. Therefore, the mean-velocity distribution is determined mostly by

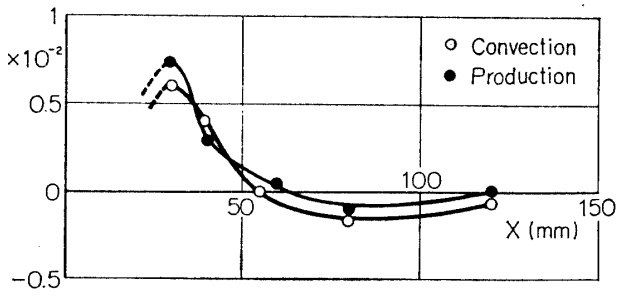

FIG. 7-3. Energy balance calculated from experimental data. Sound of 630 Hz and 700 Hz.

$$\text{convection}=\frac{\partial}{\partial X}\int_{-\infty}^{\infty}\frac{\overline{u^2}+\overline{v^2}}{U_0^2}\cdot\frac{U}{U_0}dY$$

$$\text{production}=-2\int_{-\infty}^{\infty}\left[\frac{\overline{uv}}{U_0^2}\frac{\partial U}{\partial Y}\frac{1}{U_0}+\frac{\overline{u^2}-\overline{v^2}}{U_0^2}\frac{\partial U}{\partial X}\frac{1}{U_0}\right]dY$$

This document is provided by JAXA.

fundamental components. In the energy equation the production of the fluctuation energy also takes place mostly through fundamental components. The energy of mean motion may be given first to the fundamental components and handed over to low-frequency components. On the other hand, high-frequency components can receive energy directly from the mean motion by the Reynolds stress.

In order to make a more detailed discussion on the energy balance we have to measure higher-order statistical quantities such as $\overline{u^3}$, $\overline{u^2v}$ as functions of X and Y. The energy exchange among spectral components may be clarified by taking spectra of these higher-order quantities.

8. Amplification of Ramdomness

The growth of a velocity fluctuation is, in the linear region as well as in the nonlinear region, considerd to be a deterministic process. As shown in preceding sections, wave-forms of fluctuation at small X are regular and periodic.

The turbulence is, on the other hand, characterized by random fluctuations. In the transition region, the regular fluctuations must be randomized. If we can define "randomness", it must be amplified in the transition process. An extremely small amount of irregularity or randomness may abide in an apparently regular fluctuation. The transition process is interpreted as the amplification of the original randomness on one side and the reduction of regularity on the other.

A primary effect of the nonlinearity for a system including fluctuations is the generation of higher harmonics from the fundamental component. Existing theoretical works on the nonlinear development of a regular fluctuation are based on this concept. The production of higher harmonics in the wake is, however, not likely to be a vital ring in the whole transition process by following reasons. In the present experiment the most unstable fluctuation according to the linear theory has a frequency around 630 Hz. The second and third harmonics are 1260 Hz and 1890 Hz. Components with these high frequencies may decay by the viscous effect. Experimental results indicate that high-frequency components are small in magnitude. Energy-containing components in a turbulent wake have much lower frequencies. Then the most significant process must be the generation of low-frequency components rather than the generation of higher harmonics. The generation of subharmonics in a half-jet (separated layer) has been found (reference 7 and 10). In the wake no subharmonics are found. These must be a difference in the transition process of a wake and a half-jet.

In the present experiment with two sounds we observe the generation of a component with the frequency of the difference of two frequencies. We believe that the energy-containing low-frequency components are produced by this process. In the natural transition, a residual small-amplitude disturbance in the wind-tunnel is amplified in the linear region.

Low-frequency velocity fluctuations, do not grow in the linear region because the growth rate is very small. The can be generated only by a nonlinear interac-

This document is provided by JAXA.

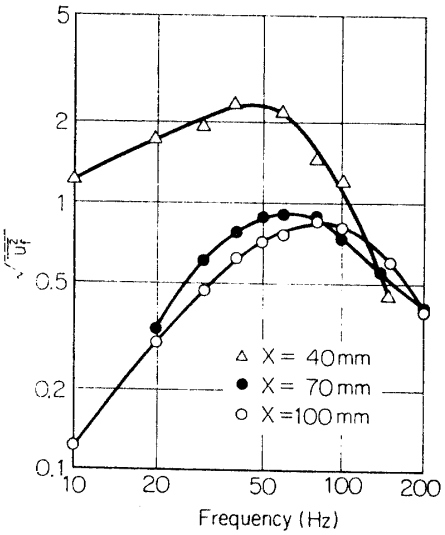

FIG. 8-1. Low-frequency portions of spectra of u-fluctuation at $Y=0$. Natural transition. Ordinate is arbitrary scale.

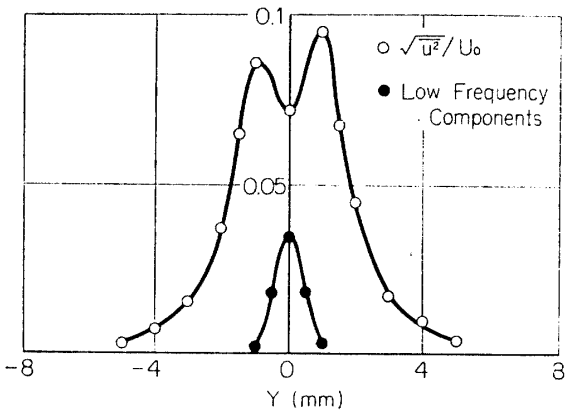

FIG. 8-2. Distributions of $\sqrt{\overline{u^2}}/U_0$ and low-frequency components at $X=40$ mm. Natural transition.

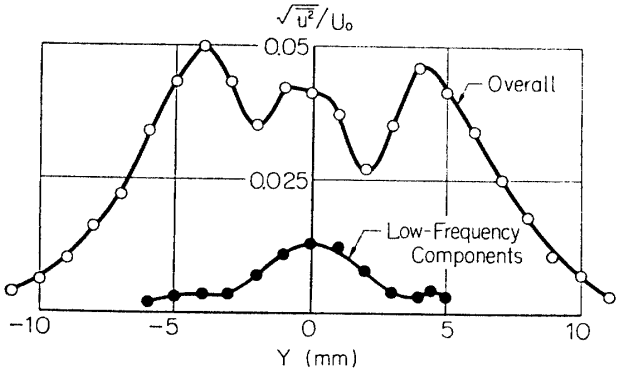

FIG. 8-3. Distributions of $\sqrt{\overline{u^2}}/U_0$ and low-frequency components at $X=100$ mm. Natural transition.

tion of high-frequency components which have large growth rates in the linear region.

The nature of irregular, slow fluctuations in the u-fluctuation in natural transition (Fig. 3-5) was investigated by observing spectra. Fig. 8-1 shows low-frequency portions of spectra at three X-stations. There rae broad peaks between 50 and 100 Hz. The frequency of the predominant fluctuation is around 630 Hz and low-frequency components are separable from this fundamental component. Setting by the central frequency of a band-pass filter around 50 Hz. Figs. 8-2 and 8-3 show distributions of low-frequency components in Y-direction in comparison with overall $\sqrt{\overline{u^2}}$. The low-frequency components are localized near the center-line at both X-stations. Generally speaking, in a fully-developed turbulent flow, distributions of high-frequency components are broader than those of low-frequency components. This fact coincides with the localized distribution of low-frequency components in the transition region. The streamwise variation of the

This document is provided by JAXA.

peak value of low-frequency components on the center line is illustrated in Fig. 8-4 together with the variation of the maximum value of overall $\sqrt{\overline{u^2}}$ at each X-station. They are extremely small at $X=30$ mm, reach a maximum at about $X=45$ mm, decrease downstream a little and increase again from $X=150$ mm.

The nature of the low-frequency components in natural transition is very similar to that of 70 Hz-component in the presence of sound of two frequencies (630 Hz and 700 Hz) in many respects.

1. Both have large amplitude near the center-line.
2. Both components are not found in v-fluctuation.
3. Streamwise developments of both components are very similar as shown in Fig. 8-5. Upper two curves show the variation of the breadth of the distribution of $\sqrt{\overline{u^2}}$ in the natural transition and that with sound of two frequencies. Lower two curves illustrate the breadth of distributions of low-frequency components and 70 Hz-componnet. If X-axis is shifted properly, two curves almost coincide.

Thus we conclude that the low-frequency components in natural transition is generated by the nonlinear interaction of high-frequency components.

The mutual suppression of amplitudes of two fluctuations and the production of the low-frequency component from high-frequency fluctuations are two fundamental effect of the nonlinear interaction. In the natural transition, the amplification of randomness may be accomplished by the following process.

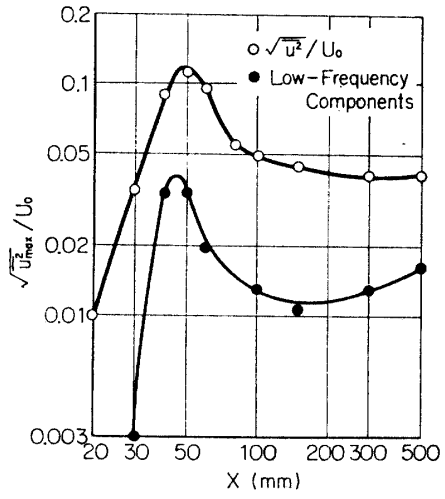

FIG. 8-4. Streamwise variations of maximum values of $\sqrt{\overline{u^2}}$ and low-frequency components at each X-station. Natural transition.

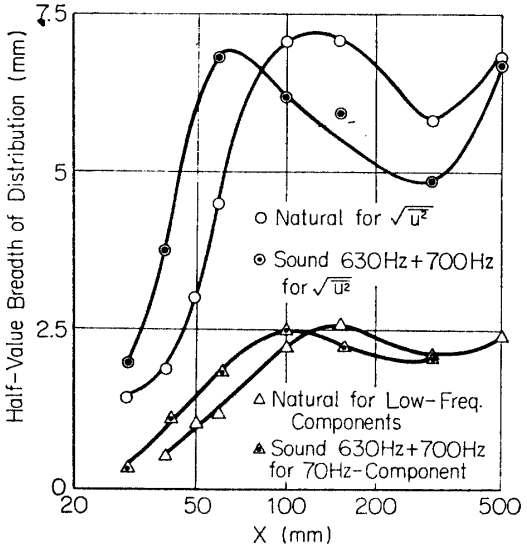

FIG. 8-5. Upper two curves: Streamwise variations of half-value breadth of distribution of $\sqrt{\overline{u^2}}$ in natural transition and with sound of 630 Hz and 700 Hz. Lower two curves: half-value breadth of distribution of root-mean-square of low-frequency components in natural transition and of 70 Hz-components with sound 630 Hz and 700 Hz.

This document is provided by JAXA.

Consider that 610 Hz- and 650 Hz-components are present in a wake. They will produce 40 Hz-component by a nonlinear interaction. If the frequency of one of two fundamental components changes by 1%, namely, from 610 Hz to 616 Hz, the frequency of low-frequency component changes to 34 Hz. Now, the variation in the frequency is 15%. Obviously, a small change results in a large relative change. Thus, the randomness in the frequency is amplified. The randomization in the amplitude may be accomplished by the mutual suppression.

Suppose there are two fluctuations, A and B. If the amplitude of A is reduced a little by some reason, A will be suppressed more by B. On the other hand, B will experience less suppression by A. This is a kind of positive feedback system. The small reduction of amplitude in A is amplified. The randomization in the frequency and amplitude will lead to the production of random turbulence. However, there are still much works to be done for clarifying the total process of laminar-turbulent transition.

9. Conclusion

Experimental results on the transition process of a two-dimensional wake with three different conditions indicate following conclusions.

1. In the natural transition a regular velocity fluctuation of a pronounced frequency grows. A slow, irregular fluctuation is observed near the center line of the wake. The wave-form of fluctuation changes gradually into turbulent pattern without accompanied by abrupt breakdowns.

2. When a sound of single frequency is introduced into the wake, the wave-form is more regular and the slow, irregular fluctuation disappears. The transition distance defined by the onset of turbulent fluctuation is larger than that in the natural transition.

3. In the presence of sound of two frequencies (f_1, and f_2), velocity fluctuations of f_1-f_2, $2(f_1-f_2)$, $\cdots$ and f_1+f_2, $2(f_1+f_2)$, $\cdots$ are produced by the nonlinear interaction. The low-frequency components —f_1-f_2, $2(f_1-f_2)$, $\cdots$— consist mainly of u-fluctuation. Fundamental components —f_1, f_2— and high-frequency components —f_1+f_2, $2(f_1+f_2)$ $\cdots$— are composed of u- and v-fluctuations. Phases of fundamental components are antisymmetrical whereas those of other components are symmetrical with respect to the center line.

4. In three cases, streamwise distributions of the mean velocity on the center line, U_c show maxima and minima. In the region where U_c decreases downstream the sign of Reynolds stress is such that the fluctuation energy is given back to the mean motion.

5. The momentum flux in the flow direction is estimated from experimental results and it is almost constant.

6. The energy balance calculated from experimental data indicate that the production of fluctuation energy is almost balanced out by the streamwise convection, the viscous dissipation being very small. The region of negative production the energy transfer from the fluctuation to the mean motion is found.

This document is provided by JAXA.

7. The extended linear theory based on the local equilibrium is not valid in the nonlinear region.

8. The nature of low-frequency components in the natural transition is very similar to that of f_1-f_2 component in the presence of sound of two frequencies.

9. The change of regular velocity fluctuation into random turbulence is considered to be a process of amplification of randomness. A small randomness in the amplitude is amplified by the mutual suppression of spectral components and the randomization in the frequency is accomplished by the generation of low-frequency components from two high-frequency components.

Department of Gas Dynamics,
Institute of Space and Aeronautical Science,
University of Tokyo, Tokyo
June 4, 1970

References

[1] Benney, D. J.: A non-linear theory for oscillations in a parallel flow. J. Fluid Mech. vol. 10, part 2, 209–236 (1961)
[2] Görtler, H. and Velte, W.: Recent mathematical treatments of laminar flow and transition problems. Phys. Fluid, Suppl. S3–S10 (1967)
[3] Kelly, R. E.: On the resonant interaction of neutral disturbances in two inviscid shear flows. J. Fluid Mech. vol. 31, part 4, 789–799 (1968)
[4] Klebanoff, P. S. and Tidstrom, K. D. and Sargent, L. M.: The three dimensional nature of boundary layer instability J. Fluid Mech. vol. 12, part 1, 1–34 (1962)
[5] Sato, H. and Kuriki, K.: The mechanism of transition in the wake of a thin flat plate placed parallel to a uniform flow. J. Fluid Mech. vol. 11, part 3, 321–352 (1961)
[6] Sato, H.: The stability and transition of a two-dimensional jet. J. Fluid Mech. vol. 7, part 1, 53–80 (1959)
[7] Sato, H.: Further investigation on the transition of two-dimensional separated layer at subsonic speeds. J. Phys. Soc. Japan, vol. 14, 1797–1810 (1959)
[8] Freymuth, P.: On transition in a separated laminar boundary layer. J. Fluid Mech. vol. 25, part 4, 683–704 (1966)
[9] Bloor, M. S.: The transition to turbulence in the wake of a circular cylinder. J. Fluid Mech. vol. 19, part 2, 290–340 (1964)
[10] Browand, F. K.: An experimental investigation of the instability of an incompressible, separated shear layer. J. Fluid Mech. vol. 26, part 2, 281–307 (1966)

This document is provided by JAXA.